INTEGRATING DROPLET MICROFLUIDICS AND CONFOCAL FLUORESCENCE SPECTROSCOPY FOR HIGH-THROUGHPUT BIOMOLECULAR ANALYSIS

by

Tushar D Rane

A dissertation submitted to Johns Hopkins University in conformity with the requirements for the degree of Doctor of Philosophy

Baltimore, Maryland

May, 2014

© 2014 Tushar D Rane

All Rights Reserved

Abstract

Droplet microfluidics has emerged as a branch of microfluidics with tremendous potential for high-sensitivity and high-throughput biomolecular analysis, leading to its adaptation for a variety of applications. However, commonly used biosample analysis schemes using droplet-based systems are limited, due to the need for multiple devices per analysis, integration with low-sensitivity detection techniques as well as the need of barcodes for droplet identification. This thesis will focus on sample-to-answer droplet microfluidic devices I have developed in collaboration with colleagues at the Johns Hopkins University to overcome these limitations. Integration of novel microfluidic design with highly sensitive confocal fluorescence spectroscopy technique has enabled these devices to achieve ultra-sensitive analysis of individual biosamples at single-molecule levels as well as high throughput multi-analyte analysis of biosamples.

Acknowledgements

First and foremost, I would like to thank my advisor Dr. Jeff Wang for providing me with guidance throughout my PhD while giving me sufficient freedom to pursue my own research ideas. He has been very patient and supportive mentor throughout this long PhD process. I will always be thankful to him for providing me the opportunity to pursue my PhD at the BioMEMS lab and training me for a career in science.

My lab mates have been a major part of my learning process throughout the PhD. It was very helpful to learn microfluidics from Chris, optics from Kelvin and molecular biology from Tim and Megan during my initial stay in the lab. Chris and Helena have also been great research partners in collaborative research projects we completed together. Furthermore, research discussions I have had with other lab members over time including Yi, Cyrus, Yunke, Dong Jin, Ye, Liben and Weihua have been very helpful. Vasudev made my stay in Baltimore very enjoyable through being a great labmate as well as roommate for a long time. Finally all other lab mates have made going through these long PhD years a breeze by maintaining a friendly atmosphere in the lab all the time.

Casual cricket in front of the MSE library helped me make some great friends at JHU. I will always remember playing cricket with Rege, Golu, Buffy, Thampy, Kiran, Coach and others. Late night and weekend hangouts with Nupura, Amritha, Radha, Ben, John, Alex and Lukas have made my stay at JHU very enjoyable. Furthermore, weekend outings with Raghupati, Nema and Panga once in a while helped me recharge when research seemed overwhelming.

Finally, my parents, my sister and my niece (a new addition to our family) have been very patient and understanding while I undertook this long path of academic training while being far away from them. I will always cherish their support and unconditional love and dedicate this thesis to them.

Table of contents

Abstract ii

Acknowledgements iii

Table of contents iv

List of tables ix

List of Figures x

Chapter1: Introduction 1

Chapter 2: Counting single molecules within droplets 5

- 2.1 Introduction 5
- 2.2 Solution 6
- 2.3 Conclusion 10
- 2.4 Supplementary section 11
  - 2.4.1 Device Fabrication and Operation 11
  - 2.4.2 Experimental Setup for Single Molecule Detection 13
  - 2.4.3 Sample Preparation 15
  - 2.4.4 Single Molecule Data Analysis 16

Chapter 3: Amplification-free single cell detection in droplets 35

- 3.1 Background 35

3.2 Solution 36

3.3 Experimental section.. 40

3.3.1 PNA Beacon.. 40

3.3.2 Control Targets and Pathogen Cells 40

3.3.3 Design and Fabrication of Microfluidic Device............................... 42

3.3.4 Optical Detection Setup 43

3.3.5 Operation of Microfluidic Device 44

3.4 Results and Discussion.. 45

3.5 Conclusion.. 50

3.6 Supplementary section 50

3.6.1 Device design and fabrication for experiments with 16s rRNA mimic 50

3.6.2 Fluorescence data analysis for experiments with 16s rRNA mimic51

3.6.3 Optimizing the incubation temperature for the PNA beacon assay in bulk.. 53

Chapter 4: Continuous Flow Digital Loop-Mediated Isothermal Amplification (LAMP) Reaction for Digital Nucleic Acid Detection 72

4.1 Introduction 72

4.2 Experimental section.. 75

4.3 Results and Discussion.. 79

4.4 Conclusion 81

4.5 Supplementary section 82

4.5.1 LAMP assay indicator evaluation 82

4.5.2 Droplet data analysis 84

Chapter 5: A Barcode-Free Combinatorial Screening Platform for Matrix Metalloproteinase Screening 107

5.1 Introduction 107

5.2 Solution 110

5.3 Conclusion 117

5.4 Supplementary section 117

5.4.1: Microfluidic device fabrication 117

5.4.2: Materials 118

5.4.3: Experimental protocol 121

5.4.4: Determining maximum reagent dilution on device 124

5.4.5 Fluorescence standard curve 125

5.4.6 Long droplet sequence generation on device 126

Chapter 6: Microfluidic platform for on-demand generation of spatially indexed combinatorial droplets 147

6.1 Background 147

6.2 Materials and Methods 152

6.2.1 Serial Sampling Loading System 152

6.2.2 Fabrication of the Master Molds for the Microfluidic Device 153

6.2.3 Microfluidic Device Fabrication 154

6.2.4 Capillary–to–Chip Interface 154

6.2.5 Device control 155

6.2.6 Reagents 155

6.2.7 Sample plug and droplet volume estimation 156

6.3 Results and Discussion 157

6.3.1 Overall Work Flow 157

6.3.2 Capillary-to-Chip Interface 158

6.3.3 Droplet uniformity using mechanical valve based droplet generation 159

6.3.4 Sample Digitization 160

6.3.5 Generation of droplets of combinatorial mixtures 161

6.4 Conclusion 164

6.5 Supplementary section 166

6.5.1 Mold Fabrication 166

6.5.2 Device Fabrication and Operation 167

6.5.3 Fusion Zone design 168

6.5.4 Serial Sample Loading System 169

6.5.4.4 Discussion... 184

Chapter 7: Conclusion and Future directions... 220

References 221

Curriculum Vitae 231

List of tables

Table 3.1: Droplet volume and its effect on the target concentration within the droplet……………………………………………………………………….66

List of Figures

Fig. 2.1: Microfluidic device design 19

Fig. 2.2: Testing the microfluidic device 21

Fig. 2.3: Single molecule quantification on the microfluidic device 23

Fig. 2.4: A cross-section of the constriction within the retractable valve....... 25

Fig. 2.5: Schematic diagram of the optical components in our two color Cylindrical Illumination Confocal Spectroscopy (CICS) system.................... 27

Fig 2.6: Estimation of the size of the CICS illumination volume. 29

Fig 2.7: Single molecule data analysis. 31

Fig 2.8: A high magnification image of a droplet squeezing through a 20 µm by 10 µm constriction. 33

Fig 3.1: Schematic of the droplet assay platform for single cell detection. 54

Fig 3.2: Microfluidic chip design.. 56

Fig 3.3: Fluorescence data collected from the artificially generated sequences of positive control (PNA beacon + rRNA mimic + human genomic DNA) and negative control (PNA beacon + human genomic DNA only) droplets. 58

Fig 3.4: Quantification of positive droplet count in a droplet sequence for different artificially generated droplet sequences. 60

Fig 3.5: Fluorescence data collected from droplets with and without E. coli cells. 62

Fig 3.6: Fluorescence data collected from droplets generated using a low concentration E. coli sample. 64

Fig. 3.7: Schematic of the chip design for experiments with 16s rRNA mimic 68

Fig. 3.8: Effect of incubation temperature on the cell lysis and PNA beacon hybridization efficiency 70

Fig. 4.1 Droplet microfluidic device for continuous flow digital LAMP analysis 85

Fig. 4.2 Sample digital LAMP signal from droplets with an EvaGreen readout. 87

Fig. 4.3 Sample digital LAMP signal from droplets with a Calcein based readout. 89

Fig. 4.4 Average droplet fluorescence intensity data from large droplet populations for different target concentrations. 91

Fig. 4.5 Target nucleic acid quantification with digital LAMP. 93

Fig. 4.6 Microfluidic device used for droplet experiments 95

Fig. 4.7 Effect of EvaGreen concentration on LAMP signal to background ratio 97

Fig. 4.8 Gel verification of LAMP reaction outcome for various EvaGreen concentrations. 99

Fig. 4.9 Effect of Manganese chloride concentration on LAMP signal to background ratio 101

Fig. 4.10 Gel verification of LAMP reaction outcome for various Manganese Chloride concentrations. 103

Fig. 4.11 Two different techniques for separation of positive and negative droplet clusters from a droplet population.. 105

Fig 5.1 MMP screening platform.. 127

Fig 5.2 A series of fluorescent droplets generated on a single device:.......... 129

Fig 5.3 Droplet composition control and serial droplet fluorescence detection on the device:.. 131

Fig 5.4 MMP-substrate assay on device:... 133

Fig 5.5 MMP activity comparison between on and off-chip experiments:.... 135

Fig 5.6 Largest reagent dilution generated on the device:............................ 137

Fig 5.7 Standard curves.. 139

Fig 5.8 MMP activity comparison between on and off-chip experiments:.... 141

Fig 5.9 Average measured droplet fluorescence intensities from two repeats of 650 unique MMP-substrate combinations.. 143

Fig 5.10 Average fluorescence intensities measured from different repeats for each unique MMP-substrate combination plotted against each other: 145

Fig 6.1 Schematic of the sample screening platform.................................... 186

Fig 6.2 'Serial Sample Loading' (SSL) system 188

Fig 6.3: Microfluidic Device Design... 190

Fig 6.4 Control of droplet volume and droplet uniformity using mechanical valve based droplet generation... 192

Fig 6.5 Demonstration of reagent injection in sample daughter droplets merging with reagents.. 194

Fig 6.6 Photographs of the incubation region indicating multiplexing capability of the device........ 196

Fig 6.7 Microfabrication Process with Single Developing Step: 198

Fig 6.8 Modified microfluidic device fabrication:........ 200

Fig 6.9 Fusion zone design for robust reagent injection in sample droplets with different volumes........ 202

Fig 6.10 A schematic illustrating the working principle of the sample plug loading system........ 204

Fig 6.11 Different views of a CAD model of the capillary adapter actually used for fabrication of the capillary adapter:........ 206

Fig 6.12 A photograph of the actual assembled Serial Sample Loading (SSL) system:........ 208

Fig 6.13 A plot of pressure variation in the sample well over time, for different peak pressures (10, 20, 30, 40 and 50 psi) applied to the sample well. 210

Fig 6.14 Micrographs demonstrating capability of the SSL system to load uniform sample plugs into a capillary:........ 212

Fig 6.15 Plots showing the linear relationship between sample plug volume and the duration of the peak pressure phase (Tpeak) for three different fixed values of peak pressure (Ppeak: 0.5, 1 and 1.5 psi) applied........ 214

Fig 6.16 Plot showing the linear relationship between the sample plug volume and the peak pressure (Ppeak) applied for a fixed duration of the peak pressure phase (Tpeak: 1 sec)... 216

Fig 6.17 Sample plug volume variation with plug number........................... 218

Chapter1: Introduction

Conventional microfluidic systems designed to miniaturize biochemical experimentation done on bench top equipment typically use single phase fluid flow. However, past few years have seen the emergence of the term ‘Droplet Microfluidics’ in the microfluidic community. Droplet Microfluidics employs two immiscible phases i.e. the dispersed or droplet phase and the continuous or carrier fluid phase to rapidly generate millions of discrete reaction chambers(i.e. droplets)(1). Droplet microfluidics offers distinct advantages over conventional microfluidic systems including shorter heat and mass transfer times (due to high surface area to volume ratio), rapid mixing and massive parallel processing (1).

Although, microdroplet generation is possible through application of a variety of non-microfluidic methods, the application of microfluidics for droplet generation allows highly monodisperse droplet generation with significant reduction in droplet size(2). Most common microfluidic configurations used for droplet generation are the ‘T-junction’ and ‘Flow focusing’ configurations. T-junction configuration involves side shearing of the dispersed phase by the continuous phase, whereas the flow focusing configuration involves forcing the dispersed phase and the continuous phase through a narrow region in the microfluidic chip for droplet generation. Flow focusing configuration allows for more symmetric shearing of the dispersed phase with reduced size and polydispersity(2). Droplet generator chips can routinely approach kHz generation rates with peak rate of 20 kHz reported in literature (3). As a result, a simple droplet generator chip can set up millions of reactions in a matter of minutes. Furthermore, the size of the reaction containers i.e. droplets can be reduced to as low as fL volumes (1) resulting in orders of magnitude savings in reagent volume over microfluidic large scale integration systems (4). Reduced reaction volumes and fast generation rates allow droplet microfluidic platform to be used for running large number of reactions without the need for increasing device size (1). Furthermore, highly monodisperse droplet generation is further supplemented with development of sophisticated droplet manipulation techniques. Basic operations required for performing chemical reactions including droplet fusion, droplet fission, droplet sorting, droplet mixing etc have been demonstrated with a variety of active as well as passive methods(1).

Inspired by nature's way of performing biochemical operations within confined discrete individual units i.e. cells, performing chemistry and biology in droplets is rapidly becoming a prominent research theme. Droplet microfluidics has been utilized for a variety of applications including single cell screening(5, 6), digital PCR (7-9), protein engineering and directed evolution(10) ,protein crystallization condition screening(11) and shape and structure controlled particle synthesis (12-14)

However, droplet microfluidics being still in its early stages still suffers from a few limitations which need to be addressed to expand the applicability of this elegant technology to a wider range of applications. To be specific, 1) Readout techniques like fluorescence imaging (15, 16) used with droplets lack the sensitivity required for detecting low abundance biomolecules of interest at single molecule level. As a result amplification schemes are typically required for detection of a nucleic acid sequence of interest, increasing the droplet platform complexity. 2) The PCR based droplet platforms used for precise nucleic acid/pathogen quantification from a biological sample require a complicated multi-device and multi-instrument workflow and 3) Although droplet microfluidics can be used to set up millions of reactions in minutes, the T-junction and flow focusing droplet generator chips commonly used for various applications (1) cannot generate droplets with arbitrary compositions by mixing many different reagents in different proportions, limiting the true high-throughput potential of droplets.

This thesis will attempt to overcome all the limitations of the droplet microfluidic technology mentioned above. The limitations mentioned above are broken down into individual problems in each chapter of this thesis. Each chapter begins with the description of a specific problem being addressed followed by a proposed solution to the problem as well as discussion of experimental results showing the efficacy of that solution. Towards the end of each chapter, a ‘supplementary section’ is included, which lists details of experimental conditions for the experimental results discussed earlier in the chapter.

Overall I believe that all the solutions proposed in this thesis combined together will contribute to the repertoire of tools available with droplet microfluidic technology for ultra-sensitive and high-throughput biomolecular analysis, thus, expanding the applicability of this elegant technique to a broader range of applications.

Chapter 2: Counting single molecules within droplets

Rane, T. D., et al. "Counting single molecules in sub-nanolitre droplets." Lab on a Chip 10.2 (2010): 161-164. Reproduced by permission of The Royal Society of Chemistry

2.1 Introduction

Droplet-based microfluidic platforms offer the distinct advantages of fast sample mixing, limited reagent dispersion, and lower sample loss or contamination when compared to traditional microfluidic devices.(1)(2) In addition, simple control strategies for kHz frequency droplet generation, transportation, storage, and sorting give the platform a propensity for high throughput analysis. While initial applications have been shown in a range of research disciplines, including biochemical analysis,(17) chemical and material synthesis,(18) and chemical reactions,(19) more recent applications have emerged that seek to expand this high throughput capability to the analysis of individual biological entities, such as single cells(20-22) or biomolecules.(23, 24)

In single cell experiments, in vitro compartmentalization in droplets enables rapid accumulation of secreted cellular factors,(25) and provides both chemical isolation and a unique means of cell selection and control.(26) Alternately, single molecule compartmentalization enables nucleic acid analysis through single-copy DNA PCR, extending the high throughput capacity of droplet-based microfluidics to digital PCR assays.(21, 23, 24) However, the current dependence on amplification techniques (e.g. PCR or fluorogenic substrate)(1) for detection of low concentration biomolecules presents limitations in droplet-based platforms; these include decreased throughput and added complexity involved with enzymatic amplification. These limitations point towards the need for integration of a highly sensitive detection platform for amplification-free detection of low-abundance biomolecules.

2.2 Solution

Confocal Fluorescence Spectroscopy (CFS) has traditionally been used for fluorescence based single molecule detection (SMD).(27-32) Resolution of single fluorophores is accomplished through reduction of a laser-illuminated probe volume to femtolitre size, thus minimizing background noise. Although well suited for SMD in continuous sample streams, CFS is ill-suited for low abundance analyte detection in discrete volumes (e.g. droplets).(33, 34) Fig. 2.1A depicts the challenges associated with SMD in droplet platforms. A single pass of the droplet through the laser illuminated volume results in low intra-droplet detection efficiencies (i.e. detection of only a small fraction of encapsulated molecules), as most biomolecules pass around the detection volume. In addition, even at nominal flow speeds the sub-nanolitre droplets pass by the detection volume in milliseconds, making it difficult to resolve tens to hundreds of molecules encapsulated within each single droplet.

In this report, we overcome challenges involved with biomolecular quantification in droplets, including short intradroplet signal acquisition times and droplet–illumination volume size mismatches. In our platform, one dimensional beam shaping using cylindrical optics (Cylindrical Illumination Confocal Spectroscopy, CICS)(35) produces a sheet-like illumination volume, maximizing intra-droplet detection efficiency (Fig. 2.1B). Furthermore, droplet confinement through a microfluidic constriction extends droplet duration through the illumination volume, providing the spatial and temporal resolution necessary to detect single biomolecules.

Controlled droplet confinement and passage through the illumination volume was accomplished using a microfluidic constriction channel patterned into a retractable PDMS valve (Fig. 2.1C). In the open valve state the constriction was not part of the fluidic path and presented no unnecessary challenge to droplet generation due to the increased fluidic resistance of the narrow channel. Water-in-oil droplets were generated using a flow-focusing configuration and transferred to a downstream storage chamber within the multilayered (36) PDMS device (details in section 2.4.1). Upon valve actuation droplets were driven through the constriction using the continuous phase at a controlled pressure, while the occasional clogging of the narrow constriction was averted by pulsing the retractable channel to remove debris. The microdevices were coupled to a custom confocal fluorescence spectroscopic system as described previously, (33-35) by loading the chip onto a stage capable of sub-micron positioning of the chip relative to the illumination volume (details in section 2.3). Two separate optical configurations were used with two different cylindrical lenses (f = 200 mm or f = 300 mm) to expand the illumination volume laterally across the constriction width, while remaining diffraction limited in the other dimensions to maximize signal to noise ratio (SNR).(35) These two configurations created detection volumes with 14.3 or 64.6 μm^2 cross-sections, respectively (details in section 2.4.2). Four separate microdevices were fabricated with constrictions ranging from ~50-400 μm^2 sized cross-sections, yielding a range of maximum possible molecular detection efficiencies (i.e. ratio of the cross sectional areas of the laser illumination and the constriction channel) in traversing droplets from 3.5% to 100%.

Fig. 2.2A shows that droplets from pL to nL sizes were stretched through the constrictions without droplet break-up. In the initial experiments, TOTO®-3 stained Lambda DNA was used as a model biomolecule. Varying concentrations of DNA were loaded in ~40 pL droplets and run through the 64.6 μm^2 illumination volume held within the 200 μm^2 constriction. The raw data trace in Fig. 2.2B shows the outline of two control droplets (no DNA) running through the constriction (red trace – Fluorescence signal from Alexa 488 droplet indicator dye, black trace – Fluorescence signal from TOTO®-3/DNA; details in section 2.4.3). Fig. 2.2C shows the encapsulation and detection of the DNA at 37 pM concentrations. At these higher concentrations, droplet stretching through the constriction becomes increasingly essential as the ~1000 DNA molecules per droplet (37 pM within 44.5 pL) must be resolved within the droplet's transit time through the CICS volume. Fig. 2.3A shows the effect that droplet transit times had on single molecule counting at 37 pM. Burst counts per droplet approach a maximum value of 312 (red line – average of last three datapoints) at ~280 ms. Droplets that traverse the constriction at a faster pace yield decreasing burst rates. The lost information is a result of non-digital molecular occupancy in the illumination volume and decreased SNRs at faster speeds. However, the 312 average fluorescence bursts per droplet in the plateau region agree well with the expected value (320 bursts for the maximum possible detection efficiency of 32.3%). The small discrepancy from the expected value is attributable to molecular loss into the continuous phase and experimental variation in laser and constriction alignment (details of single molecule data analysis and thresholding in section 2.4.4).

In all subsequent experiments, pressures that yielded equal droplet durations through the constriction were selected, yielding equal drop-to-drop acquisition times. This constraint enabled molecular quantification through the expected linear increase in single molecule fluorescent bursts with increasingmolecular concentrations (Fig. 2.3B). In addition, the ability to mold intradroplet detection efficiencies via alterations in the constriction channel to laser illumination cross-section ratio is apparent in Fig. 2.3C. As shown, the average fluorescent bursts per droplet show a linearly increasing trend with decreasing constriction size at equivalent DNA concentrations (maximum possible detection efficiencies of 16.15, 32.3, 64.6, and 100%; details in sections 2.4.1 and 2.4.2).

The results so far, indicate the effectiveness of the droplet-SMD platform in quantifying low abundance fluorescent biomolecules encapsulated within droplets. However, the utility of the droplet-SMD platform can also be extended to sequence specific nucleic acid assays using common single fluorophore nucleic acid probes.(27, 29-31, 34, 37) As shown in Fig. 2.3D, a smaller CICS illumination volume (14.3 μm^2) was used to increase SNR for single fluorophore studies. At 40 pM concentrations (~1000 molecules per 44.5 pL droplet), Cy5 molecular beacons (MB) (34) for E. coli rRNA sequences show few background peaks due to thermal fluctuation of the hairpin probe (Fig. 2.3D top panel; average peaks per droplet 0.282 ± 0.11). However, the presence of target is detectable upon target hybridization as an increase in fluorescence peak counts per drop (Fig. 2.3D bottom panel; average peaks per droplet 9.075 ± 0.76). These single fluorophore studies were performed using a 200 μm^2 constriction; however, the smaller constriction sizes used above demonstrate the ability to mold intradroplet detection efficiencies to meet a variety of experimental requirements.

2.3 Conclusion

In conclusion, for the first time we have demonstrated direct and amplification-free single molecule detection of biomolecules in subnanolitre droplets. As shown, biomolecular quantification using SMD requires only a microfluidic constriction channel for droplet confinement and elongation. Thus, the droplet-SMD microdevice presents a unique alternative to the complex PCR devices currently used for intra-droplet detection. Furthermore, by applying homogeneous probes for single molecule counting we were able to detect nucleic acids using a sequence specific probe. Future integration of the droplet-SMD platform with existing in-drop cell control and lysis techniques(1, 2) or single molecule probe schemes(27, 29-31, 37) presents a general method for high-throughput single cell analysis.

2.4 Supplementary section

2.4.1 Device Fabrication and Operation

As discussed in the text, all devices were fabricated using multilayer soft lithography. Two layers of polydimethylsiloxane (PDMS) were constructed, one for droplet generation and transport and another for the pneumatic valve. The mold for the device was made using three separate photoresist layers. First, a 10 μm tall pad of SPR220-7.0 (Shipley) was used to create the portion of the valve that would close tight against the underlying glass coverslip. After development, a reflow process at 200 °C for 120 minutes resulted in the semi-circular cross-section necessary for effective valve closure. SU-8 was then used to pattern a small constriction channel (20 μm wide with varying heights of 2.5 – 20 μm) on top of SPR220-7.0 pad that would remain open while the valve is in the actuated state. Finally, the 35 μm tall layer containing the droplet generator module was patterned to connect the constriction to the rest of the device. A separate mold for the pneumatic valve (control) layer was made at a 40 μm height, again using SU-8 3025 photoresist (See Fig. 2.4 for a cross-section of the constriction within the retractable valve).

PDMS prepolymer (SYLGARD® 184, Dow Corning) was prepared at 1:7 mixing ratio and cast onto the control layer mold to result in a final thickness of ~ 3 mm upon curing at 80 °C for 10 minutes. The fluidic layer molds were silanized using vapor deposition of chlorotrimethylsilane (Sigma-Aldrich) before spin coating with PDMS prepolymer at a mixing ratio of 1:15 (1300 rpm for 60 seconds). The excess curing agent in the thick control layer (1:10 is the standard mixing ratio) was added to ensure fusion with the second PDMS layer. The thin PDMS layer was then partially cured at 80 °C for 5 minutes before the thick PDMS sheet containing the mechanical valve was peeled off its mold and aligned to the fluidic layer. The two layers were fused together upon curing at 80 °C for 30 minutes. During these steps holes for fluidic and valve access were punched using gauge 20 syringe needles (McMaster-Carr). Finally, the entire chip was bonded to a coverglass (Fisherfinest, 12-548-5R, 35x50-1) after activation of the PDMS surface via plasma oxidation. Samples were delivered to the microfluidic chip using 0.02 inch I.D. Tygon tubing (Cole-Parmer) fitted with 23-gauge needle tips (McMaster-Carr). A mixture of Mineral oil (20% v/v), Tegosoft DEC (73% v/v), and ABIL WE09 (7% w/v)(38) was used as the continuous phase for droplet generation. Upon generation drops were carried to a large volume (~2 uL) storage channel, where droplets could be collected for downstream analysis. During on-chip single molecule detection (SMD), the continuous phase was used to force drops through the constriction at a controlled speed. The discrete phase always consisted of high concentration of Alexa488 dye, which served as an indicator dye to monitor droplet edges on the fluorescence spectroscopy platform. The signal from the indicator dye also provided feedback to control the speeds at which droplets traversed the constriction.

2.4.2 Experimental Setup for Single Molecule Detection

Spectroscopy data was acquired using a custom-built, dual laser excitation, dual emission channel, single molecule spectroscopy platform, as described previously (Fig. 2.5).(39) The system was capable of Cylindrical Illumination Confocal Spectroscopy (CICS) with 488 nm (Melles Griot) and 633 nm (Thorlabs) laser illumination and detection in narrow wavelength bands centered on 560 nm and 670 nm (Fig. 2.5). The two laser beams used in the setup were spatially aligned using beam steering mounts (Newport) and combined using a dichroic mirror (z633RDC, Chroma Technology). The joint laser beam was coupled with an optical fiber to isolate the laser optics from rest of the setup. The beam emerging from the optical fiber is collimated and expanded before hitting a cylindrical lens (f = 200 mm), which was used to shape it in the form of a sheet and focus it into the back focal plane of a microscope objective (100X, oil-immersion, 1.3 NA UPlanFl, Olympus). The objective tightly focused the beam into the microfluidic device, and collected emitted fluorescence in an epi-fluorescence configuration. The collected fluorescence signal was spectrally separated from the excitation light using a second dichroic mirror (z488/633RPC, Chroma Technology). Upon passing through a confocal aperture, the collected fluorescence was separated into two emission bands by a third dichroic mirror (XF2016, Omega), passed through bandpass filters (560AF55 and 670DF40, Omega Optical), and finally imaged on Silicon Avalanche Photodiodes (SPCM-AQR-13 and SPCM-CD2801, PerkinElmer Optoelectronics) using f = 30 mm doublet lenses (Thorlabs). The slit-like confocal aperture used in this configuration measured 750 µm by 50 µm. The actual size of the CICS illumination volume for the 633 nm laser in this configuration was estimated using the experimental data shown in Fig. 2.6. The 633 nm laser beam was focused on a reflective silicon wafer surface and the reflected laser beam was imaged on a CCD camera (Allied Vision Technologies GmbH), after passing through the confocal aperture. The intensity profile of the image thus obtained was analyzed to estimate the width of the illumination volume (20.13 µm). This was followed by a z-scan to estimate the size of the illumination volume along the axis of the laser beam. During the z-scan, the reflective silicon wafer piece was moved along the axis of the laser beam, with respect to the laser beam focus and the reflected laser beam intensity was collected using the APD corresponding to the 670DF40 bandpass filter (Red APD). The variation of the reflected laser intensity with changing position of the reflective surface respective to the laser beam focus is shown in the right panel in Fig. 2.6. A Lorentzian function was fit to the data and 1/e2 radius of the illumination volume was estimated to be 3.2 µm. Hence, the overall cross section of the illumination volume corresponding to the 633 nm laser was found to be ~64.6 µm2. The CICS setup in this configuration was used for the Lambda DNA experiments. In a second configuration for single fluorophore experiments, a separate cylindrical lens (f = 300 mm, Thorlabs) was used to shape the laser beam into a sheet and to focus it into the back focal plane of the objective (same as above). An aperture of size 600 µm by 150 µm was used in this configuration to obtain a smaller observation volume. The size of the actual illumination volume was estimated as described above and was found to be ~14.3 µm2 in cross section. The single molecule burst data was collected from the APDs by a PC using a PCI 6602 counter DAQ card (National Instruments), controlled using a custom software written in LabView (National Instruments). The microfluidic devices were positioned using a combination of a piezo stage (BPC203, Thorlabs) and a manual XYZ stage (Newport), allowing focusing of the CICS illumination volume at desired positions on the devices.

2.4.3 Sample Preparation

For the Lambda DNA experiments, Lambda DNA (37 pM; Invitrogen) was stained with TOTO®-3 dye (Invitrogen) at a concentration of 1 µM for at least 30 minutes before droplet generation. The indicator dye Alexa 488 was then added to the stained DNA and the sample was diluted to achieve the concentration of DNA required for a particular experiment. Final concentration of indicator dye in the discrete phase was kept to a constant of 100 nM in all the experiments with Lambda DNA. The single fluorophore experiments were conducted using a DNA molecular beacon (MB; 5'-Cy5-CATCCGCTGCCTCCCGTAGGAGTG- BHQ2-3'; Integrated DNA Technologies) with the probe sequence complementary to a conserved region of the 16S rRNA in a wide-range of bacteria.(34) Complementary DNA oligonucleotides were hybridized in 10 mM phosphate buffer (pH 7.8) and 900 mM NaCl at 100X of the MB concentration to saturate available probe. The MB-target mixture was heated to 95 °C and then gradually cooled to room temperature for 1 hour to ensure adequate hybridization, prior to loading into the microdevice for droplet generation. The final concentration of molecular beacons in the discrete phase was 40 pM, both in the 'MB only control' and the 'MB hybridized with target' experiment. The concentration of the indicator dye Alexa 488 in the discrete phase was kept to a constant of 10 nM in each case.

2.4.4 Single Molecule Data Analysis

An image of the droplets generated on each chip was taken prior to obtaining single molecule burst data using a custom stereoscope interface for the single molecule spectroscopy platform (Nikon SMZ1000). The average droplet size was estimated from a minimum of ten droplets for each particular experiment. This data allowed the droplet counts per droplet to be normalized to an average droplet size (44.5 pL for all experiments), so that slight experimental variation in droplet size did not affect overall results.

Data analysis was performed using custom software written in MatLab. Briefly, the leading and falling edge of each droplet were identified as the location in a data trace where the signal from the Alexa488 indicator dye reached three standard deviations above the background fluorescence of the continuous phase. A size filter was used to remove small satellite droplets from the analysis, while single molecule data from the Red APD (TOTO-3/Cy5 channel) was analyzed at each droplet location, as identified by the indicator dye signal (from the Green APD). Integration time for photon binning was set at 0.1 ms for all peak counting experiments.

For each sample, three data traces were analyzed with each trace containing at least 10 droplets visible in the form of fluorescence signal from indicator dye. For each droplet analyzed, the number of fluorescent peaks from the Red channel was normalized with the average droplet volume estimated from the picture, as described earlier. The number of peaks per unit volume, thus obtained, was converted to number of peaks per drop of a standard size (44.5 pl). The peak counting algorithm introduced by Huang et. al. (40) was adopted to minimize thresholding artifacts. Traditionally, in single molecule counting experiments threshold values for fluorescent burst detection are set around three standard deviations from the mean background signal. Setting a lower threshold for detection in discrete volume droplets would result in lower false negatives, but cause a subsequent increase in false positive fluorescent bursts from background noise. However, as shown in Fig. 2.7 the same data trace can be analyzed with different thresholds to obtain a linear trend (in which there is no interference from background noise) that can be interpolated to the zero threshold to estimate the true molecule count per droplet.(40) In this manner, we were able to obtain molecular counts per droplet that closely matched the expected value, as determined by the maximum possible detection efficiencies (sections 2.4.1 and 2.4.2) and concentrations (section 2.4.3). Acquisition of single molecule data from the droplets with the laser probe focused through the thin layer of the continuous, oil phase (see Fig 2.8) was observed to cause a slight decrease in signal-to-noise ratio compared to that obtained for data acquisition from a fluid filled microfluidic channel (data not shown). However, this was not shown to have any effect on the estimation of intra-droplet molecular concentrations (figure 2.3B and C).

Fig. 2.1: Microfluidic device design A. A droplet moving through a microfluidic channel is shown. Inset shows the size of the droplet relative to the illumination volume of a standard Confocal Fluorescence Spectroscopy (CFS) setup. **B.** In contrast, elongation of a droplet squeezing through a microfluidic constriction is shown. The inset shows the sheet-like illumination volume of a Cylindrical Illumination Confocal Spectroscopy setup relative to the elongated droplet in the microfluidic constriction. **C.** The multilayered microfluidic device designed for the experiments in this paper is shown. A flow focusing geometry was used for droplet generation. The left panel shows droplets being generated using a food dye as the discrete phase. The rightmost panels show the retractable constriction region in either the open (left) or actuated (right) state, as described in text. (scale bar: 50 mm).

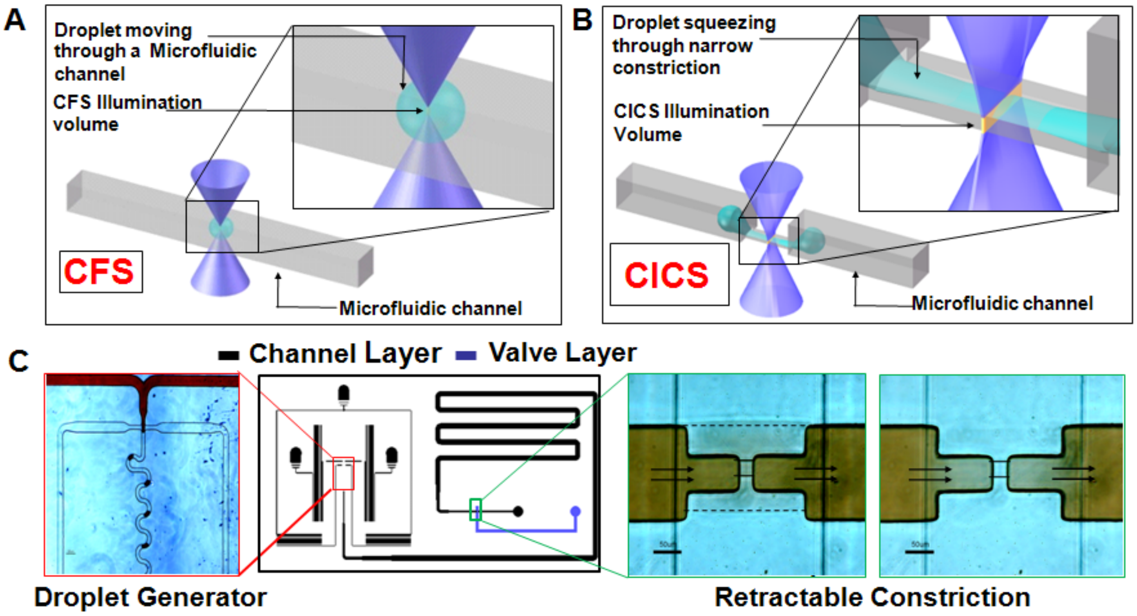
A
Droplet moving through a Microfluidic channel
CFS Illumination volume
CFS
Microfluidic channel
B
Droplet squeezing through narrow constriction
CICS Illumination Volume
CICS
Microfluidic channel
C
Channel Layer
Valve Layer
Droplet Generator
Retractable Constriction

Fig. 2.2: Testing the microfluidic device A. Retractable constriction in action: Two very different sized droplets can be seen stretching through the constriction without breakup. **B.** Sample single molecule trace data for control sample (TOTO®-3 dye only). The discrete phase consisted of 100 nM TOTO®-3 dye along with 100 nM Alexa 488 dye (Indicator dye). The red trace shows fluorescence signal from the indicator dye, while the black trace shows the fluorescence signal from TOTO®-3 dye. **C.** Similar single molecule trace data with the discrete phase consisting of TOTO®-3 labeled, 37 pM Lambda DNA and 100 nM Alexa 488 dye.

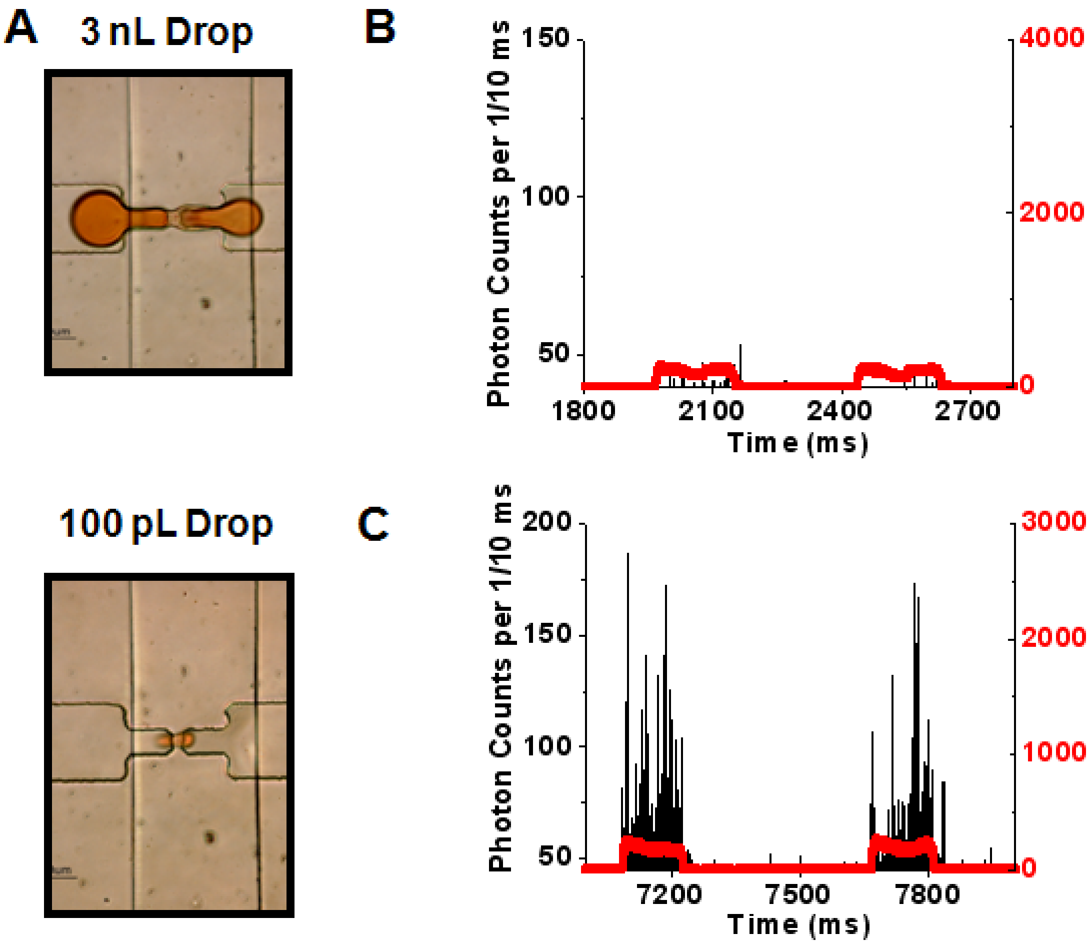
A
3 nL Drop
B
Photon Counts per 1/10 ms
150
100
50
4000
2000
0
1800
2100
2400
2700
Time (ms)
100 pL Drop
C
Photon Counts per 1/10 ms
200
150
100
50
3000
2000
1000
0
7200
7500
7800
Time (ms)

Fig. 2.3: Single molecule quantification on the microfluidic device A. Data showing the effect of droplet transit time on the mass detection efficiency within droplets. The data was obtained using a microfluidic chip (Fig 2.1C) with a 200 μm^2 constriction. The discrete phase consisted of 1 mM TOTO-3, 37 pM Lambda DNA and 100 nM Alexa 488 dye. The number of single molecule fluorescent bursts increase with increasing droplet transit time through the microfluidic constriction, finally reaching a plateau (average value of 312 ± 31.9; red line) at transit times >280 ms. **B.** SMD-droplet platform response to changing molecular concentrations. Droplets were generated using discrete phase consisting of a range of DNA concentrations and passed through a 200 μm^2 constriction for single molecule detection. **C.** Manipulation of mass detection efficiency within droplets by simply changing the constriction size is demonstrated. As the constriction size decreases, larger sections of each droplet pass through the illumination volume and hence, mass detection efficiency increases. All the experiments were conducted on a CICS setup with detection volume cross section size 64.6 μm^2 and DNA concentrations of 0.37 pM (details of data normalization in section 2.4.4). **D.** The tunable nature of the droplet-CICS platform to attain single fluorophore sensitivity is illustrated using a Cy5 molecular beacon complementary to a sequence on 16S rRNA from E. coli. The top row shows three representative sample droplets from a ‘molecular beacon (MB) only’ control sample. The black trace shows single molecule data from the Cy5 dye on the MBs. The bottom row shows sample droplets made from the same concentration molecular beacon hybridized with a synthetic target DNA. The average number of single molecule bursts per droplet in the control sample was 0.282 ± 0.11, compared to 9.075 ± 0.76 in the target sample. This experiment was conducted on a chip with a constriction cross sectional area of 200 μm^2 and CICS illumination volume of 14.3 μm^2. Each data point represents the interpolated y-intercept at zero threshold values from three sets of experiments with standard deviation; see details of single molecule analysis and thresholding in section 2.4.4

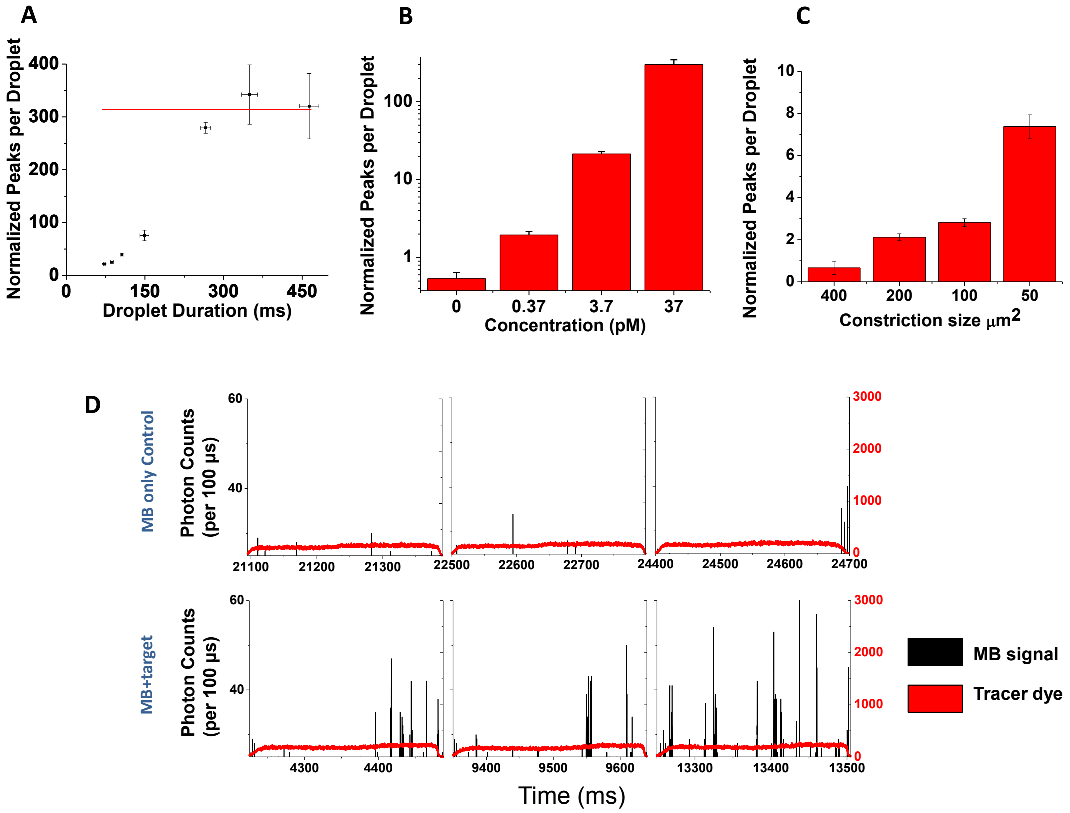
A
Normalized Peaks per Droplet
400
300
200
100
0
0
150
300
450
Droplet Duration (ms)
B
Normalized Peaks per Droplet
100
10
1
0
0.37
3.7
37
Concentration (pM)
C
Normalized Peaks per Droplet
10
8
6
4
2
0
400
200
100
50
Constriction size μm2
D
MB only Control
Photon Counts (per 100 μs)
60
40
3000
2000
1000
0
21100
21200
21300
22500
22600
22700
24400
24500
24600
24700
MB+target
Photon Counts (per 100 μs)
60
40
3000
2000
1000
0
4300
4400
9400
9500
9600
13300
13400
13500
Time (ms)
MB signal
Tracer dye

Fig. 2.4: A cross-section of the constriction within the retractable valve. Upon pressurization of the top control layer, the actuated valve caused the main portion of the channel to close while the smaller constriction channel was left as the only open path for droplet travel.

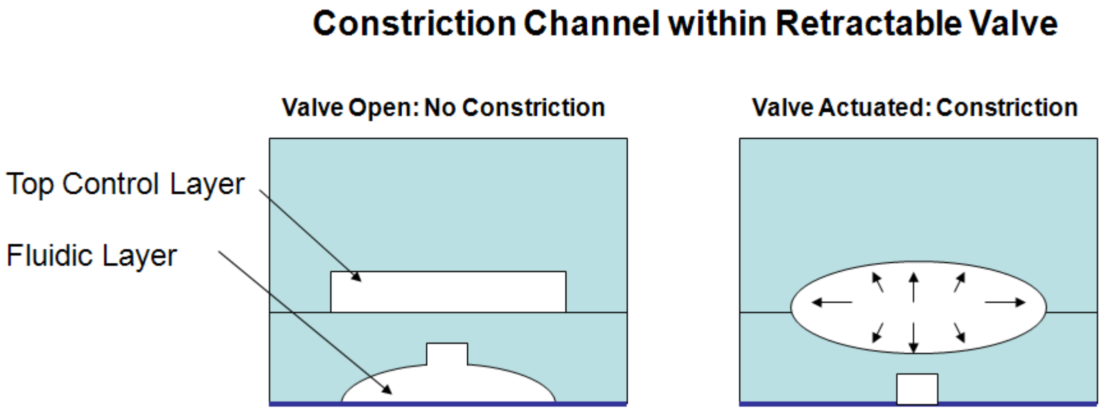
Constriction Channel within Retractable Valve
Valve Open: No Constriction
Valve Actuated: Constriction
Top Control Layer
Fluidic Layer

Fig. 2.5: Schematic diagram of the optical components in our two color Cylindrical Illumination Confocal Spectroscopy (CICS) system.

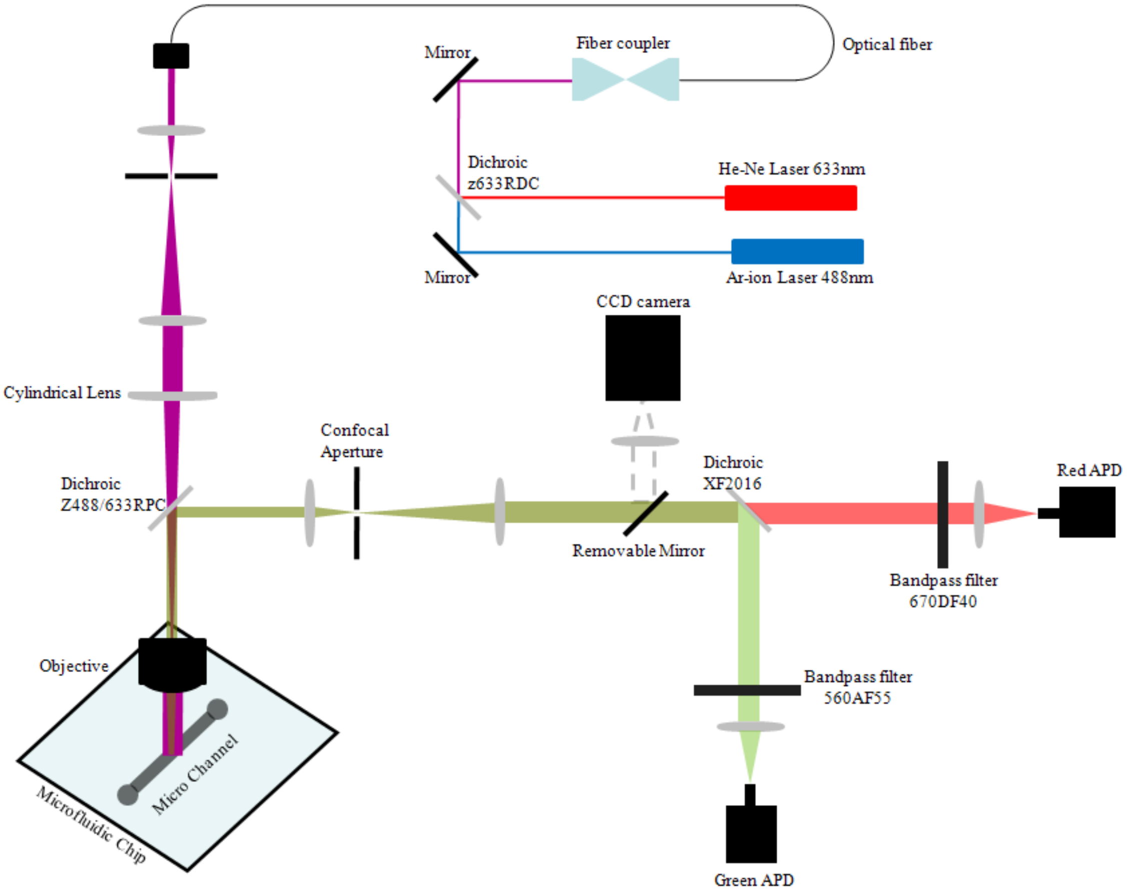
Optical fiber
Mirror
Fiber coupler
Dichroic
z633RDC
He-Ne Laser 633nm
Mirror
Ar-ion Laser 488nm
CCD camera
Cylindrical Lens
Confocal
Aperture
Dichroic
Z488/633RPC
Dichroic
XF2016
Red APD
Removable Mirror
Bandpass filter
670DF40
Objective
Bandpass filter
560AF55
Micro Channel
Microfluidic Chip
Green APD

Fig 2.6: Estimation of the size of the CICS illumination volume. Left panel: The reflected image of the CICS illumination volume and the intensity profile of the image are shown. This image was acquired using the 633 nm laser on the CICS setup focused on a reflective silicon wafer surface and imaged with a CCD camera, after passing through the confocal aperture. The width of the illumination volume was measured to be 20.13 µm. Right panel: The reflected intensity data from a z-scan conducted to estimate the size of the CICS illumination volume along the axis of the laser beam is plotted. The X axis shows the location of the laser beam focus relative to the surface of the silicon wafer, while the Y axis shows the normalized reflected intensity of the laser beam collected using an APD.

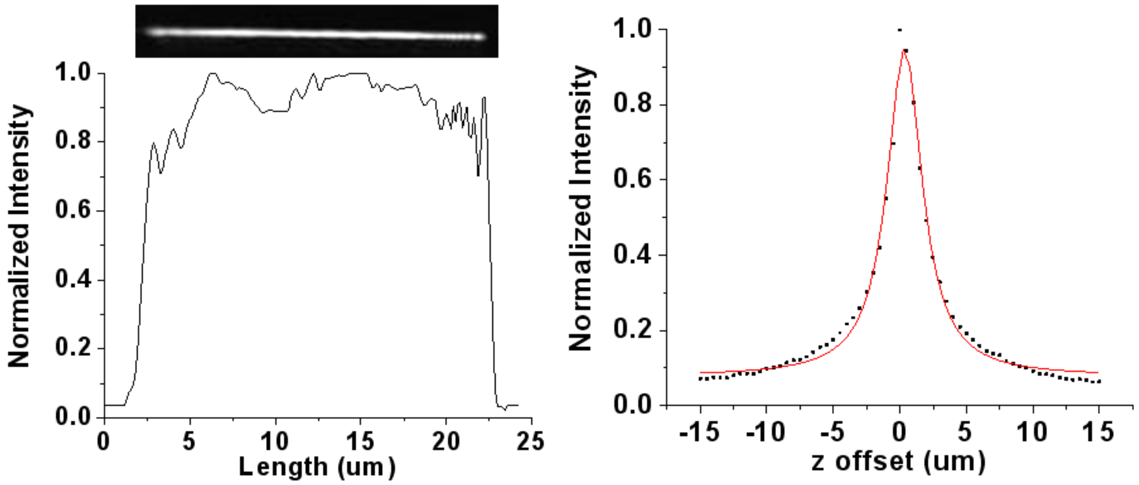
Normalized Intensity
1.0
0.8
0.6
0.4
0.2
0.0
0
5
10
15
20
25
Length (um)
Normalized Intensity
1.0
0.8
0.6
0.4
0.2
0.0
-15
-10
-5
0
5
10
15
z offset (um)

Fig 2.7: Single molecule data analysis. A simple linear interpolation using the fluorescence burst counts with the threshold between 90 and 120 gives a molecule count of 7.38 ± 0.56, which is close to the expected number of 9.92 molecules per droplet (0.37 pM Toto-labeled lambda DNA within 44.5 pL droplets; 50 μm^2 constriction within the 64.6 μm^2 illumination volume for a maximum possible detection efficiency of 100%). This number corresponds to the 50 μm^2 data point in figure 2.3C.

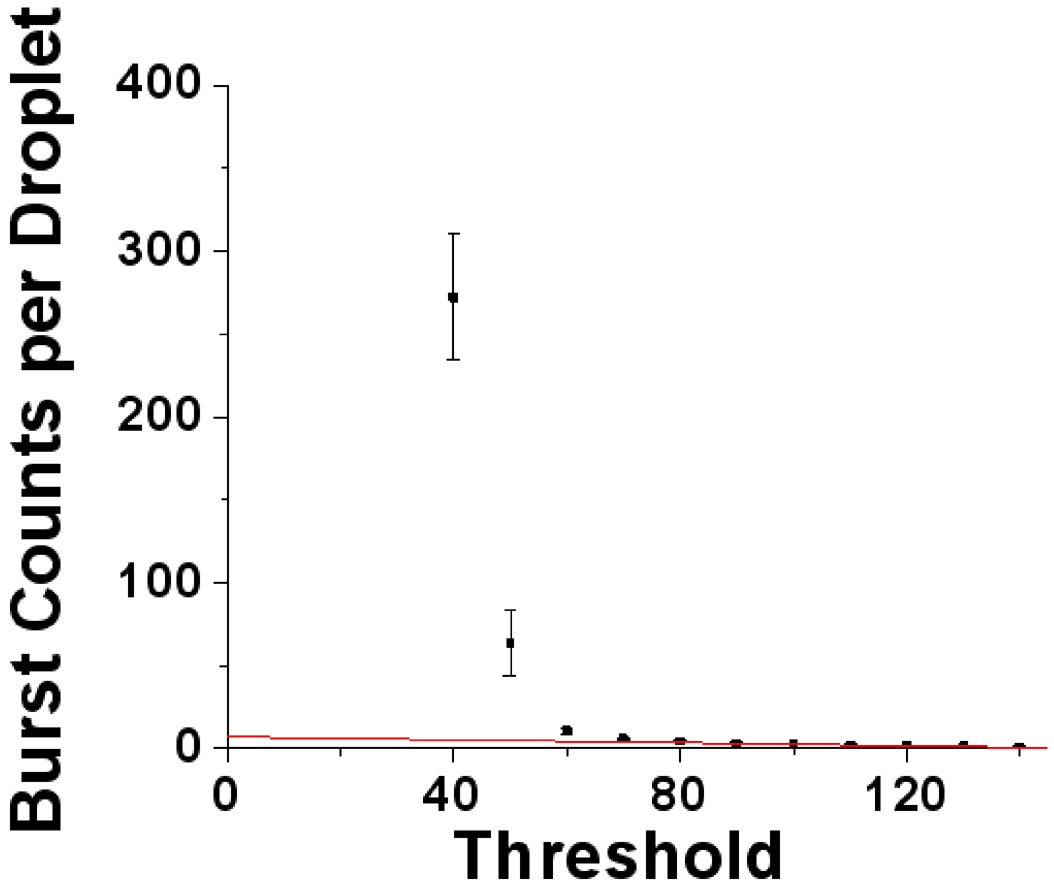
Burst Counts per Droplet
400
300
200
100
0
0
40
80
120
Threshold

Fig 2.8: A high magnification image of a droplet squeezing through a 20 µm by 10 µm constriction. This lateral view clearly shows the continued presence of the continuous phase surrounding the droplet as it is pushed through the constriction.

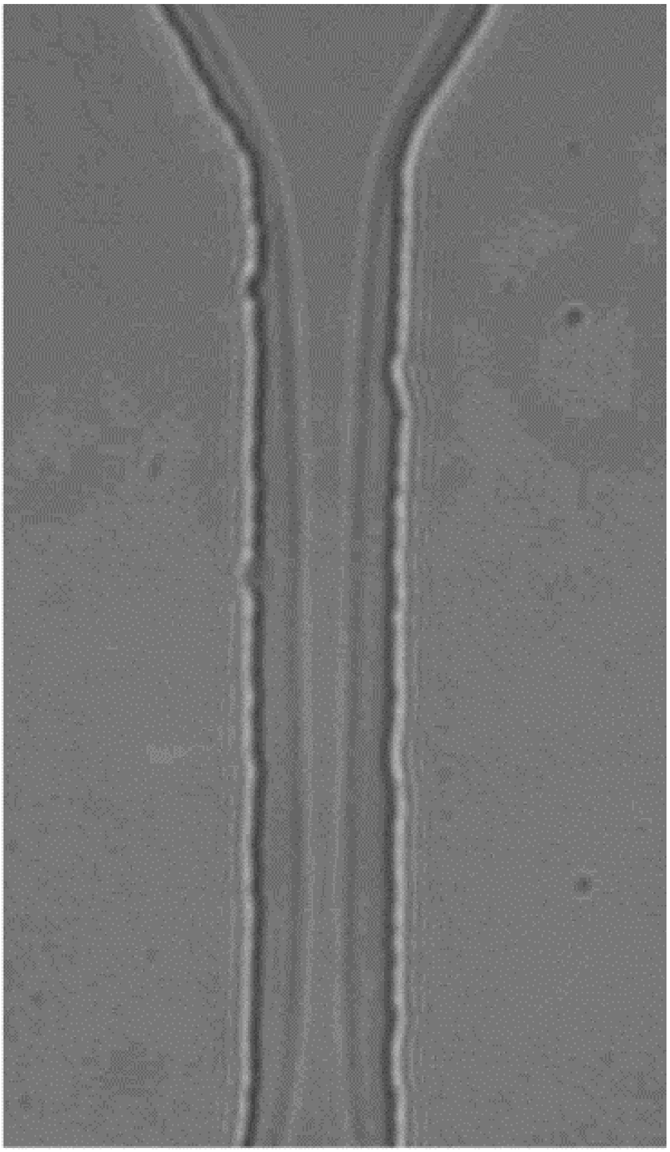

Chapter 3: Amplification-free single cell detection in droplets

Rane, Tushar D., et al. "Droplet microfluidics for amplification-free genetic detection of single cells." Lab on a Chip 12.18 (2012): 3341-3347. Reproduced by permission of The Royal Society of Chemistry

3.1 Background

Droplet-based microfluidic systems have introduced otherwise 'analog' microfluidic systems (i.e. continuous flow microfluidics) to the benefits of the 'digital' operation format. Analogous to the benefits of digital technology in electronics, droplet microfluidics allows 'digital operations' like mixing precise reagent quantities, splitting a reagent into precise small volumes etc. possible in microfluidic systems. Such digital operations can be very beneficial in biological analyses. For instance, amplification of individual DNA molecules by separating them from each other using DNA sample splitting into small volumes, i.e. digital PCR, can be used for quantification of DNA and sensitive detection of rare mutant DNA present in the background of a large number of wild-type DNA(4, 7, 41, 42).

At a cellular level, droplets can also be used for confinement and manipulation of single cells into small droplets, making them ideal for conducting high throughput single cell studies. However, this application of droplets is in its infancy with only a select few reports having started harnessing this potential of droplet microfluidics. For instance, Huebner et al.

demonstrated quantification of protein expression in single cells encapsulated within droplets, from a naturally fluorescent protein(20). Joensson et al. demonstrated detection of cell-surface biomarkers using enzymatic amplification in droplets(43). Boedicker et al. demonstrated analysis of single bacterial cells for their susceptibility to antibiotics in droplets, using a fluorescent cell viability indicator assay(25). Brouzes et al. developed optically-coded droplet assay for high-throughput screening of a drug library for its cytotoxic effect against U937 cells(5). Zeng et al. proposed a single cell PCR assay for genetic detection using a microfluidic droplet generator array(6). This platform, although capable of high throughput screening, requires off-chip PCR reactions and a complex multicolor flow cytometer for amplicon detection.

3.2 Solution

In this article we report a droplet microfluidic device that facilitates amplification-free genetic detection of single cells. This device offers a simple and yet fully integrated approach to include all the assay steps, including cell isolation, lysis, probe-target binding and fluorescent detection, performed within microfluidic droplets. We exploit the relatively unexplored probe hybridization based assays for detection of an intracellular genetic marker of interest. Single cell sensitivity is achieved in our platform through a two pronged approach. Initially, stochastic confinement of single cells within small droplets (pL volume) is used to maintain a low abundance intracellular target of interest from single cells at high concentrations. Cell encapsulation in droplets is inherently a probabilistic process, presenting a unique challenge for ensuring encapsulation of a single cell in each droplet and hence, quantification of target cells present in a sample. However, cell encapsulation within droplets has been demonstrated to be a Poisson process in the droplet microfluidic literature (44-47). As a result, despite multiple cell encapsulation in a small fraction of droplets, the underlying Poisson distribution and hence the target cell count in the sample can be estimated. Secondly, the microfluidic platform is coupled with highly sensitive confocal fluorescence spectroscopy for sensitive detection of target biomolecules from individual droplets(33, 48). Simple temperature incubation requirements for cellular lysis and hybridization allow us to streamline all the assay steps in a single droplet. Our platform utilizes 16S ribosomal RNA (rRNA) as the genetic biomarker for pathogen detection. The 16S rRNA gene is often used for phylogenetic studies as it is highly conserved between different species of bacteria and archaea(49-51). In addition, 16S rRNA is typically present at 10^4-10^5 copies per cell(52). Thus, using 16S rRNA as a surrogate biomarker offers the dual benefits of high specificity as well as a relatively large number per cell as compared to DNA. Confinement of these molecules within the small volume of a droplet, coupled with sensitive fluorescence detection readout like confocal fluorescence spectroscopy (39, 48, 53) makes amplification-free detection at single cell levels possible. A simple target concentration calculation can illustrate the concentrating power of microfluidic droplets. Typical volumes handled by pipettors are in microliters. Assuming a single bacterial cell containing 20,000 16S rRNA molecules is lysed in a 1μL volume, the target 16S rRNA molecule is present at the fM concentration, a concentration level that usually necessitates target amplification prior to detection. However, if the same cell is lysed while confined within a pL-sized droplet, the resulting nM target (Table 3.1) is readily detectable, eliminating the need for target amplification. The picoliter to nanoliter sized droplets indicated in Table 3.1 can be easily generated using flow focusing droplet generators(1).

In situ detection of 16S rRNA encapsulated in a droplet requires fluorescent molecular probes capable of homogeneous detection in a solution phase without the need to remove (wash away) free probes. Molecular beacons are widely used fluorescence resonance energy transfer (FRET) probes that fluoresce upon hybridization with complimentary targets(54). Since unhybridized beacons are minimally fluorescent, they form excellent probes for homogeneous detection of nucleic acid targets(55, 56). However, standard oligonucleotide molecular beacons suffer from the complication of negative charge based repulsion as well as the requirement of high salt concentrations when used to detect a large target molecule with extensive secondary structure like 16S rRNA. Instead, we use a peptide nucleic acid (PNA) beacon to carry out intra-droplet 16S rRNA detection. PNA is a synthetic DNA analogue synthesized by attaching nucleic acid bases to a peptide backbone. The absence of negative charge on the PNA backbone prevents the problems of charge-based repulsion from the target nucleic acid as well as removes the requirement for higher salt concentration for effective target binding(57). Lower salt concentrations promote denaturation of the 16S rRNA targets, providing easier access for the probe molecules to bind their complementary region on the rRNA(57).

The operational procedure of the microfluidic single cell detection platform is illustrated in Fig. 3.1. Initially a pathogenic cell sample is mixed with PNA beacon. The mixture is diluted and compartmentalized into uniform picoliter sized droplets. These droplets then traverse through an incubation zone where exposure to a high temperature results in pathogenic cell lysis as well as PNA beacon hybridization with target 16S rRNA molecules. Thermal lysis of cells is a commonly used cell lysis technique, which has been shown to be efficient at cell lysis and post-lysis analysis of cellular contents using PCR for a variety of cell types including bacterial(58, 59) and human cells(60) as well as virii(61). The beacon becomes fluorescent once hybridized with a complementary sequence on a conservative site of the 16S rRNA target, resulting in a substantial increase in fluorescence of the droplet containing a pathogenic cell. Consequently, the cell of interest is identified and quantitated by detecting the bright fluorescent droplets using confocal fluorescence spectroscopy.

3.3 Experimental section

3.3.1 PNA Beacon

The PNA beacon sequence used for our experiments is N-BHQ3-E-GCT-GCC-TCC-CGT-AGG-A-KK-Cy5-C. The probe sequence used in our experiments is complementary to the bacterial domain S-D-Bact-0338-a-A-18(57). In its natural state the beacon folds on itself in solution, so that the quencher BHQ3 and the fluorophore Cy5 are in close vicinity with each other, leading to effective quenching of Cy5 fluorescence (Fig. 3.1, inset). However, when bound to a complementary target, the fluorophore moves away from quencher and starts fluorescing.

3.3.2 Control Targets and Pathogen Cells

The synthetic target used in the characterization experiments (referred to as 'rRNA mimic' hereafter) is a 200 bp oligonucleotide target mimicking a portion of the E. coli 16S rRNA sequence (5'-CTAGT AGGTG GGGTA ACGGC TCACC TAGGC GACGA TCCCT AGCTG GTCTG AGAGG ATGAC CAGCC ACACT GGAAC TGAGA CACGG TCCAG ACTCC TACGG GAGGC AGCAG TGGGG AATAT TGCAC AATGG GCGCA AGCCT GATGC AGCCA TGCCG CGTGT ATGAA GAAGG CCTTC GGGTT GTAAA GTACT TTCAG CGGGG-3')(62). The oligonucleotide was synthesized by Integrated DNA Technologies (Coralville, Iowa). Two types of control samples were prepared including 1) a 'positive control' containing synthetic targets hybridized with PNA beacon (100nM) in the presence of background human genomic DNA

(1μg/100μL) and 2) a ‘ negative control’ containing PNA beacon (100nM) in the presence of background human genomic DNA (1ug/100ul). The synthetic target concentration was different for different experiments as indicated in the results section. These samples underwent incubation at 65^{o}C for 1 hour followed by gradual cooling to room temperature in a thermocycler to promote hybridization of the PNA beacon with the synthetic target. These samples were then stored at -20^{o}C until the experiments were conducted on the microfluidic chips. Prior to the experiments on chip, 10nM Alexa Fluor® 488 dye was added to these samples as an indicator to visualize the droplet boundary and detect the passage of a droplet through the detection region(48). Alexa Fluor® 488 exhibits minimal spectral crosstalk with the Cy5 dye labeled to the PNA beacon and thus does not interfere with rRNA detection.

For the experiments with an actual pathogen sample, we used E. coli as a model pathogen. Prior to the experiments, E. coli cells (ER2566 strain, New England Biolabs, Inc) were grown overnight at 37^{o}C on a shaker (MaxQ 2000, Thermo Fisher Scientific Inc.) in an incubator (Napco 8000WJ, Thermo Fisher Scientific Inc.). We used M9 minimal media (TEKnova, Inc.) for culturing the bacterial cells. E. coli cells from this overnight culture were spun down and resuspended in PBS at concentrations required for an experiment. For all of our experiments, we maintained the PNA beacon concentration constant at 100 nM. The hybridization buffer used for all the experiments including those with the synthetic target was maintained at a constant composition of 40% formamide, 100 mM NaCl and 25 mM Tris-HCl. 10 nM Alexa Fluor® 488 was added as an indicator dye to these cell samples before introducing them on the microfluidic chip .

3.3.3 Design and Fabrication of Microfluidic Device

Fig. 3.2 shows the layout of the microfluidic chip used for conducting the single cell pathogen detection assay. We used a flow focusing droplet generator to produce uniform picoliter volume droplets. As seen from Table 3.1, smaller droplet sizes lead to higher target concentrations from single cells. Hence, the signal to background ratio for this detection platform can be tuned by varying the droplet size. The sample droplets produced at the droplet generator region are channeled to a droplet 'incubation zone' on the chip. The chip is designed with two different heights of photoresist. All the areas on the chip other than the 'incubation zone' are made with 50 μm photoresist height. The incubation zone is fabricated with 350 μm tall layer of photoresist to allow droplets to spend sufficient time on chip for completion of cell lysis and probe hybridization with target 16S rRNA molecule.

The chip was fabricated with polydimethylsiloxane (PDMS) using the standard soft lithography technique. Briefly, a silicon wafer was spin coated with a 50 μm thick layer of SU8-3025 Photoresist (PR) (MicroChem Corp.) and patterned through photolithography. This thin PR layer was hard baked onto the wafer. Another thick SU8-3050 layer was then spin coated on the same wafer and patterned using the second mask to fabricate the incubation zone of the chips. The second layer was also hard baked on the wafer and the patterned wafer was then used as a mold to fabricate PDMS chips.

To fabricate PDMS structures from the silicon wafer molds, Sylgard™ 184(Dow Corning) base and curing agent were mixed in a 10:1 ratio by weight. This mixture was degassed in vacuum and then poured on top on the silicon wafer molds. The mixture on the wafers was cured at 80^{o}C for 30 mins. The cured PDMS was then peeled off the silicon wafer and individual devices were cut out. Access holes for fluid entry were punched into the chips and the chips were then bonded to No. 1 coverglass (Fisherfinest) using oxygen plasma bonding.

3.3.4 Optical Detection Setup

Confocal fluorescence spectroscopy (CFS) offers the sensitivity as well as high speed required for rapid screening of droplets. We used a custom built CFS setup for our experiments. The details of a similar setup construction were discussed previously(35, 48). The setup is capable of dual laser excitation (488 nm and 633 nm) as well as simultaneous dual color detection, including the 'green' (centered at 520 nm) and 'red' (centered at 670 nm) wavelength bands. A custom metal plate was designed to act as an interface between the microfluidic chip and the CFS setup. This metal plate was mounted on a Piezo stage (Thorlabs) to allow precise positioning of the chip with respect to the objective on the CFS setup. The metal plate was also used to position a peltier heater below the 'incubation zone' on the microfluidic chip. The peltier heater was maintained at a fixed incubation temperature throughout an experiment on chip.

3.3.5 Operation of Microfluidic Device

The chips were treated with Aquapel (PPG Industries) to render the channels hydrophobic prior to each experiment(22). Following this treatment, oil phase was introduced onto the chip through the oil inlet and allowed to flow on chip for a few minutes to wet the channels with oil phase. The oil phase used for our experiments consisted of FC-40 oil (3M) and 2% EA surfactant by weight (Raindance Technologies, Inc).

An E. coli and PNA beacon mixture was then introduced onto the chip through the sample inlet for each experiment. Before initiating droplet generation on chip, the chip was placed onto the custom metal plate attached to the CFS setup. The chip was held in place using vacuum lines on the metal plate. The chip was placed such that the peltier heater on the metal plate was located below the incubation zone on the chip. The peltier heater was maintained at a constant temperature of 65^{o}C throughout the course of an experiment. The excitation laser beam from the CFS setup was focused on the fluorescence detection region on the chip. After the chip was ready for fluorescence data collection, droplet generation was initiated on chip by pressurizing both oil and sample inlets. The droplets took approximately one hour to traverse the incubation region on chip before reaching the fluorescence detection region. The droplets were imaged after passing through the incubation region for each experiment to estimate the droplet size and account for any variations in droplet size between experiments. Fluorescence data was then continuously collected from the droplets passing the fluorescence detection region on chip while droplets were still being generated upstream on the chip.

3.4 Results and Discussion

Prior to our experiments with live cell samples, we conducted some tests with the rRNA mimic. The objective of these tests was two-fold: First to establish the sensitivity of the assay and second to simulate different cell concentrations in a cell sample to test quantification ability of our platform. To conduct this assay, PNA beacon was mixed with different concentrations of the rRNA mimic in the background of human genomic DNA as described in the experimental section. These experiments were conducted on a separate microfluidic device discussed in Section 3.6.1. Briefly, this microfluidic device is capable of using valves to generate arbitrary sequences of droplets generated using two independent samples (positive and negative control samples described in the 'Experimental' section above).

Fig. 3.3 illustrates sample fluorescence spectroscopy traces from two of these experiments. Fig. 3.3a indicates fluorescence data collected from an artificially generated sequence of one positive droplet per 2 droplets. The positive droplet is generated using a sample consisting of PNA beacon hybridized with 6.25 nM rRNA mimic in the background of human genomic

DNA while the negative droplet is generated using a sample containing PNA beacon with human genomic DNA only. This experiment simulates a situation in which the cell concentration in a cell sample is such that approximately 50% of the droplets are empty while the other 50% have one or more cells encapsulated in them. Fig. 3.3b shows similar fluorescence data for rRNA mimic concentration of 1.56 nM. In this case, the sequence used was one positive droplet per 5 droplets. This experiment simulates a situation in which the cell concentration in a cell sample is such that approximately 80% of the droplets are empty while the other 20% have one or more cells encapsulated in them. The histograms in Fig. 3c and 3d correspond to the fluorescence data traces in Fig 3a and Fig 3b respectively. These histograms show the distribution of the burst size (sum of photons detected per droplet) for a total of 300 droplets for each corresponding condition in Fig. 3.3a and b. The histogram shows two distinct peaks indicating two populations of droplets i.e. positive droplets with rRNA mimic and negative droplets without rRNA mimic.

Sequences of droplets as shown in Fig. 3 with different ratio of the number of positive droplets to the negative droplets were run for extended periods of time and the fluorescence data collected was analyzed to differentiate between positive and negative droplets and test the reliability of the platform in differentiating between these two populations of droplets for long periods of time. This experiment was repeated for two different concentrations of rRNA mimic (6.25 nM and 1.56 nM) hybridized with the PNA beacon. The fluorescence data was analyzed to generate burst size for each droplet. A burst size threshold was determined to differentiate between 'positive' and 'negative' droplets as described in section 3.6.2 in the Supplementary section. Three different batches of 100 droplets each were analyzed to generate an 'observed positive droplet count per 100 droplets' for each condition (i.e. positive to negative droplet count ratio) for each rRNA mimic concentration.

The results from this data analysis are plotted in Fig. 3.4. It shows that the expected and observed positive droplet count for each condition (i.e. positive to negative droplet count ratio) are in excellent agreement with each other for both rRNA mimic concentrations tested. These plots thus show that the platform can reliably differentiate different positive to negative droplet count ratios from each other at close to nanomolar target concentration in positive droplets. As seen from Table 3.1, these target concentrations in positive droplets correspond to the expected 16S rRNA concentrations obtained in picoliter sized droplets following a single pathogen cell lysis within the droplet. Thus, the results indicate the capability of our detection platform to quantify target cell count in a sample provided the cells are encapsulated in droplets with volumes in the picoliter regime.

We used E. coli as a model pathogen for single cell detection. Initially we tested the PNA beacon with E. coli cells in bulk under different temperature conditions to find the best conditions for optimal cell lysis and hybridization efficiency (see section 3.6.3). Briefly, we tested E. coli cell incubation with PNA beacon at three temperature conditions viz. Room Temperature (RT), 65^{o}C and 95^{o}C. Fluorescence stemming from PNA beacons hybridized with complementary target rRNAs was obtained from each sample using the CFS setup. Our results indicate that incubation at RT barely led to cell lysis and probe hybridization. However, similar fluorescence signal for both 65^{o}C and 95^{o}C temperatures indicated similar assay efficiency at these temperatures (Fig. 3.8). We used 65^{o}C incubation for on chip experiments to avoid any problems associated with droplet evaporation and instability at high temperature incubation. We then conducted tests with E. coli cell samples on our microfluidic chip (Fig. 3.2). As a first test to estimate the background fluorescence from the PNA beacon encapsulated within droplets, we generated droplets using a sample containing only PNA beacons without E. coli cells. Fig. 3.5a shows the fluorescence signal collected from a few representative droplets generated using this sample. As discussed in the experimental section, this sample contained an indicator dye (Alexa Fluor® 488) for easy visualization of droplets in the fluorescence data. The indicator dye is present in all the droplets regardless of presence or absence of PNA beacon or target cells. Hence, every droplet can be seen as a peak in the indicator dye fluorescence data (Green trace). The red trace in Fig. 3.5a shows fluorescence signal collected from the PNA beacon (i.e. Cy5 dye on the beacon). In Fig 3.5a, we observe a very small amount of PNA background fluorescence in the red trace that is associated with the intrinsic background of free PNA beacons resulting from stochastic opening of the beacons due to thermal fluctuations. Fig. 3.5b indicates similar fluorescence data from a high concentration E. coli cell sample. A standard curve indicating the CFU/ml (CFU: Colony Forming Unit) concentration vs OD (Optical Density at 600nm) measurement was generated to estimate the CFU/ml concentration of an E. coli sample used for an experiment. In this case, the droplet size and the starting E. coli concentration lead to a concentration estimate of 15.7 CFU/droplet. Although the actual distribution of cells within the droplets is expected to be a Poisson distribution, on an average, we expect target 16S rRNA from at least one cell to be present in virtually all the droplets in this case. The fluorescence data collected from the droplets indeed indicates a strong rise in fluorescence from each droplet in the red trace i.e. PNA beacon trace, confirming our expectation.

Finally Fig. 3.6 illustrates the fluorescence data collected from the droplets generated using a sample containing low concentration of E. coli cells. The droplet size and initial E. coli concentration lead to a concentration estimate of 1 CFU per 20 droplets. In this case, we expect a large fraction of droplets to be empty with no target E. coli cells while a few droplets are expected to contain target E. coli cells. Thus, we expect digital fluorescence signal from these droplets i.e. a large number of droplets with weak background fluorescence from the PNA beacon with a few droplets showing strong fluorescence signal in the red trace. The trace in Fig. 3.6 indeed matches our expectation indicating the feasibility of using our approach to detect pathogens from a sample with intact pathogenic cells at single cell level.

3.5 Conclusion

In conclusion, we proposed a novel scheme for sequence-specific detection of single cells using genetic biomarkers. We demonstrated the functioning of our platform with a 16S rRNA mimic target as well as intact E. coli cells as a model pathogen. The success of our experiments with a pathogen sample with intact pathogenic cells indicates the promise in utilization of our platform with clinical samples with appropriate testing and optimization of assay conditions. Although the functioning of the platform was demonstrated for pathogen detection, the platform is versatile enough to be applied towards other single cell studies.

3.6 Supplementary section

3.6.1 Device design and fabrication for experiments with 16s rRNA mimic

We designed a dual layer PDMS device for our experiments with the rRNA mimic. The schematic illustrating the operation of this device is shown in Fig. 3.7. The device consisted of one oil inlet and two sample inlets. One of the sample inlets took the 'positive control' (PNA beacon + rRNA mimic + Human

Genomic DNA) as input while the other sample inlet took the 'negative control' (PNA beacon + Human Genomic DNA) as input, according to the description in the article text. Both of these sample inlets are separated from the oil flow channel through two valves. These valves are fabricated using standard multilayer soft lithography as has been described previously(48). The actuation of these valves can controlled using custom software written in Matlab™. Alternating actuation of these valves was used to generate droplet trains consisting of different proportions of droplets generated from the positive and negative control samples. The droplet train thus generated simulates the train of droplets we expect to be generated while working with a cell sample i.e. a series of droplets with (positive) and without cells (negative) encapsulated in them. These droplet trains are then routed to a downstream detection region on chip, where fluorescence detection is conducted through Confocal Fluorescence Spectroscopy.

3.6.2 Fluorescence data analysis for experiments with 16s rRNA mimic

Both the positive and negative control samples being input to the device described above in 3.6.1 had an indicator dye (Alexa 488 10nM) added to them for identification of the droplet region in the oil background from the fluorescence data collected from the droplet train. Custom software written in Matlab™ was used for processing the raw fluorescence data. As described in the article, our fluorescence setup is capable of dual excitation with a 488nm and a 633nm wavelength laser. The fluorescence collected from the sample excited by these lasers is then split into two wavelength bands centered at 520nm (Green) and 670nm (Red). Fluorescence intensity from these two wavelength bands is sensed by two individual avalanche photodiodes and converted into photon counts per unit time using custom software written in LabVIEW. The fluorescence signal in the green band is due to the fluorescence of the indicator dye while the fluorescence in the red band is from the Cy5 dye on the PNA beacon. Initially the droplet region for each individual droplet is identified from the fluorescence signal trace corresponding to the green band by setting a threshold on fluorescence intensity. Varying this threshold doesn't have much effect on identification of the droplet region due to uniform fluorescence intensity of the indicator dye encapsulated within the droplets. The photons in the red band from the region corresponding to each individual droplet were then summed to obtain a burst size for each droplet. This burst size was normalized to a standard droplet size to overcome any bias due to small size differences in different droplets. Since the droplet sequence in the droplet train was known, first 10 control sample droplets were used to set a threshold for differentiating between 'positive' and 'negative' droplets. Specifically the threshold was set at a stringent [burst size mean + 20* (burst size standard deviation)] to differentiate between positive and negative droplets. This stringent threshold prevented any false positives occurring due to small fluctuations in the fluorescence intensity of 'negative' droplets over time. For each different droplet train, three batches of 100 droplets each were analyzed to obtain a positive droplet count per 100 droplets. The mean and standard deviation obtained from this analysis was then plotted as shown in Fig. 3.4 in the article.

3.6.3 Optimizing the incubation temperature for the PNA beacon assay in bulk

Prior to our experiments with E. coli cell samples on chip, we conducted some experiments in bulk to optimize the temperature incubation conditions for the assay with live cell samples. Briefly we mixed different quantities of E.coli cells with PNA beacon and incubated them at different temperatures. Fluorescence detection was then conducted on these samples using Confocal Fluorescence Spectroscopy (CFS). PNA beacon hybridization with complementary target (16S rRNA) released after lysis of the E. coli cells leads to increase in fluorescence collected from a sample. We tested three different temperatures viz. Room Temperature (RT), 65^oC and 95^oC. The results shown in Fig. 3.8 indicate that the cell lysis and PNA hybridization was inefficient at RT incubation. Incubation at 65^oC and 95^oC on the other hand resulted in comparable cell lysis and PNA hybridization efficiency. We used 65^oC incubation for our experiments on chip to prevent any possible problems with droplet evaporation or instability due to high temperature incubation.

Fig 3.1: Schematic of the droplet assay platform for single cell detection. A statistically dilute mixture of pathogenic cells and PNA beacons is encapsulated into picoliter sized droplets, which are then incubated at elevated temperatures to facilitate cell lysis and beacon-target hybridization. PNA beacons encapsulated in a droplet containing a cell start fluorescing after hybridization with complementary 16S rRNA targets released from the cell. The specific cell of interest is detected and quantified by screening the fluorescent droplets using confocal fluorescence spectroscopy (CFS).

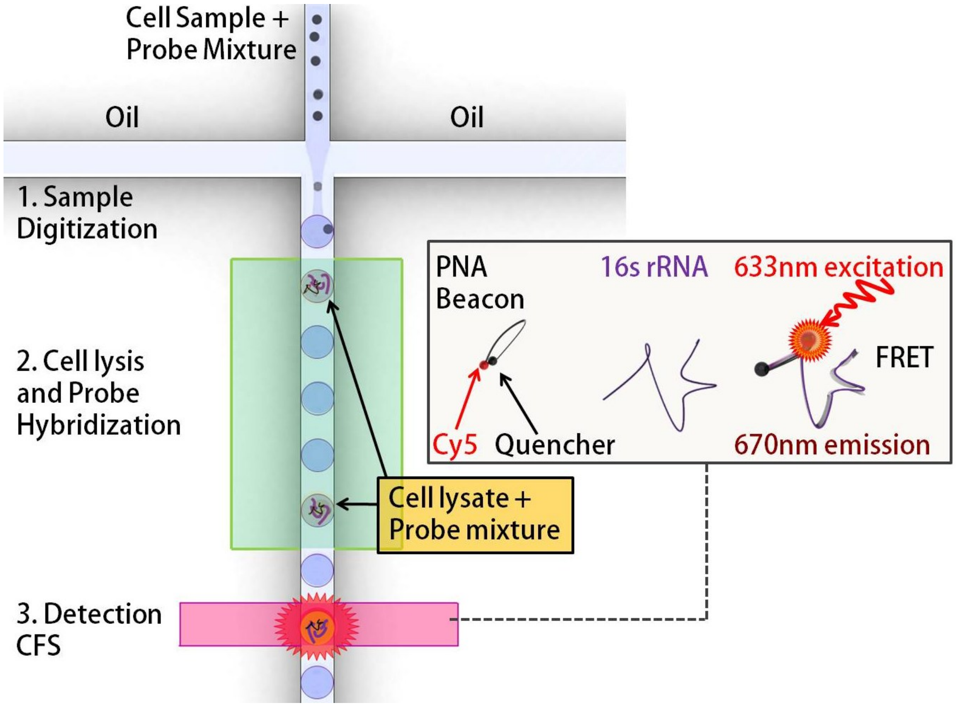
Cell Sample + Probe Mixture
Oil
Oil
1. Sample Digitization
2. Cell lysis and Probe Hybridization
3. Detection CFS
Cell lysate + Probe mixture
PNA Beacon
16s rRNA
633nm excitation
FRET
Cy5
Quencher
670nm emission

Fig 3.2: Microfluidic chip design. The top image is the actual mask design used for fabricating our microfluidic chip. The chip design consists of two different layers fabricated using two different heights of photoresist (50 µm and 350 µm). The chip features an oil inlet with two sample inlets. The chip is capable of generating droplets from a sample, droplet incubation at a high temperature (Peltier heater region) and fluorescence detection from the droplets using CFS. The bottom left image shows a stream of sample droplets generated on an actual chip, while the bottom right image is a photograph of an actual PDMS chip used for our experiments.

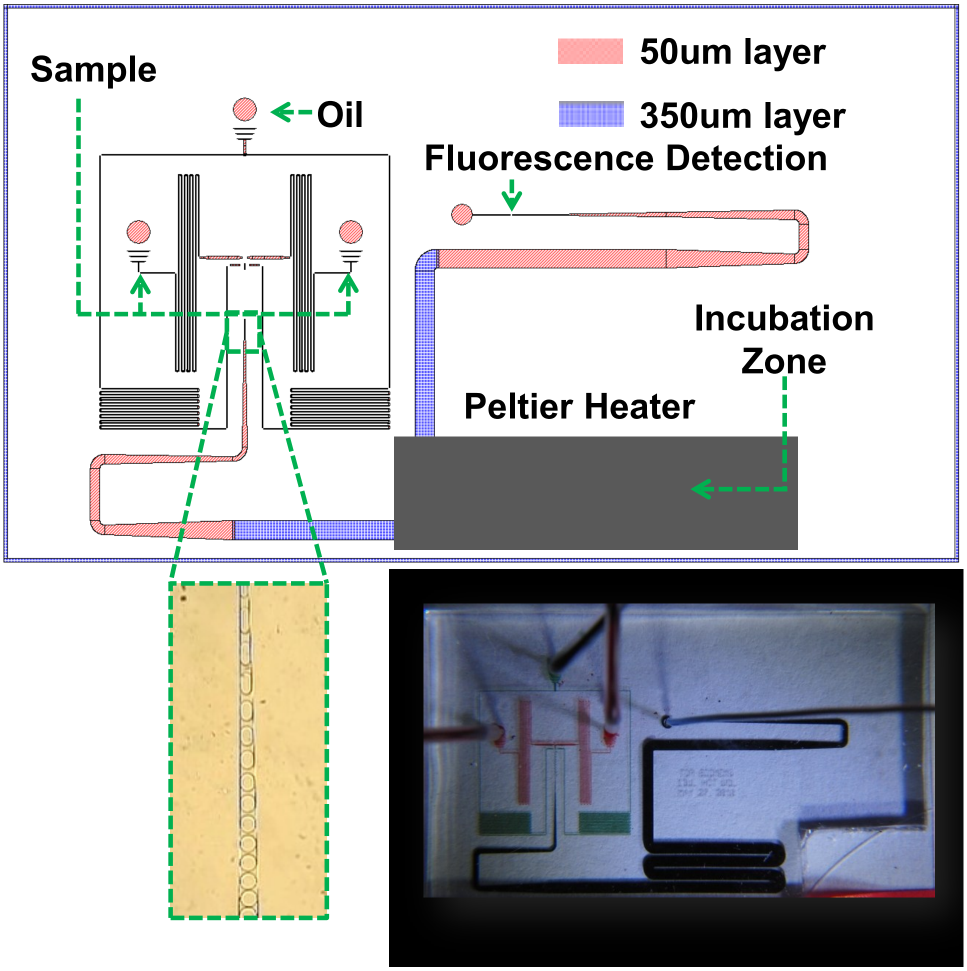
Sample
Oil
50um layer
350um layer
Fluorescence Detection
Incubation Zone
Peltier Heater

Fig 3.3: Fluorescence data collected from the artificially generated sequences of positive control (PNA beacon + rRNA mimic + human genomic DNA) and negative control (PNA beacon + human genomic DNA only) droplets. The fluorescence observed is emitted by the Cy5 dye conjugated to the PNA beacon. **a**) The plot shows fluorescence data from a droplet sequence with one positive droplet per two droplets where the positive droplets contained 6.25 nM rRNA mimic concentration. The fluorescence data shows a clear difference between the positive droplets with strong fluorescent bursts and negative droplets with low background fluorescent bursts. **b**) The data shown is similar to subfigure ‘a’ but with the positive droplets containing rRNA mimic concentration of 1.56 nM and the droplet sequence being one positive droplet per 5 droplets. **c** and **d**) The histograms show the distribution of the burst size (sum of photons detected per droplet) for 300 droplets from each condition observed in the fluorescence data traces. Histograms in subfigures ‘c’ and ‘d’ correspond to the fluorescence data traces in ‘a’ and ‘b’ respectively. The bimodal nature of both histograms indicates clear demarcation between positive droplets with large burst size and negative droplets with small burst size. (The x axis has a breakpoint in both histograms for clear visualization of the bimodal histograms)

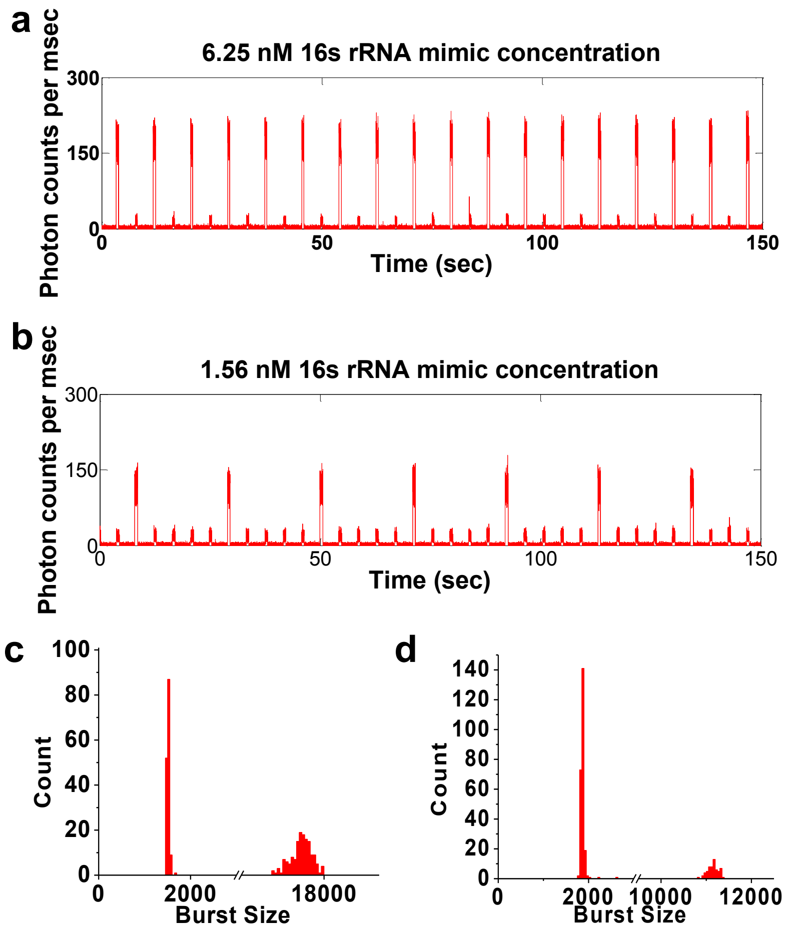
a
6.25 nM 16s rRNA mimic concentration
Photon counts per msec
300
150
0
0
50
100
150
Time (sec)
b
1.56 nM 16s rRNA mimic concentration
Photon counts per msec
300
150
0
0
50
100
150
Time (sec)
c
Count
100
80
60
40
20
0
0
2000
18000
Burst Size
d
Count
140
120
100
80
60
40
20
0
0
2000
10000
12000
Burst Size

Fig 3.4: Quantification of positive droplet count in a droplet sequence for different artificially generated droplet sequences. For each rRNA mimic concentration, different droplet sequences with different 'expected' positive droplet counts were generated and fluorescence data was collected as shown in Fig. 3.3. This data was analysed to obtain the 'observed' positive droplet count for each sequence using burst size thresholding. Excellent linearity and close to 1 slope in the relationship between 'expected' positive droplet count and the 'observed' positive droplet count for both rRNA mimic concentrations tested indicate the quantification ability of our platform. (**a:** rRNA mimic concentration 6.25nM, linear fit $y=1.0115x-0.1498$, $R^2=0.9998$, **b:** rRNA mimic concentration 1.56nM, linear fit $y=1.0076x+0.2831$, $R^2=0.9995$)

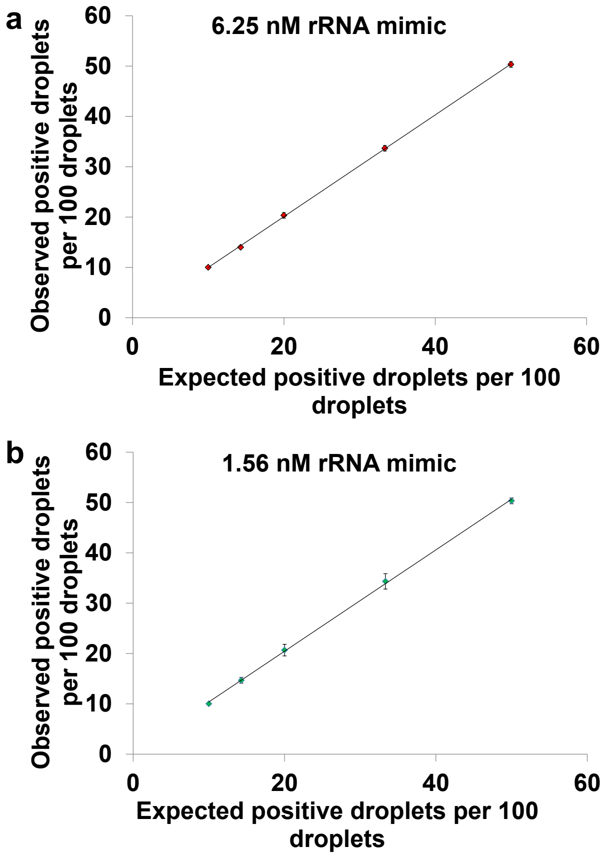
a
6.25 nM rRNA mimic
Observed positive droplets per 100 droplets
0
10
20
30
40
50
60
0
20
40
60
Expected positive droplets per 100 droplets
b
1.56 nM rRNA mimic
Observed positive droplets per 100 droplets
0
10
20
30
40
50
60
0
20
40
60
Expected positive droplets per 100 droplets

Fig 3.5: Fluorescence data collected from droplets with and without E. coli cells. The green traces indicate the fluorescence signal collected from the indicator dye (Alexa 488) present in all droplets regardless of presence or absence of E. coli cells. Each peak in the green trace indicates a droplet passing through the detection region of the CFS setup. The corresponding time points in the red traces indicate the fluorescence signal collected from the PNA beacon present within the same droplet. **a)** The fluorescence data shown here corresponds to droplets generated using a control sample (PNA beacon only). **b)** The fluorescence data shown here corresponds to a high concentration E. coli sample. The estimated E. coli sample concentration for this sample was 15.7 CFU/droplet (CFU: Colony Forming Unit).

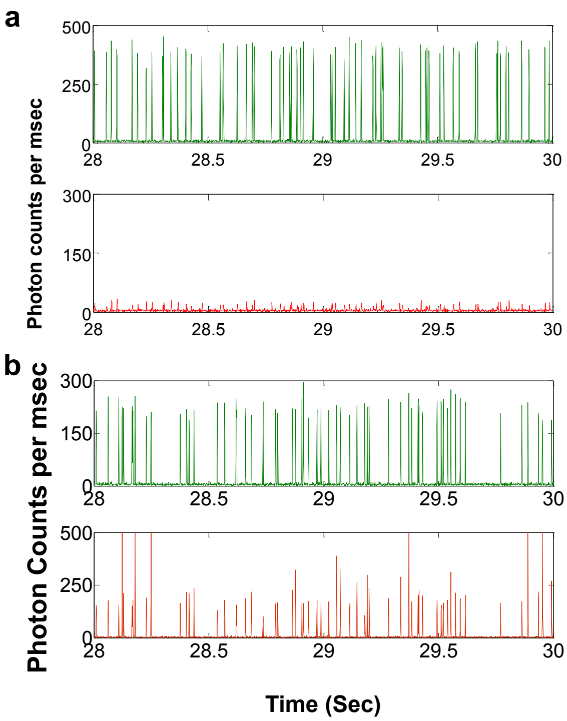
a
500
250
0
28
28.5
29
29.5
30
300
150
0
28
28.5
29
29.5
30
Photon counts per msec
b
300
150
0
28
28.5
29
29.5
30
500
250
0
28
28.5
29
29.5
30
Photon Counts per msec
Time (Sec)

Fig 3.6: Fluorescence data collected from droplets generated using a low concentration E. coli sample. Similar to Fig. 3.5, the green trace shows fluorescence from the indicator dye while the red trace indicates the fluorescence from the PNA beacon encapsulated within the droplets. The E. coli concentration for this sample was estimated at 1 CFU per 20 droplets. In this case, we expect majority of droplets to have no E. coli cells with a few droplets having E. coli cells. The inset shows a zoom in of a small section of the fluorescence data trace

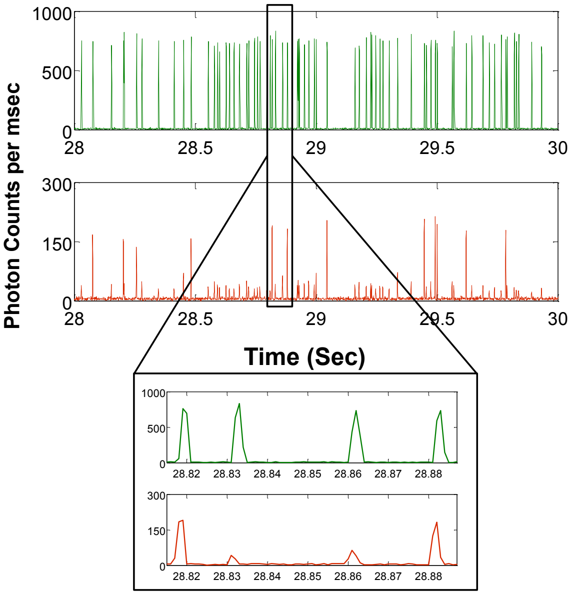
1000
500
0
28
28.5
29
29.5
30
300
150
0
28
28.5
29
29.5
30
Photon Counts per msec
Time (Sec)
1000
500
0
28.82
28.83
28.84
28.85
28.86
28.87
28.88
300
150
0
28.82
28.83
28.84
28.85
28.86
28.87
28.88

Table 3.1: Droplet volume and its effect on the target concentration within the droplet: The following table illustrates the concentrating power of droplets with respect to single cells. In this table, we assume that an intracellular target of interest is present at the concentration of 20000 targets per cell. This number is well within the range of 16s rRNA count per E. coli cell (52), (63). The table shows how the concentration of the same number of target molecules (from a single cell) changes from nanomolar to femtomolar concentrations depending on the volume in which they are released.

Target Molecules per droplet	20000	
Droplet diameter (um)	**Droplet volume (pL)**	**Target concentration in droplet (nM)**
15	1.77	1.88E+01
25	8.18	4.06E+00
35	22.45	1.48E+00
50	65.45	5.07E-01
75	220.89	1.50E-01
100	523.60	6.34E-02
1000	523598.78	6.34E-05

Fig. 3.7: Schematic of the chip design for experiments with 16s rRNA mimic

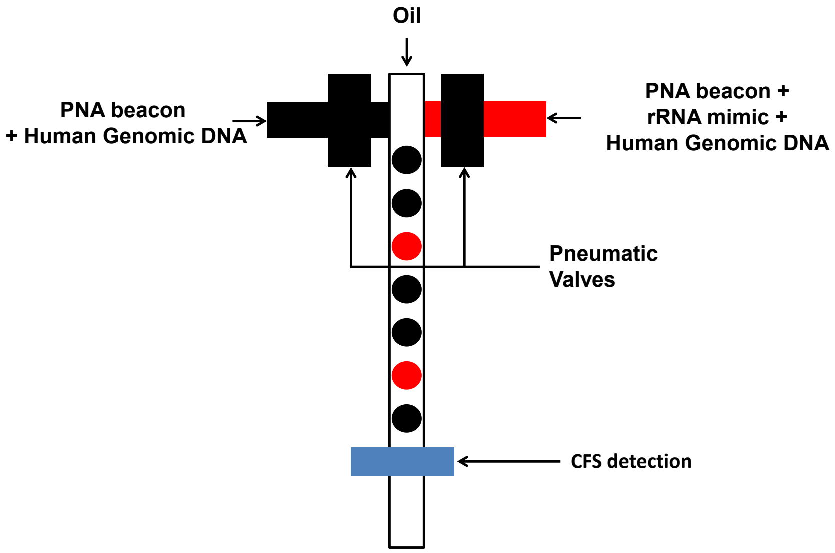
Oil
PNA beacon
+ Human Genomic DNA
PNA beacon +
rRNA mimic +
Human Genomic DNA
Pneumatic
Valves
CFS detection

Fig. 3.8: Effect of incubation temperature on the cell lysis and PNA beacon hybridization efficiency

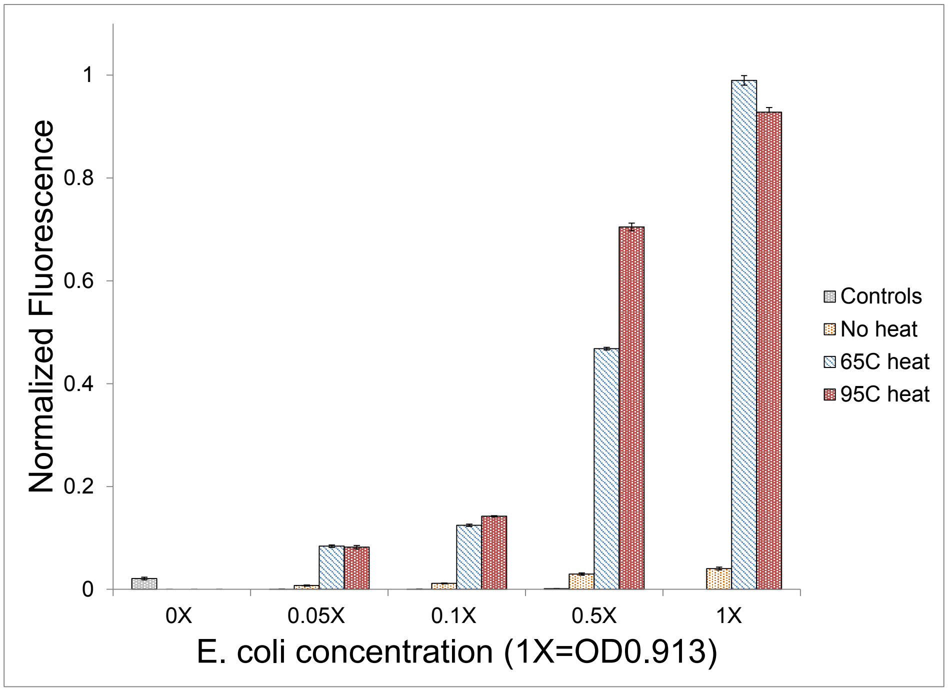
Normalized Fluorescence
0
0.2
0.4
0.6
0.8
1
0X
0.05X
0.1X
0.5X
1X
E. coli concentration (1X=OD0.913)
Controls
No heat
65C heat
95C heat

Chapter 4: Continuous Flow Digital Loop-Mediated Isothermal Amplification (LAMP) Reaction for Digital Nucleic Acid Detection

4.1 Introduction

Digital PCR (polymerase chain reaction) is rapidly becoming the technique of choice for ultra-sensitive quantification of nucleic acid molecules present in biological samples (7-9, 64, 65). Digital PCR involves breaking down a biological sample mixed with PCR reagents into a large number of individual reactions such that each reaction contains either one copy or no copies of the target nucleic acid. As PCR is run in parallel on all these reactions through thermocycling, an accurate molecular count of a nucleic acid of interest present in the biological sample can be obtained through simple counting of positive PCR reactions from the total pool of reactions.

Since the first demonstration of this concept in a 96 well plate format (41), a variety of microfluidic platforms have been proposed for practical implementation of the digital PCR technique. These platforms can be broadly classified into two different types. One type involves microfabrication of a large array of micro-wells on a substrate (4, 66, 67). This format is capable of real-time digital PCR monitoring. However, the sample volume that can be analyzed and the well size are fixed by the microfabricated design. Any change in sample volume or individual reaction volume (well size) requires a change in microfluidic design. The second type involves generation of a large number of tiny droplets (nanoliter to picoliter sized) from the sample mixed with PCR reagents(7, 8). Each of the individual droplets then functions as an independent reaction container. Similar to the micro-well format, however, commercial instruments available for conducting this type of analysis can typically process fixed sample volumes with fixed droplet size. Furthermore, the analysis workflow for droplet-based analysis is fragmented and requires 3 separate instruments/devices for completion of analysis viz. 1) A droplet generator instrument 2) A thermocycler and 3) A droplet reader instrument to detect reaction outcome from droplets. This mode of analysis reduces potential for higher throughput due to idle time on two of the three instruments while one instrument is processing the samples to be analyzed.

Implementing the droplet-based digital nucleic acid analysis workflow on a single sample-to-answer device can overcome the issues mentioned above. On such a device, all three steps of analysis viz. droplet generation, droplet incubation as well as droplet detection are performed on the same device in a continuous flow manner. Continuous flow operation implies that there is no idle time involved in the sample processing workflow and the speed at which fluorescence can be reliably detected from droplets is the only rate limiting step limiting the throughput of this system. Secondly delivery of small sample plugs separated by immiscible oil phase plugs as has been reported in the past (25, 68) can be used to deliver any sample volume that needs to be processed for a particular sample. This sample volume could range from a few tens of nanoliters to virtually any large volume that needs to be processed without any loss of sample in the process.

Despite this potential for improved throughput, larger sample volume processing capability and hence, wider dynamic range, implementing continuous flow digital PCR in droplet format is difficult due to the need for thermocycling. Attempts have been made in the past to realize digital PCR in a continuous flow format. However, these attempts have had limited success in terms of target nucleic acid quantification (23, 69).

Loop-mediated isothermal amplification (LAMP) is a great alternative to PCR for nucleic acid amplification. LAMP functions through auto-cycling strand displacement DNA synthesis. LAMP through its simple requirement for single temperature incubation is very suitable for implementation in a continuous flow format. Furthermore, since LAMP uses a set of 4 different primers recognizing six independent sequences on a target nucleic acid, it can also provide better specificity than PCR (70, 71).

The schematic shown in Fig. 4.1a illustrates the simple functioning scheme of the device we designed for continuous flow digital nucleic acid detection. A sample to be analyzed is mixed with LAMP reagents and then digitized into tiny picoliter-sized droplets on to the device. The image shown in Fig. 4.1b as well as supplementary video 1 shows the droplet generation process on the device. The droplets then flow to an incubation region where they are exposed to temperature suitable for the LAMP reaction. The image shown in Fig. 4.1c and supplementary video 2 show droplets in this region of the device. Finally these droplets move to a downstream detection region on the device, where fluorescence detection is conducted on these droplets using confocal fluorescence spectroscopy. All three steps required for analysis occur simultaneously on the device. As a result, the throughput of the device is only limited by the speed at which fluorescence can be detected from the droplets.

4.2 Experimental section

Device Fabrication: An image of the whole microfluidic device is included in Fig. 4.6. The devices were fabricated using polydimethylsiloxane (PDMS) as the structural material. To avoid evaporation of droplets during transit through the incubation region, we devised a fabrication scheme to fabricate thin PDMS devices. Initially the molds for the devices were fabricated on 4inch Si wafers using standard photolithography technique with SU8-3025 (MicroChem Corp.) as the structural material. Initially a relatively thick layer of PDMS [Sylgard 184(Ellsworth Adhesives), 10:1 base to curing agent ratio] is coated on a blank wafer at a slow spin speed of 100 rpm on a spin coater (Laurell Technologies, Corp). This layer is cured at 80^{o}C for 10 min. While the thick PDMS layer is being cured, a thin layer of PDMS (6:1 base to curing agent ratio) is the spin coated on the device mold at 350rpm. This thin layer of PDMS is cured at 80^{o}C for 6 min. A rectangular piece, large enough to cover the whole device area, is then cut out from the cured thick PDMS layer. This rectangular piece is partially bonded to the cured thin PDMS layer on the device mold by baking at 80°C for 5 min. Finally the bonded thick and thin layers are peeled off the mold. The thick layer just acts as a support to allow for manipulation of the thin layer. Access holes are then punched on the device at the input and output ports. The thin layer is then bonded to thickness #1 cover glass (Ted Pella, Inc) using standard O_2 plasma treatment. The thick layer being partially bonded to the thin layer, can then be easily peeled off without breaking the bond between the thin layer and the coverglass. Small cubes of PDMS (10:1 base to curing agent ratio) with holes punched at the center are then bonded to the thin PDMS layer using O2 plasma treatment. Finally another thickness #1 coverglass is bonded to the thin PDMS layer, effectively sandwiching this layer between two pieces of coverglass in the incubation region on the device. Images of the actual device can be seen in Fig. 4.6.

Materials: The following reagents were used for LAMP reactions on and off-chip: Betaine (Sigma-Aldrich Co., LLC), $MgSO_4$ (New England Biolabs), ROX reference dye (Life Technologies), dNTPs (Life Technologies), BSA (New England Biolabs), Calcein (Anaspec, Inc), Manganese Chloride (Sigma-Aldrich Co., LLC), EvaGreen dye (Biotium Inc), Bst 2.0 WarmStart DNA Polymerase and isothermal reaction buffer (New England Biolabs). A typical reaction mixture consisted of 1X isothermal reaction buffer, 0.8M Betaine, 7mM $MgSO_4$, 25µM Calcein, 0.75mM Manganese Chloride, 0.25µM ROX reference dye, 0.1mg/mL BSA, 1.4mM dNTPs and 0.32 U/µL BST WarmStart DNA Polymerase. For experiments with EvaGreen, Calcein and Manganese chloride were replaced with 0.5X EvaGreen dye where 1X is the manufacturer recommended concentration.

The primers for the experiments in this article were designed to be specific to a region on the 16s rRNA gene for Neisseria Gonorrhoeae. The primers were designed using the LAMP primer design software PrimerExplorer. For the experiments with synthetic target, a double stranded target was generated using fusion PCR and then purified from the gel band specific to the target after running electrophoresis on the PCR product. For the experiments with genomic DNA, DNA extracted from Neisseria Gonorrhoeae (Strain FA1090, ATCC® 700825™) was purchased from ATCC®. The base sequences of primers used for LAMP experiments are as follows

F3: 5- ATC CTG GCT CAG ATT GAA CG -3

B3: 5- ATA TCG GCC GCT CGG ATA -3

FIP: 5- GCC ACC CGA GAA GCA AGC TTC TTT TGG CGG CAT GCT TTA CAC AT -3

BIP: 5- TAC CGG GTA GCG GGG GAT AAT TTT CTG CTT TCC CTC TCA AGA CG -3

LoopF: 5- TGC TGC CGT CCG ACT TG -3

LoopB: 5- CTG ATC GAA AGA TCA GCT AAT ACC G -3

The base sequence of the target region flanked by the primers F3 and B3 is

5- ATC CTG GCT CAG ATT GAA CGC TGG CGG CAT GCT TTA CAC ATG CAA GTC GGA CGG CAG CAC AGG GAA GCT TGC TTC TCG GGT GGC GAG TGG CGA ACG GGT GAG TAA CAT ATC GGA ACG TAC CGG GTA GCG GGG GAT AAC TGA TCG AAA GAT CAG CTA ATA CCG CAT ACG TCT TGA GAG GGA AAG CAG GGG ACC TTC GGG CCT TGC GCT ATC CGA GCG GCC GAT AT -3

For all experiments, the final concentration of all primers in the reaction mixture was kept constant at 1) 0.2μM for F3, B3 2) 1.6uM for FIP and BIP and 3) 0.8uM for LoopF and LoopB respectively. The oil phase used for experiments on-chip consisted of FC40 (3M) with 5% perfluoropolyether-polyethyleneglycol surfactant (RAN Biotechnologies, Inc) by weight

Device operation: Reagents (oil phase and sample) were delivered to the device through custom assembled flow controllers with flow feedback (IDEX Health and Science, LLC). For the duration of an experiment, the device was mounted on a platform designed such that the incubation region on the device was placed on a custom peltier heater assembly. This peltier heater assembly was used to maintain the incubation region on the device at a temperature of 63C suitable for the LAMP reaction. Fluorescence was continuously detected from droplets passing through the detection region on the device by a custom built confocal fluorescence spectroscopy setup. The optical setup is capable of dual excitation (488nm and 552nm) as well as dual band detection (506-534nm and 608-648nm).

4.3 Results and Discussion

Reliable quantification with digital LAMP reaction requires assay readout with good signal to background ratio (SBR). We compared two different assay outcome indicators for the LAMP assay viz. 1) DNA binding dye EvaGreen® and 2) A Calcein dye based indicator (71). The details of the experiments are included in section 4.5.1. Briefly, EvaGreen indicates a positive LAMP reaction through increased fluorescence resulting from the binding of the dye to the large amount of double stranded DNA generated by the LAMP reaction. Calcein dye is non-fluorescent when bound with Manganese ions. However, large amount of DNA generated during LAMP reaction results in generation of pyrophosphate as a byproduct, which sequesters Manganese from Calcein, resulting in return of the dye to its original fluorescence. We tested both readouts for SBR under different conditions using the synthetic dsDNA target containing a base sequence specific to Neisseria Gonorrhoeae (Fig. 4.7, 4.8, 4.9 and 4.10). Our results indicate that the maximum SBR possible with EvaGreen was approx. 2 whereas the maximum SBR possible with Calcein was approx. 6.5.

We then tested both of these assay outcome indicators on the droplet device (Fig. 4.1). To conduct this test, a low concentration of the synthetic target was mixed with LAMP reagents and then processed on the droplet device. Figures

4.2 and 4.3 show a sample digital fluorescence signal obtained from droplets using the two different detection techniques. In both cases, an indicator dye (ROX) is encapsulated in the droplets. The fluorescence channel corresponding to this dye shows steady fluorescence intensity across droplets whereas assay readout specific fluorescence channel shows characteristic digital signal with droplet intensities varying between two different levels. Calcein-based detection clearly shows much stronger difference between positive droplets (positive LAMP reaction) and negative droplets (negative LAMP reaction). As data is collected from a large number of droplets, the two droplet populations (positive and negative) can be easily separated from each other in both cases as long as the positive droplet population is a significant fraction of the total droplet population. However, for droplet populations with rare positive droplets, it was not possible to reliably threshold the droplet intensity data to identify positive droplets from the droplet population with EvaGreen based readout due to low SBR. So for all subsequent experiments we used Calcein-based readout as the detection technique.

We then tested the capability of the continuous flow device to function for long periods of time while processing samples with different target concentrations. Fig. 4.4 shows average droplet intensity data for different target concentrations. The data corresponding to each target concentration is obtained from a population of 100000 droplets each. Each droplet has two data points associated with it 1) A Blue data point indicated average Calcein fluorescence intensity and 2) A Green data point indicating average ROX flu0rescence intensity. As expected for all different target concentrations, the ROX fluorescence intensity shows minimal variation whereas the Calcein fluorescence intensity shows two distinct populations.

Target quantification from the droplet intensity data requires proper separation of the two populations of droplets (positive and negative) from each other. We tested two different techniques to conduct this separation 1) Standard thresholding with a fixed manually specified threshold and 2) Automated clustering using expectation maximization algorithm in Matlab. For thresholding analysis, a threshold approximately centered between the two peaks in the droplet intensity histograms was used whereas for automated clustering, two gaussians were fit to the histogram data using default fitting conditions in Matlab (Details in section 4.5.2). The positive droplet fraction identified for different input target concentrations using these two techniques is plotted against the expected target concentration in Fig. 4.5. The data points follow a characteristic exponential curve predicted by the Poisson distribution of target molecules within droplets.

4.4 Conclusion

In summary, we demonstrated a continuous flow digital nucleic acid sensing system using LAMP reaction as a means of nucleic acid amplification. Using this system, we obtained throughputs on the order of million droplets per 110 minutes. With an average drop volume of 10pL, this corresponds to processing of 10uL of sample volume per 110mins. Considering that a continuous flow system is the only format with the possibility of delivery of small reaction volumes per sample sub micro liter, a sample volume of 100nL per sample would imply that our device is capable of processing 100 samples per 110 mins. Furthermore, the throughput of this system is only limited by the speed at which fluorescence can be detected from droplets reliably. Since we are operating in a conservative region where the transit time per droplet is ~1-2msec per droplet, there is plenty of room to further enhance the throughput, making this an attractive alternative to the traditional digital PCR workflow for digital nucleic acid sensing. On the other hand, applications which require rare molecule sensing from large volumes of a biological sample can benefit from the capability of this device to screen as large a volume as required due to continuous flow format of operation.

4.5 Supplementary section

4.5.1 LAMP assay indicator evaluation

Evaluation experiments to estimate signal to background ratios from the LAMP assay indicators under different conditions were done in a tube format. In one set of experiments, EvaGreen was used as the assay indicator dye. The assay conditions were kept the same as described in Materials and Methods section in the main article, except that the BSA concentration used was 0.01mg/mL and the EvaGreen concentration was varied between 0.5X to 5X where 1X is the recommended concentration from the manufacturer. The positive controls consisted of 2.15e7 copies/mL concentration synthetic target. The LAMP reactions were assembled with 20µL final volume and incubated in PCR strips on a thermocycler at 63oC for 1hr. Following incubation, the reaction mixtures were manually pipetted into a glass bottom 384 well plate and fluorescence was detected from the wells using a Typhoon 9410 Variable Mode Imager (GE Healthcare). The outcome of the reactions was also verified through gel electrophoresis as shown in Fig. 4.8. We observed that the signal to background ratio (positive to negative control fluorescence ratio) varied between 1.7 to 1.95 for EvaGreen concentration varying between 0.5X to 2X. No positive amplification reaction was observed for higher concentrations of the EvaGreen dye. Similar evaluation experiment was conducted for the Calcein based LAMP assay indicator. The Calcein concentration was kept fixed at 25µM while the Manganese chloride concentration was varied between 0nM to 2000nM. The analysis steps were the same as indicated for the EvaGreen experiment described earlier. We observed that the signal to background ratio (positive to negative control fluorescence ratio) in this case varied between ~1 to 6.7 for Manganese Chloride concentration varying between 0nM to 1000nM (Fig. 4.9). No amplification was observed for 2000nM Manganese Chloride concentration as indicated by gel electrophoresis results in Fig. 4.10

4.5.2 Droplet data analysis

Droplet fluorescence was detected from the device using a confocal fluorescence spectroscopy setup capable of dual excitation (488nm and 552nm) as well as dual band detection (506-534nm and 608-648nm). Since all samples tested on the device included ROX as an indicator dye, ROX fluorescence thresholding was used to identify droplets from a fluorescence data trace. The droplets collected from the fluorescence data traces were filtered to remove droplets with very short (<0.5ms) and very long transit times (>5ms), indicative of satellite droplets and merged droplets respectively, from data analysis. Average fluorescence intensity of all the filtered droplets was then calculated. The average fluorescence intensity data was then either 1) thresholded with a constant threshold to separate the populations of positive and negative droplets or 2) clustered into positive and negative droplet populations using expectation maximization algorithm implemented in Matlab through the function 'gmdistribution.fit'. An example of population identification using both techniques is shown in Fig. 4.11. Using this population data a positive droplet fraction from the total droplet population is estimated. From each experiment, an image of droplets is analyzed to estimate the volume of the droplets for that particular experiment. This volume estimate was used to estimate the known target molecule concentration per droplet for each experiment. The droplet volume varied around ~8pL for all the experiments.

Fig. 4.1 Droplet microfluidic device for continuous flow digital LAMP analysis a) A schematic showing three steps of digital LAMP analysis that are conducted on the droplet microfluidic device b) An image of the droplet generation region on the microfluidic device c) An image of the droplet incubation region on the microfluidic device

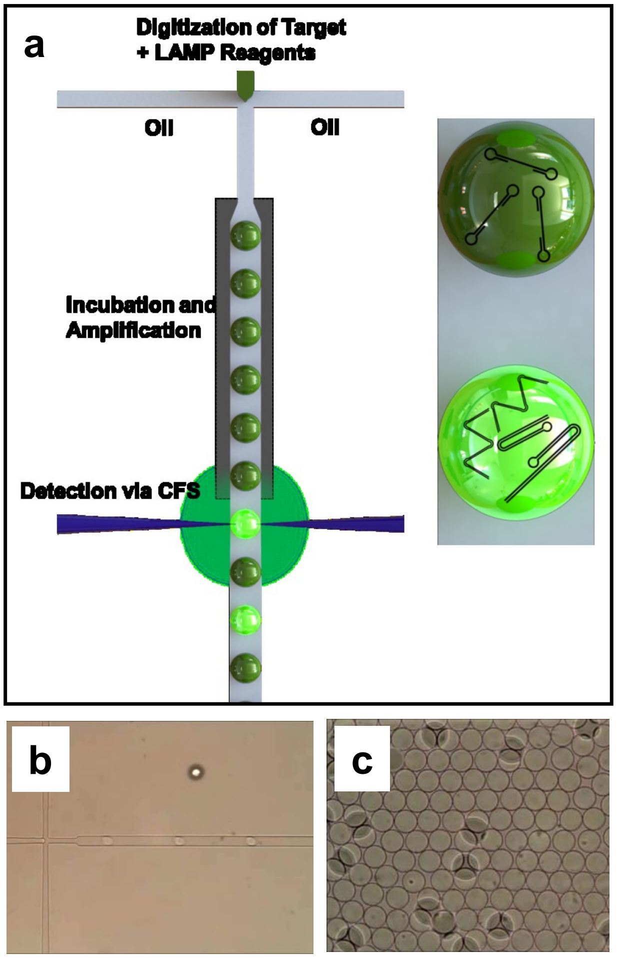
a
Digitization of Target
+ LAMP Reagents
Oil
Oil
Incubation and
Amplification
Detection via CFS
b
c

Fig. 4.2 Sample digital LAMP signal from droplets with an EvaGreen readout. Blue trace: EvaGreen fluorescence signal, Green trace: ROX (indicator dye) fluorescence signal. The inset shows individual droplets in the fluorescence data traces. The indicator dye fluorescence intensity can be seen uniform across droplets whereas the EvaGreen fluorescence intensity varies between two levels: high intensity indicating positive LAMP reaction and low intensity indicating negative LAMP reaction

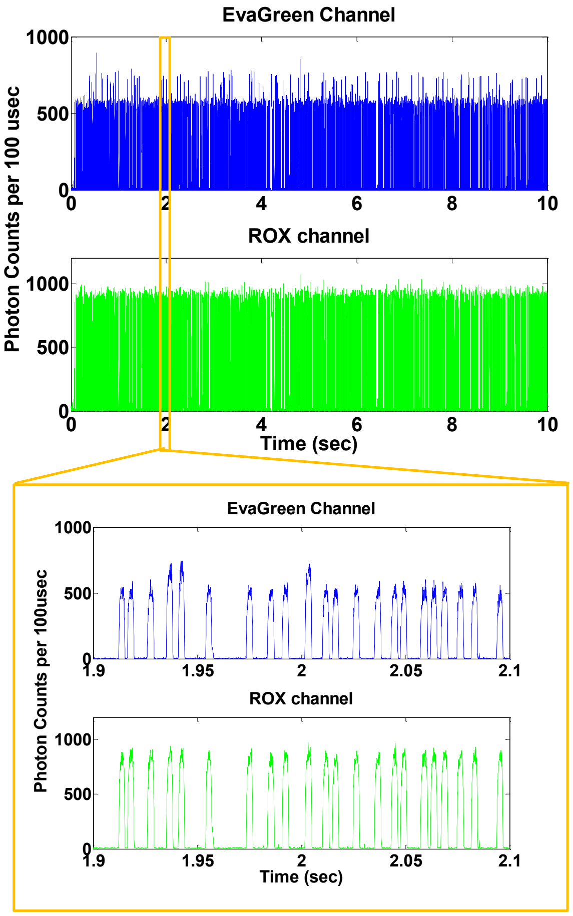
EvaGreen Channel
ROX channel
Photon Counts per 100 usec
1000
500
0
0
2
4
6
8
10
Time (sec)
EvaGreen Channel
ROX channel
Photon Counts per 100usec
1.9
1.95
2
2.05
2.1
Time (sec)

Fig. 4.3 Sample digital LAMP signal from droplets with a Calcein based readout. Blue trace: Calcein fluorescence signal, Green trace: ROX (indicator dye) fluorescence signal. The inset shows individual droplets in the fluorescence data traces. The indicator dye fluorescence intensity can be seen uniform across droplets whereas the Calcein fluorescence intensity varies between two levels: high intensity indicating positive LAMP reaction and low intensity indicating negative LAMP reaction

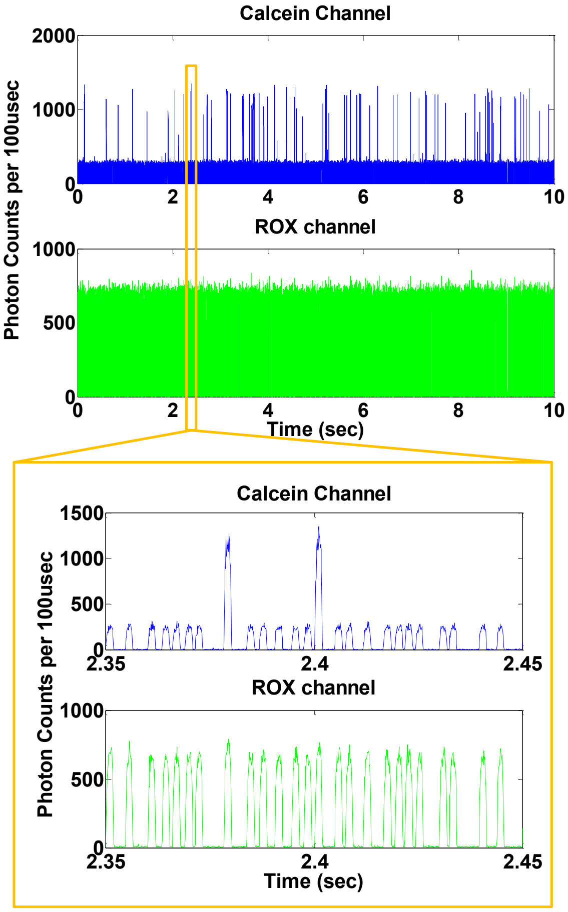
Calcein Channel
2000
1000
0
0
2
4
6
8
10
ROX channel
1000
500
0
0
2
4
6
8
10
Time (sec)
Photon Counts per 100usec
Calcein Channel
1500
1000
500
0
2.35
2.4
2.45
ROX channel
1000
500
0
2.35
2.4
2.45
Time (sec)
Photon Counts per 100usec

Fig. 4.4 Average droplet fluorescence intensity data from large droplet populations for different target concentrations. Each droplet has two data points associated with it. A blue data point indicating average Calcein fluorescence intensity and a corresponding green data point indicating average ROX intensity. Data from a population of 100000 droplets is shown for each target concentration. The ROX intensity shows minimal variability across droplets whereas the Calcein intensity varies between two levels as expected from Fig. 4.3. The fraction of the positive droplet population can be seen decreasing with decreasing target concentration.

1X target concentration

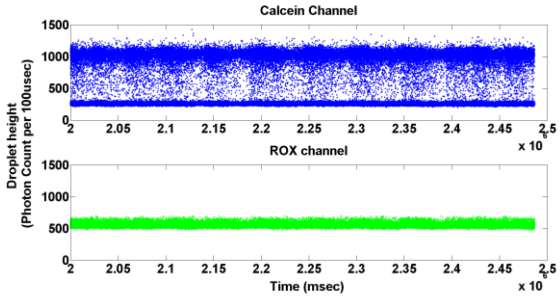

0.111X target concentration

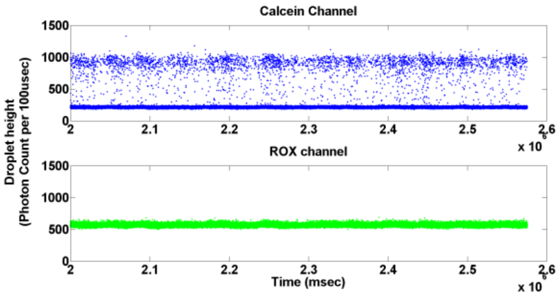

0.0061X target concentration

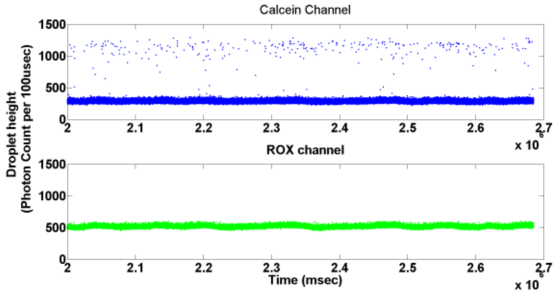

0X target concentration

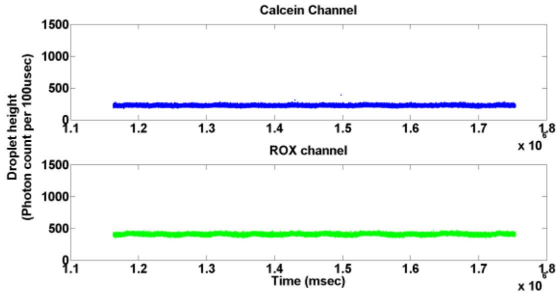

Fig. 4.5 Target nucleic acid quantification with digital LAMP. The plot of the positive droplet fraction against the expected target concentration in copies per droplet shows an exponential relationship predicted by Poisson distribution. Both thresholding and clustering approaches for positive droplet identification agree well for higher target concentrations. However, clustering leads to overestimation of target concentration for lower input target concentrations

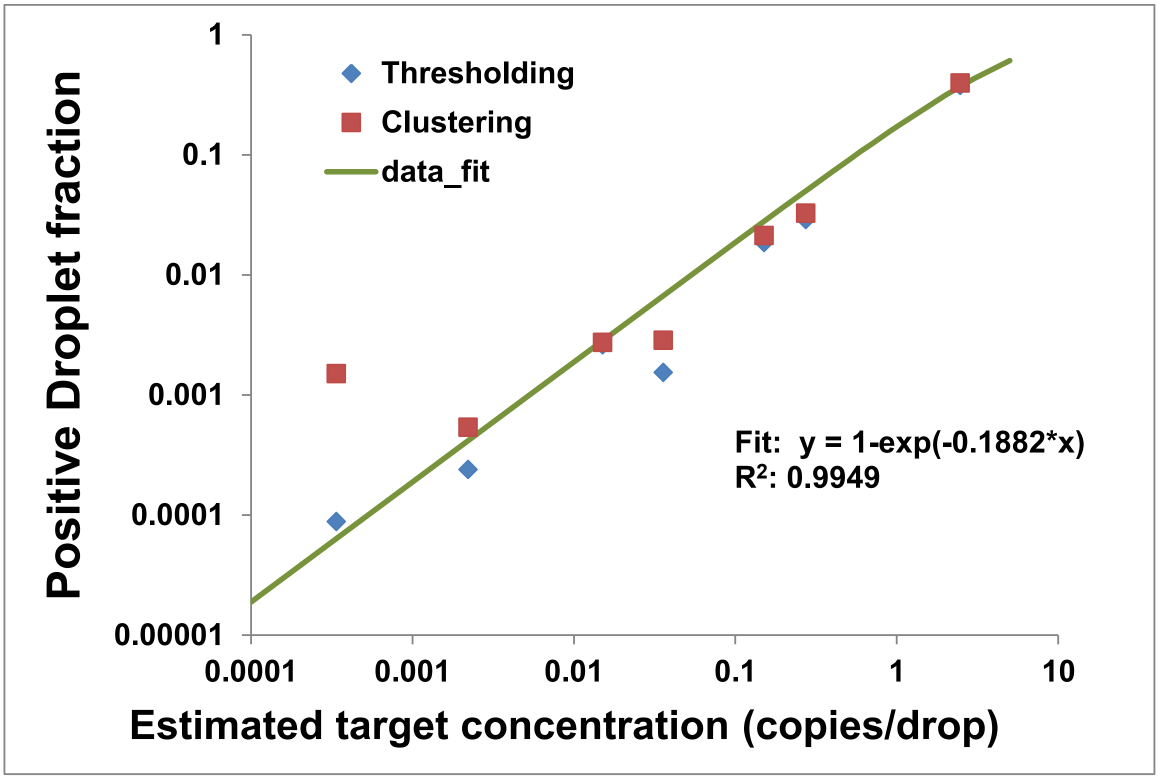
Positive Droplet fraction
1
0.1
0.01
0.001
0.0001
0.00001
0.0001
0.001
0.01
0.1
1
10
Estimated target concentration (copies/drop)
◆ Thresholding
■ Clustering
data_fit
Fit: y = 1-exp(-0.1882*x)
R²: 0.9949

Fig. 4.6 Microfluidic device used for droplet experiments. The left panel shows the thin structure of the device while the right panel indicates different ports on the device with bonded PDMS cubes for tubing attachment

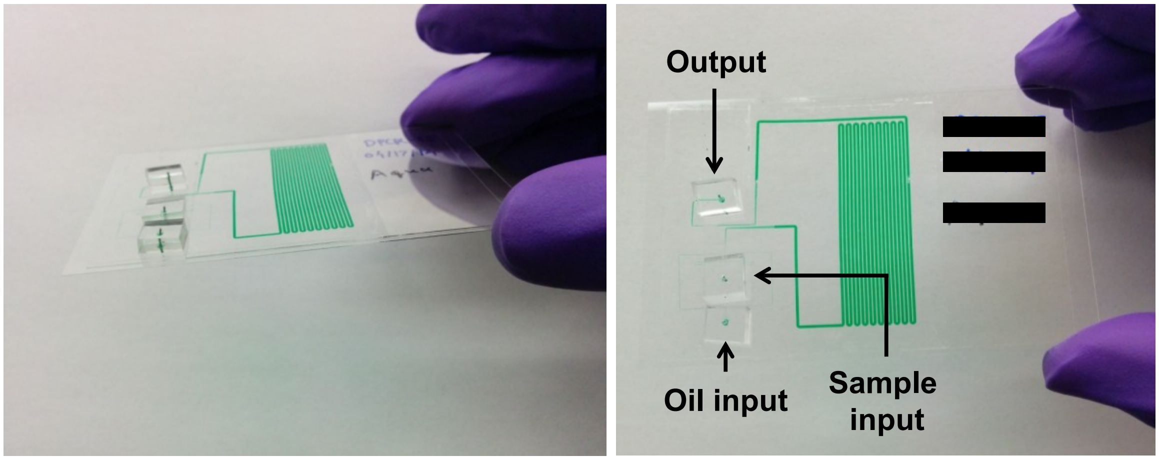
Output
Oil input
Sample input

[redacted]

Fig. 4.7 Effect of EvaGreen concentration on LAMP signal to background ratio

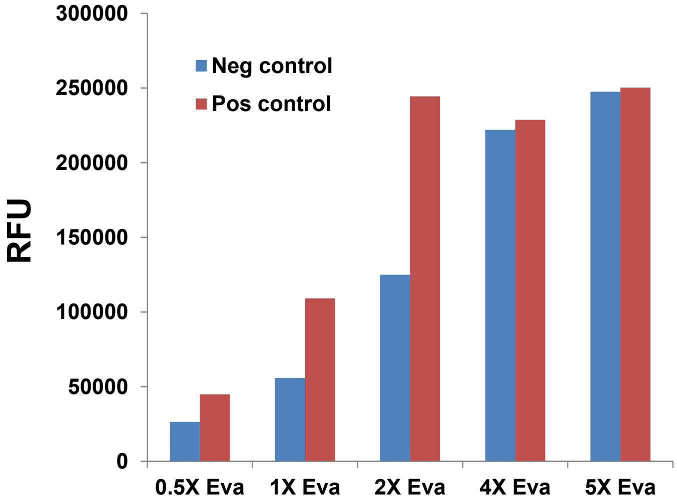

300000
250000
200000
150000
100000
50000
0
RFU
Neg control
Pos control
0.5X Eva
1X Eva
2X Eva
4X Eva
5X Eva

Fig. 4.8 Gel verification of LAMP reaction outcome for various EvaGreen concentrations.

Top row (Negative controls). 1: 100bp ladder, 2-5: 0.5X-5X EvaGreen concentrations with RT (Room temperature) incubation, 6-11: 0.5X-5X EvaGreen concentrations with 63°C incubation.

Bottom row (Positive controls). 1: 100bp ladder, 2-5: 0.5X-5X EvaGreen concentrations with RT incubation, 6-11: 0.5X-5X EvaGreen concentrations with 63°C incubation

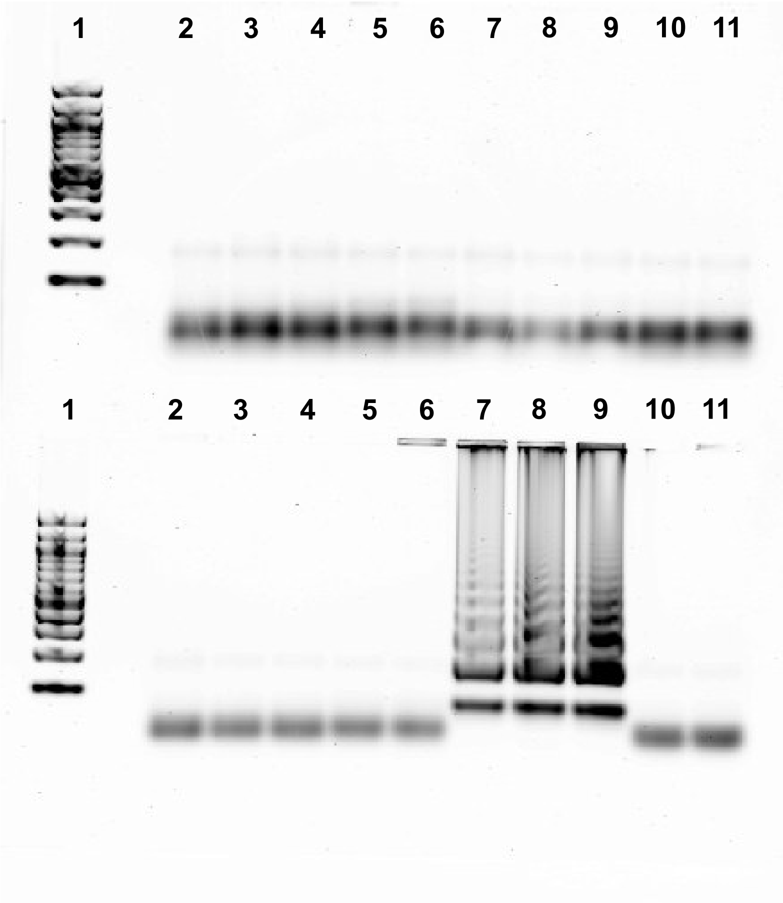
1
2
3
4
5
6
7
8
9
10
11
1
2
3
4
5
6
7
8
9
10
11

Fig. 4.9 Effect of Manganese chloride concentration on LAMP signal to background ratio

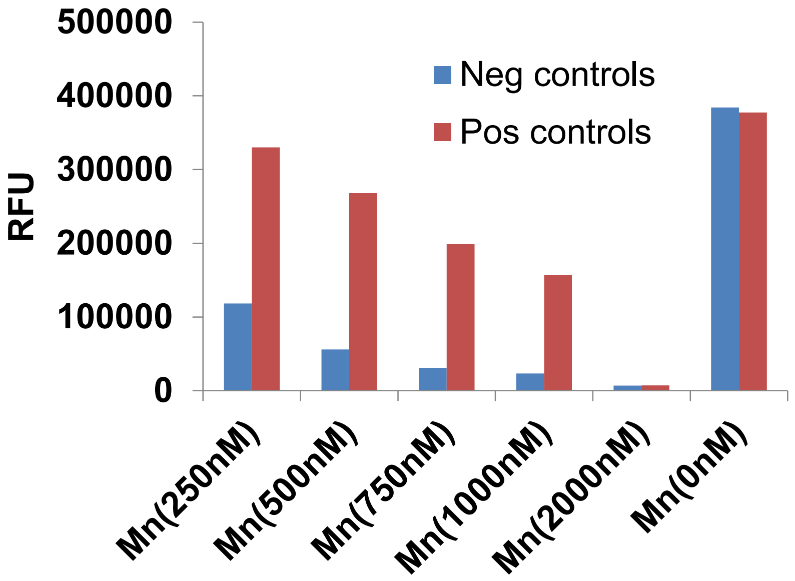
500000
400000
300000
200000
100000
0
RFU
🟦 Neg controls
🟥 Pos controls
Mn(250nM)
Mn(500nM)
Mn(750nM)
Mn(1000nM)
Mn(2000nM)
Mn(0nM)

Fig. 4.10 Gel verification of LAMP reaction outcome for various Manganese Chloride concentrations.

Top row (Negative controls). 1: 100bp ladder, 2-7: 250nM, 500nM, 750nM, 1000nM, 2000nM and 0nM Manganese Chloride concentrations respectively with 63^{o}C incubation

Bottom row (Positive controls). 1: 100bp ladder, 2-5: 2-7: 250nM, 500nM, 750nM, 1000nM, 2000nM and 0nM Manganese Chloride concentrations respectively with 63^{o}C incubation

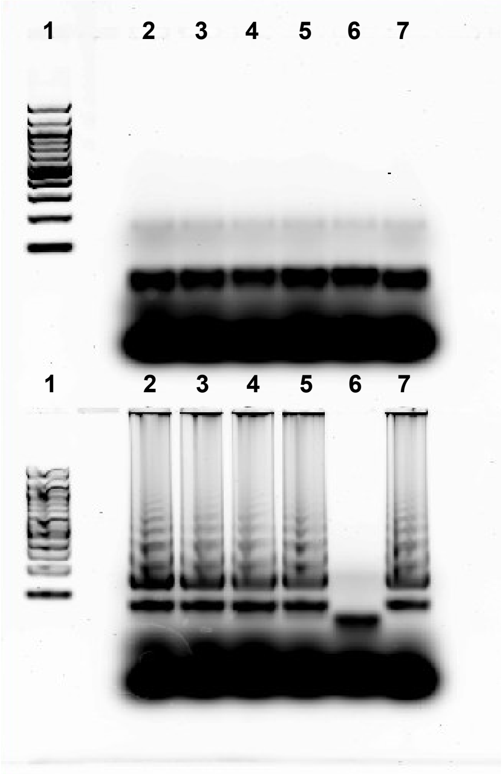
1
2
3
4
5
6
7
1
2
3
4
5
6
7

Fig. 4.11 Two different techniques for separation of positive and negative droplet clusters from a droplet population. The two histograms indicate the droplet intensity data from the same droplet population with the insets showing a zoomed in version of the histogram. The histogram on top is separated into negative (blue) and positive (green) droplet populations using automated clustering using expectation maximization algorithm whereas the histogram on bottom is separated into the positive and negative droplet populations using a fixed threshold.

Approach 1: Clustering

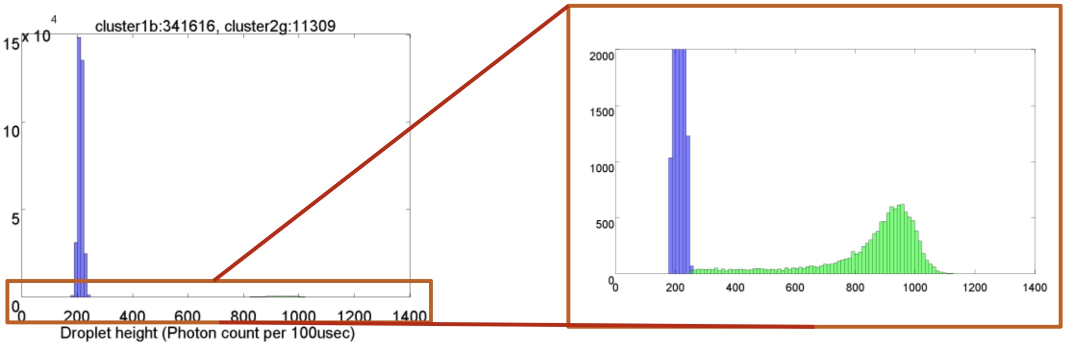

Approach 2: Thresholding

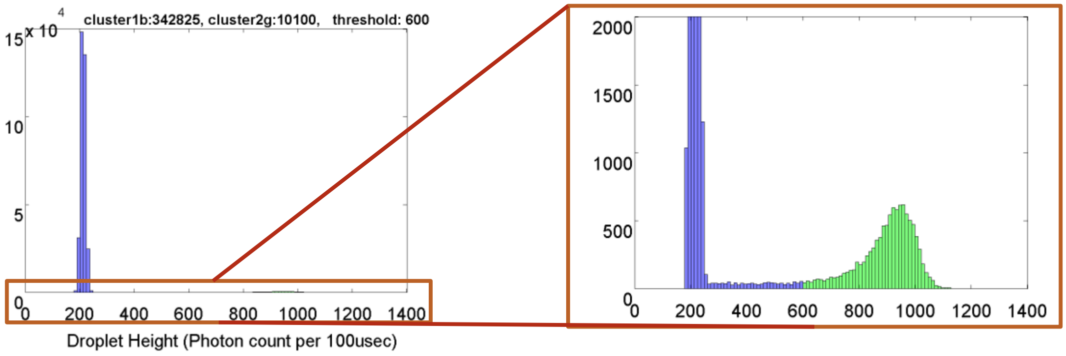

Chapter 5: A Barcode-Free Combinatorial Screening Platform for Matrix Metalloproteinase Screening

5.1 Introduction

Matrix metalloproteinases (MMPs) are a family of enzymes involved in a plethora of biological functions. Through their activity against biological molecules like proteinases, latent growth factors, cell-surface receptors, growth factor binding proteins etc, they are able to regulate a number of biological processes (72). Furthermore, this family also plays an important role in pathological conditions like cancer, arthritis, psoriasis, pulmonary emphysema and endometriosis (73). It is, thus, critical to infer the presence of particular subtypes of MMP family in biological samples for better understanding of their role in pathological processes. Short FRET peptide substrates can be used to sense MMPs through their cleavage activity. However their relative non-specificity demands sophisticated mathematical techniques like Proteolytic Activity Matrix Analysis (PrAMA) (74) to infer the presence of a specific set of MMPs based on the cleavage signature of an unknown biological sample against a panel FRET peptide substrates. Functioning of techniques like this requires large datasets of individual purified MMP cleavage signatures against a large panel of peptide substrates, generating which can be extremely costly and time consuming through the standard 96 well plate workflow.

Droplet microfluidics holds tremendous promise for high throughput analysis of biological samples. The power of droplet microfluidics is evident from the scientific literature harnessing this versatile platform for a variety of applications like single cell analysis (75), single molecule analysis (76), particle generation (77), and enzyme kinetics analysis (78). This technology has really matured in digital analysis of individual biological samples at single molecule level (9, 76, 79). However the potential of this technology to address the needs of combinatorial screening applications by replacing standard biochemical assays conducted in a multi-well plate format (μL regime) to the droplet format (nL-pL regime) still remains unattained.

A variety of droplet-based schemes have been proposed by other research groups to suit the needs of combinatorial screening applications. Brouzes et al proposed a scheme for high-throughput screening of single cells through high-speed electrocoalescence of a reagent droplet library with cell sample droplets(75). Despite high-speed operation, this scheme is practically limited to a small number of reagent-sample combinations due to the need for a composition identifying unique barcode in each droplet. Furthermore, the reagent and sample droplet volumes are fixed resulting in fixed sample to reagent ratio in each droplet. Another scheme proposed by Abate et al provides an alternative through the picoinjection technology. This technology is capable of injecting small quantities of individual reagents into droplets at high speeds. However, picoinjector technology is also limited by the need for unique barcodes and reagent quantity control is only possible with pressure and flow rate variation, both of which cannot be varied for each individual droplet. (80). Picoinjector technology has been applied to MMP screening against FRET substrates (81). However, due to the limitations discussed above the multiplexing capacity of these demonstrations is limited to small number of unique MMP-substrate combinations, albeit with large number of repeats of each condition.

We proposed an alternative strategy in recent past to overcome the limitations of these technologies (82). This strategy combines the control offered by microfluidic valves with the high throughput capacity of droplets. Barcode-free, continuous flow operation of this strategy implies unlimited potential screening capacity on a single device with precise composition control over each individual droplet. In this article we demonstrate the true potential of this technology using MMP screening as a sample application. A droplet based scheme using valves has also been proposed by Jambovane et al for MMP screening (83). However, application of imaging as a detection mechanism severely limits the throughput of this scheme both from the point of view of data acquisition as well as processing. A simple modification to a continuous flow format of operation can completely change the throughput capacity of a single device as demonstrated in this article.

5.2 Solution

A schematic of the device we designed for this application is illustrated in Fig 5.1. The device features a central channel with an oil phase input at the upstream end, followed by a reagent injection region, an incubation region and a fluorescence detection region respectively as one moves downstream. The device also has twelve individual reagent inputs. We also included 'pressure relief' channels on this device, to decouple the dependence of droplet size generated on the device from the changing flow resistance of the incubation region. The valves corresponding to the pressure relief channels are opened during reagent injection and droplet displacement operations on the device.

The device operation sequence is illustrated in Fig 5.1. The most upstream reagent input is dedicated to dispensing reaction buffer into droplets. For every droplet generated on the device, initially a buffer droplet is dispensed in the central channel. As all reagents are constantly maintained under pressure, opening the valve corresponding to a particular reagent results in release of a reagent droplet into the central channel. The valve opening time as well as the pressure magnitude applied to the reagents can be used to control the volume of the reagent dispensed into the central channel. After using this mechanism to dispense a buffer droplet, this droplet is moved in front of the input corresponding to the next reagent to be injected, using flow of oil phase from the oil input to the central channel, and the injection of next reagent is completed. This sequence of steps can be repeated as many times as desired to inject up to 12 reagents in each droplet using this device. After a complete reaction mixture droplet is assembled, this droplet is moved to the downstream incubation region. The length of the incubation region can be modified to achieve desired incubation time of the droplets on the device. Following incubation, the droplets move to a fluorescence detection region where they are interrogated by a confocal fluorescence spectroscopy system for the reaction outcome. All three steps of device operation can be seen in the supporting videos included with this thesis (supplementary videos 3, 4 and 5).

This scheme of combinatorial droplet generation has a few salient features which set it apart from other droplet microfluidic platforms described above. Under this scheme up to 12 different reagents can be injected into a reagent droplet at various independently controlled proportions. The device can operate in a completely automated manner through execution of a predetermined valve actuation sequence. This automation also implies that various reaction mixtures can be generated in a predetermined order as desired. This feature also provides the device with the ability to generate exactly as many repeats of a reaction mixture as desired. Simultaneous operation of all three steps i.e. droplet generation, incubation as well as fluorescence detection implies that this device has virtually unlimited screening capacity. Even at a very conservative estimate of ten different reagent concentrations for each reagent in a droplet, a single device is capable of producing a trillion different droplet compositions. Most importantly, since the order of droplets is maintained throughout the device, droplets are automatically spatially coded, precluding the need for composition identifying unique barcodes.

We designed a microfluidic device to execute the workflow proposed in Fig 5.1. The details of device fabrication can be found in section 5.4.1. The device was then tested for its capability to generate various combinations of input reagents in a predetermined sequence using fluorescent dyes as reagents. In our first test, we generated all possible combinations of four different concentrations of three different fluorescent dyes on our microfluidic device (Fig 5.2). Each white square in the collage in Fig 5.2 includes three images of a droplet taken with red, green and blue filters from top to bottom respectively (details in sections 5.4.2). A progressive sequence of changing droplet compositions can be seen as one moves from left to right in each row, beginning with increasing concentrations of individual dyes followed by all combinations of pairs of dyes followed by all combinations of triplets of dyes.

This mode of operation, however, is inherently limited in screening capacity by the space available on the device in the incubation region. The true potential of our scheme lies in the continuous flow mode of operation wherein all the steps of droplet generation, incubation and detection are occurring simultaneously on the device in synchronization with each other.

To test this mode of operation, we generated a sequence of droplets on the device using two different fluorescent dyes (Alexa Fluor 488 and Alexa Fluor 546, hereafter Alexa488 and Alexa546 respectively). The sequence consisted of a gradient of Alexa488 followed by a gradient of Alexa546 followed by four different fixed intensities of Alexa 488 dye with a gradient of Alexa 546 dye at each fixed intensity of Alexa 488 dye. The two data traces in Fig 5.3 show two repeats of this droplet sequence. The bar chart at the bottom of Fig 5.3 shows the mean and standard deviation of each droplet's fluorescence intensity in the sequence over ten repeats of the droplet sequence. The data traces show the ability of our scheme to independently control the concentration of different components in droplets and sense the effect of this varying concentration in a serial manner. As designed the sequence of droplets is constantly maintained throughout the device resulting in fluorescence data collection from the droplets, exactly in the order that they were generated. The presence of strongly fluorescent droplets right next to weakly fluorescent droplets in a channel indicates minimal carryover of material from droplet to droplet. Finally the small error bars in the bar chart indicate repeatable and robust operation of the device without any human intervention.

An important characteristic of a combinatorial reaction generation system like ours is the reagent concentration dynamic range of the system. The upper end of this range is fixed by the input reagent concentration. The response time of the valves used in our scheme as well as the minimum pressure that can be applied to a reagent for reliable injection puts a lower limit on the smallest reagent volume that can be injected into a droplet. However, this limitation theoretically doesn't limit the lower end of the reagent concentration dynamic range as the buffer droplet size can always be made as large as necessary to achieve the required concentration. Practically however we observed that large volume droplets due to their long length tend to breakup during transit through the incubation region on the device. Given these constraints we were able to achieve a maximum dilution of 6 parts per 1000 on our device (section 5.4.4). This number is however limited to our current device design as well as the oil-surfactant system used in our experiments. An increase in channel height in the incubation region, to decrease droplet length, as well as choice of a modified oil-surfactant system for better droplet stability may further reduce the dilution limit we were able to achieve without droplet breakup on our device.

We then tested the applicability of our droplet system for screening of Matrix Metalloproteinases (MMPs) against a variety of peptide substrates on our device for their specificity and activity. The peptide substrates used are short peptide sequences labeled with a fluorophore (5-FAM) and a quencher (QXL™520) on either ends. In the presence of an MMP, the peptide sequence is cleaved resulting in separation of the fluorophore from the quencher and a consequent increase in the fluorophore's fluorescence. The rate of increase in fluorescence of an MMP-substrate sample can then serve as a proxy for the activity of the MMP against the peptide substrate.

Fig 5.4 shows data traces obtained from two repeats of a droplet sequence containing various combinations of MMPs and substrates. The data trace in the top panel indicates fluorescence emitted by the fluorophore on the peptide substrates. However, for a droplet sequence with an unknown outcome (as against a fluorescent dye dilution series), it can be difficult to estimate the position of each droplet in the whole long sequence as well as to ensure that the device is operating robustly without any unwanted merging/breakup of droplets. So we also included some 'beacon' droplets in the droplet sequence, generated through different dilutions of a fluorescent dye different from the fluorescent dye on the MMP substrates. These droplets are indicated in the data trace from the Alexa546 channel. The known repeating pattern of these droplets allows us to easily discern repeats of a droplet sequence from the data. Furthermore, their predetermined location in the droplet sequence allows us to ensure that the device is operating in a robust manner without any unwanted merging/breakup of droplets as any unwanted merging/breakup would result in a change in the position of a beacon droplet in the whole sequence. It should be noted that these beacon droplets are not limited by different fluorescence intensities that can be easily distinguished by the detection system similar to fluorescence intensity based barcodes. The possibility of varying intensities, varying count as well as varying spacing between beacon droplets provides for virtually unlimited possible beacon droplets marking different positions in an extremely long droplet sequence.

We then compared the substrate cleavage rates for various MMP-substrate combinations we observed on our device against cleavage rates we observed in off-chip experiments. Some representative results are indicated in Fig 5.5 while others are included in Fig 5.8. Our comparison indicates that the cleavage rates of enzymes MMP1, MMP2 and MMP9 matched across platforms fairly well for various substrates. However, the substrate cleavage rates for MMP8 and MMP13 were consistently low on the device when compared with cleavage rates in off-chip experiments. Interaction of proteins with oil-surfactant system used in droplet devices has been reported in literature (84, 85). Our results indicate that the oil-surfactant system we used interacts with MMP8 and MMP13, reducing their activity. Some solutions have been proposed in the literature to engineer better surfactants with substantially reduced interaction with proteins (84, 85). These solutions can potentially make this platform suitable for a broad range of enzymatic screening. As a proof of principle of screening large number of enzyme-substrate combinations on a single device, we generated a droplet train consisting of 650 unique droplet compositions (data shown in section 5.4.6). The activity patterns from two repeats of this sequence shows excellent similarity. We, however, did observe that following long term operation of the device the hydrophobic treatment wears off resulting in more sticking of droplet contents to the channel surface. Superhydrophobic treatments have been proposed in literature to fabricate antifouling surfaces. Integration of these surfaces with our device design can potentially increase the time span for which a device can function without significant channel surface fouling.

5.3 Conclusion

In summary, we demonstrated a droplet device for combinatorial screening applications without the need for composition identifying unique barcodes. We expect this format of droplet devices to increase the applicability of droplet microfluidics to applications requiring the capability of rapid heterogenous reaction generation.

5.4 Supplementary section

5.4.1: Microfluidic device fabrication

The microfluidic devices for our experiments were fabricated using standard multilayer soft-lithography techniques. The fluidic layer mold for the devices was fabricated through dual layer photolithography. Initially a layer of SPR-220 7.0 (MicroChem Corp.) photoresist is patterned on a 4 inch silicon wafer. This positive photoresist was used to generate the channel regions on the device to be compressed by the control layer. Following this step, a layer of SU8-3025 (MicroChem Corp.) was patterned on the same wafer to generate the rest of the fluidic layer network on the device. An independent control layer mold was prepared on a separate silicon wafer by patterning a single layer of SU8-3025 on the wafer. These molds were then used to fabricate devices using multi-layer soft lithography. Initially a ~1mm thick layer of polydimethylsiloxane (Sylgard Elastomer 184, Ellsworth Adhesives, 6:1 base to curing agent ratio) was spin-coated on the control layer mold. This layer was partially cured in an oven at ~80°C for 5-6 minutes. The PDMS membrane on the mold was then peeled off and trimmed to prepare for alignment with the fluidic layer. A thin layer of PDMS was spin coated on the fluidic layer mold and partially cured in the oven at ~80°C for 3-4 minutes. The PDMS membrane from the control layer mold was then aligned with the fluidic layer using a stereoscope. These two layers were allowed to bond for 10 minutes at ~80°C. Following this, ~50g of PDMS (10:1 base to curing agent ratio) was poured on these two layers to form the thick body of the device. This thick PDMS layer was allowed to cure for at least 25 minutes at ~80°C. The devices were then peeled off the mold and holes were punched at the input and output ports. The devices were bonded to Thickness #1 cover glass (Ted Pella, Inc.) using oxygen plasma treatment. Before use, the devices were treated with Aquapel (PPG Industries) to render the fluidic channels on the device hydrophobic.

5.4.2: Materials

We used a 'MMP Substrate Sampler kit' (Anaspec, Inc Catalog#: 71170) as a source of MMP substrates for our experiments. This kit consists of 16 substrates (SB1-SB16), all of which consist of short peptide sequences labeled with the fluorophore 5-FAM and quencher QXL™520. The exact sequences of peptides from this kit included in our experiments are appended below this section. The kit also included a fluorescence reference standard (5-FAM-Pro-Leu-OH), which was used to generate standard curves correlating fluorescence intensity with substrate concentration. A 'Matrix Metalloproteinase (MMP) Multipack-1' (Enzo Life Sciences, Catalog #: BML-AK013-0001) was used as a source of MMPs for our experiments. This kit consists of active recombinant MMP catalytic domains. We used the fluorescent dyes Alexa Fluor 350, Alexa Fluor 488 and Alexa Fluor 647 (Life Technologies) as indicator dyes for the experimental results shown in Fig 5.2. The input concentrations of these three dyes used for experimental results in Fig 5.2 were 25uM, 10uM and 10uM respectively. Alexa Fluor 546 was used in the form of an oligo labeled with the dye as an indicator dye for our experiments including this dye. All the reagents including fluorescent dyes were diluted to the required concentrations with the reaction buffer included with the MMP substrate sampler kit. 10ug/mL of BSA was added to the reaction buffer to prevent adsorption of reagents to device and tubing walls. The oil phase for our experiments consisted of FC-40 (3M) and 1H, 1H, 2H, 2H-Perfluoro-1-octanol (SigmaAldrich) (4:1 v/v). The surfactant oil phase consisted on FC40 with 2% fluorosurfactant (RAN Biotechnologies) by weight.

Input reagent concentrations for various experiments

The input dye concentrations used for the image in Fig 5.2 were Alexa350: 25uM, Alexa488: 10uM and Alexa647: 10uM. Four different concentrations of these dyes generated in droplets from each of these inputs were 0X, 0.1X, 0.2X and 0.3X where X is the original input concentration of each dye.

The input dye concentrations used for data in Fig 5.3 were Alexa488: 50nM and Alexa546: 50nM. Five different concentrations of each dye apparent in droplet format from Fig 5.3 were 0X, 0.1X, 0.2X, 0.3X and 0.4X where X is the original input concentration of each dye

For the experimental results in Fig 5.4 and 5.5, the input concentration of all MMPs was 5ng/uL while the concentration of all substrates was 5uM. 1X MMP concentration in droplets for these figures refers to 1ng/uL concentration while 1X substrate concentration refers to 1uM concentration.

For the experimental results in Fig 5.8, the input concentration of all MMPs was 7.5ng/uL while the concentration of all substrates was 7.5uM. 1X MMP concentration in droplets for these results refers to 1ng/uL concentration while 1X substrate concentration refers to 1uM concentration.

For the experimental results in section 5.4.6, the input concentration of all MMPs was 7.5ng/uL while the concentration of all substrates was 7.5uM. 1X MMP concentration in droplets for these results refers to 0.5ng/uL concentration while 1X substrate concentration refers to 0.5uM concentration.

Peptide substrate sequences:

SB2: QXL520TM -Pro-Leu-Ala-Leu-Trp-Ala-Arg-Lys(5-FAM)-NH2

SB3: QXL520 TM -Pro-Leu-Gly-Cys(Me)-His-Ala-D-Arg-Lys(5-FAM)-NH2

SB4: 5-FAM-Pro-Leu-Ala-Nva-Dap(QXL520 TM)-Ala-Arg-NH2

SB5: 5-FAM-Pro-Leu-Gly-Leu-Dap(QXL520 TM)-Ala-Arg-NH2

SB8: QXL520 TM -Arg-Pro-Lys-Pro-Leu-Ala-Nva-Trp-Lys(5-FAM)-NH2

SB9: QXL520 TM -Arg-Pro-Leu-Ala-Leu-Trp-Arg-Lys(5-FAM)-NH2

SB11: 5-FAM-Pro-Cha-Gly-Nva-His-Ala-Dap(QXL™520)-NH2

SB12: 5-FAM-Arg-Pro-Lys-Pro-Tyr-Ala-Nva-Trp-Met-Lys(QXL520 TM)-NH2

SB15: QXL520 TM -γ-Abu-Pro-Gln-Gly-Leu-Dab(5-FAM)-Ala-Lys-NH2

5.4.3: Experimental protocol

5.4.3.1 On-chip experiments

A set of solenoid valves was used to control the on/off status of the valves on the device. Initially, all the reagent inputs on the device were primed with the respective reagent. Any residual reagents in the central channel following this process were flushed out using the oil phase. Following this, the valve actuation sequence corresponding to the reagent combinations to be generated on the device was executed by a computer. The valve actuation sequence for each droplet consisted of the following steps 1) Buffer droplet generation 2) Droplet displacement in front of other reagent inputs for reagent injection 3) Droplet displacement to the incubation region through injection of oil phase in the central channel 4) Further displacement of droplet in the incubation channel through injection of a surfactant oil phase in the central channel. 5) Closing all valves on the device for dissipation of pressure in the central channel. After ensuring proper operation of the device on a microscope, the device is moved to a fluorescence detection setup. The fluorescence detection setup we used for our experiments is capable of dual channel excitation (488nm, 552nm) as well as dual band detection (506-534nm and 608-648nm). The detection volume of the fluorescence detection setup was placed at the detection region of the device for continuous sensing of fluorescence from droplets passing that region. The device was maintained at room temperature for all the experiments.

5.4.3.2 Off-chip experiments

For off-chip experimental results used in Fig 5.5 and 5.8, MMP and substrate concentrations identical to those being compared against in the droplet format were generated in 20uL reactions in a 96 well plate format. The fluorescence from the 96 well plate with these reaction mixtures was then monitored on a CFX96 Real-Time PCR detection system (Bio-Rad Laboratories, Inc).

5.4.3.3 Data Analysis on-chip experiments

Fluorescence data obtained from droplet sequences generated on chip was further processed through custom software written in Matlab. This software identified various droplets in a data trace and generated various statistics obtained from the data collected from each droplet. The average droplet fluorescence intensity identified by this software for each droplet was then used to estimate MMP activity rates shown in Fig 5.5 and 5.8. Each repeat of a droplet sequence consisted of substrate only controls for each substrate type and concentration. The average fluorescence intensity of a substrate-only control droplet was subtracted from the average fluorescence intensity of a MMP-substrate combination droplet (with same substrate concentration) and this intensity difference was converted to substrate concentration difference using the standard curve in section 5.4.5. The substrate concentration difference thus obtained was then divided by the droplet transit time on the device (~12min) to estimate MMP activity rates for that particular MMP-substrate combination.

5.4.3.4 Data Analysis off-chip experiments

For a fair comparison between on-chip and off-chip experiments, MMP activity rate was estimated from off-chip experiments in a manner similar to on-chip experiments. The fluorescence intensity reading from a substrate only control sample was subtracted from a MMP-substrate combination reaction for the same substrate concentration at the same time point (12mins after injection of enzyme into the reaction mixture). The difference in fluorescence intensities was again converted to substrate concentration difference, using the standard curve for off-chip experiments in section 5.4.5. This substrate concentration difference was then divided by the time for which the enzyme was added to the reaction mixture (12 min) to estimate MMP activity rate for that particular MMP-substrate combination.

5.4.4: Determining maximum reagent dilution on device

To generate maximum reagent dilution on the device, we tested the smallest reagent injection possible on our device. To conduct this experiment we generated various dilutions of Alexa Fluor 546 dye on our device. The Alexa Fluor 546 input was maintained under a low pressure of 1psi while the buffer input was maintained at a high pressure of 10psi. We then generated a droplet sequence which included droplets containing Alexa Fluor 546 injections generated using valve opening times of 0.0125, 0.05, 0.0875, 0.125, 0.1625, 0.2, 0.2375 and 0.275 seconds for the valve corresponding to the Alexa Fluor 546 input. We also included a buffer-only droplet at the beginning of the droplet sequence as well as an Alexa Fluor 546 droplet without any dilution at the end of the sequence. Fluorescence data collected from four repeats of this droplet sequence can be seen in Fig 5.6. We observed that a valve opening time of 0.0875 seconds was necessary to observe reliable injection of reagent into the droplets. The maximum dilution of the dye obtained for this valve opening time was 0.0066X, calculated as the ratio of the average fluorescence intensity of the droplet corresponding to 0.0875 second valve opening time to the average fluorescence intensity of the undiluted Alexa Fluor 546 droplet at the end of the droplet sequence.

5.4.5 Fluorescence standard curve

Various concentrations (2, 1, 0.5, 0.25, 0.125, 0.0625, 0.03125 and 0.015625 μM) of the fluorescence reference standard included in the MMP substrate sampler kit were used to generate a standard curve relating fluorescence intensity with substrate concentration. To generate the standard curve for the optical setup used with the microfluidic device, a train of droplets was generated using different concentrations of the reference standard for fluorescence measurement to closely mimic the experimental conditions on the device. Excellent linear relation was observed between reference standard concentration and the measured fluorescence intensities (Fig 5.7).

Similarly fluorescence intensities of the same set of concentrations of the reference standard were measured on the CFX96 Real-Time PCR detection system used for fluorescence monitoring from off-chip experiments. The plot of the measured fluorescence intensities against the corresponding reference standard concentrations shows linear relation between the two variables (Fig 5.7).

5.4.6 Long droplet sequence generation on device

As a proof of principle, we generated a large sequence of droplets containing 650 unique MMP-substrate combinations on a single device. Average fluorescence intensities obtained from two repeats of droplets corresponding to each unique combination are shown in the two matrices in Fig 5.9. Plots of measured fluorescence intensities from different MMP-substrate combinations against each other for different repeats show good linear correlation indicating repeatable operation of the device over long periods of time (Fig 5.10).

Fig 5.1 MMP screening platform. Step 1: Droplet assembly through microfluidic valve (thin black colored channels) controlled injection of desired MMP(s) and substrate(s) in a buffer droplet Step 2: Incubation of assembled MMP-substrate droplets in the incubation channel on the device. Step 3: Serial interrogation of droplets through Confocal Fluorescence Spectroscopy while preserving the order of generation, precluding the need for a barcode to identify the composition of each droplet

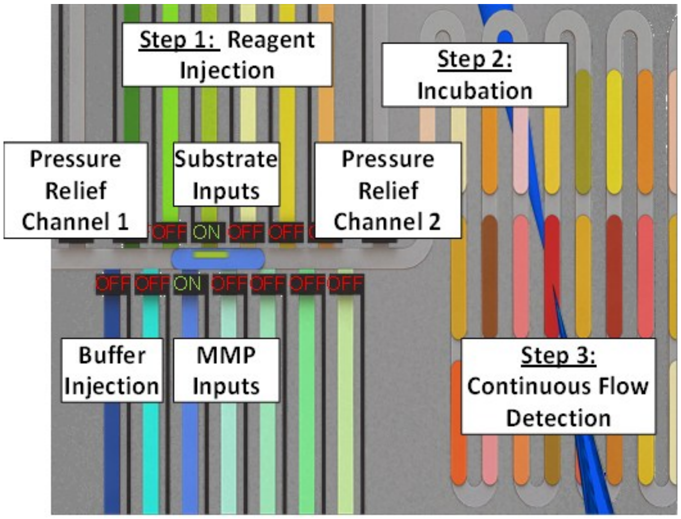
Step 1: Reagent Injection
Step 2: Incubation
Pressure Relief Channel 1
Substrate Inputs
Pressure Relief Channel 2
OFF
ON
OFF
OFF
OFF
OFF
ON
OFF
OFF
OFF
OFF
Buffer Injection
MMP Inputs
Step 3: Continuous Flow Detection

Fig 5.2 A series of fluorescent droplets generated on a single device: Each white square contains three images of a single droplet collected using DAPI, FITC and Cy5 filter sets on a fluorescence microscope from the bottom to top respectively. The droplets represent all possible combinations of four different intensities of three different fluorescent dyes (Alexa350, Alexa488 and Alexa 647) generated on the device.

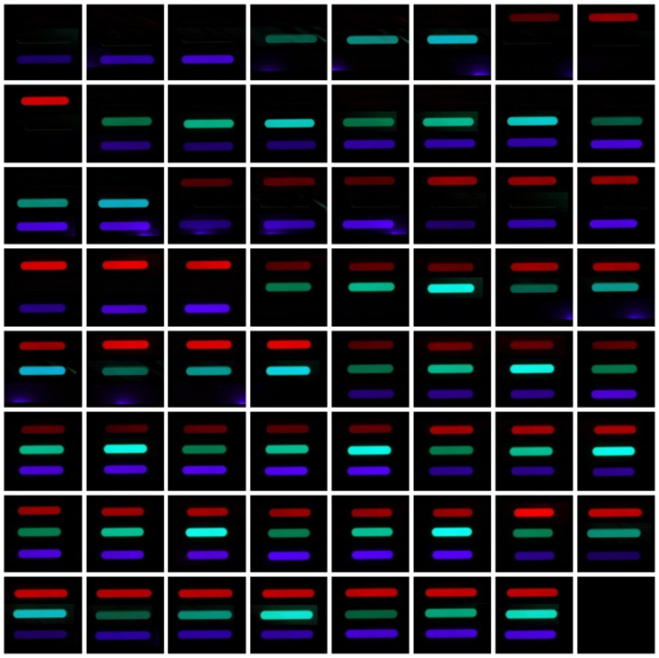

Fig 5.3 Droplet composition control and serial droplet fluorescence detection on the device: The two data traces show two repeats of a sequence of 24 droplets generated on the device. The green trace indicates fluorescence from the Alexa488 channel (506-534nm) while the orange trace indicates fluorescence from the Alexa546 channel (608-648nm). The fluorescence data indicates the capability of the device to independently control the concentration of different reagents in individual droplets. The plot on the bottom indicates average fluorescence of each individual droplet in the sequence. The error bars indicate the standard deviation in average fluorescence over ten repeats of the sequence.

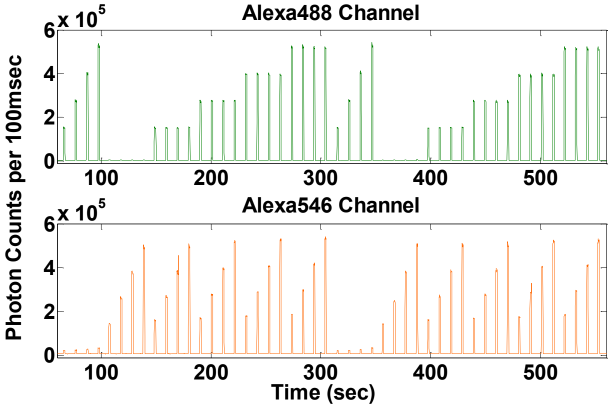
Alexa488 Channel
x 10^5
6
4
2
0
100
200
300
400
500
Alexa546 Channel
x 10^5
6
4
2
0
100
200
300
400
500
Photon Counts per 100msec
Time (sec)

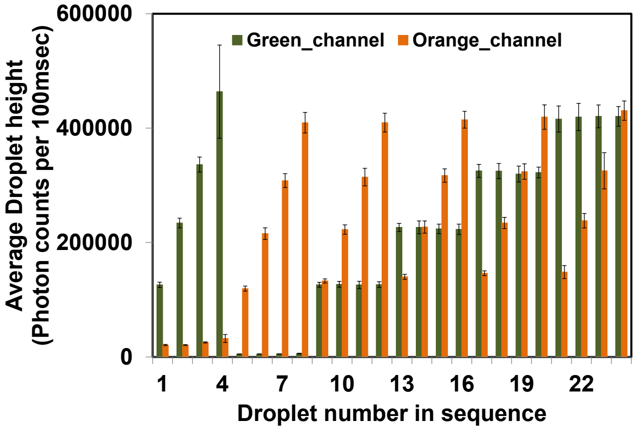
Green_channel
Orange_channel
600000
400000
200000
0
Average Droplet height
(Photon counts per 100msec)
1
4
7
10
13
16
19
22
Droplet number in sequence

Fig 5.4 MMP-substrate assay on device: The two data traces indicate fluorescence obtained from two repeats of a sequence of droplets containing different MMP-substrate combinations. The FAM channel indicates fluorescence from the FRET-peptide substrates cleaved by different MMPs. Alexa546 dye is used to insert a few 'beacon' droplets (Green peaks in Alexa546 channel) into the droplet sequence without interfering with the assay channel. The presence of beacon droplets in the sequence at predetermined positions with respect to other droplets can be used as an indicator of proper operation of the device without any unwanted droplet merging/splitting. The fluorescence from the non-beacon droplets in the Alexa546 channel is due to bleeding of some fluorescence from the FAM channel into the Alexa546 channel

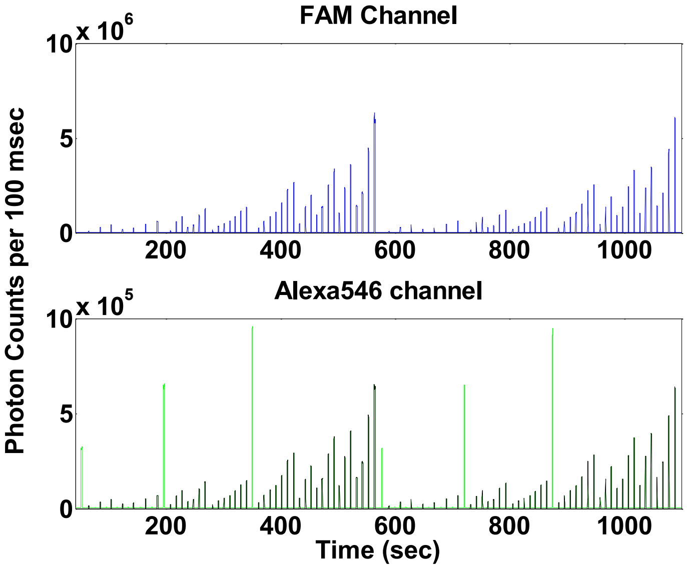
FAM Channel
10 x 10^6
5
0
200
400
600
800
1000
Alexa546 channel
10 x 10^5
5
0
200
400
600
800
1000
Time (sec)
Photon Counts per 100 msec

Fig 5.5 MMP activity comparison between on and off-chip experiments: The cleavage rates of different MMP types against different substrates estimated from corresponding droplets on the device are compared against cleavage rates estimated for same reaction conditions from off-chip experiments. (**MMP1_1:** MMP1 at 1X concentration, **SB9_2_chip:** Substrate SB9 at 2X concentration on-chip, **SB12_1_bulk:** Substrate SB12 at 1X concentration off-chip)

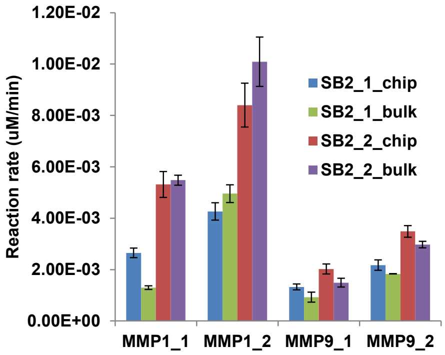
Reaction rate (uM/min)
1.20E-02
1.00E-02
8.00E-03
6.00E-03
4.00E-03
2.00E-03
0.00E+00
MMP1_1
MMP1_2
MMP9_1
MMP9_2
SB2_1_chip
SB2_1_bulk
SB2_2_chip
SB2_2_bulk

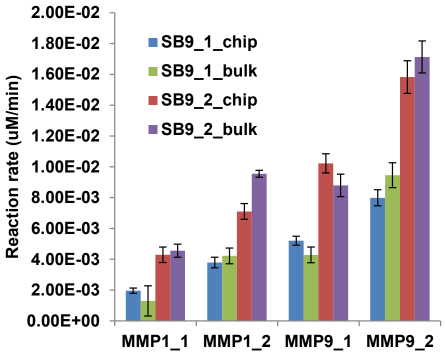
Reaction rate (uM/min)
2.00E-02
1.80E-02
1.60E-02
1.40E-02
1.20E-02
1.00E-02
8.00E-03
6.00E-03
4.00E-03
2.00E-03
0.00E+00
MMP1_1
MMP1_2
MMP9_1
MMP9_2
SB9_1_chip
SB9_1_bulk
SB9_2_chip
SB9_2_bulk

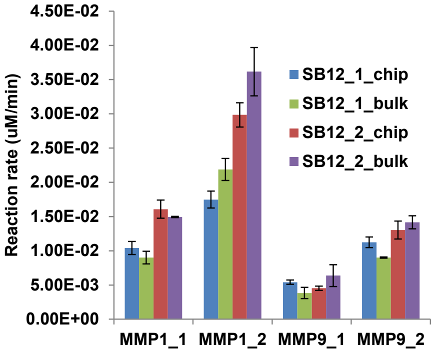
Reaction rate (uM/min)
4.50E-02
4.00E-02
3.50E-02
3.00E-02
2.50E-02
2.00E-02
1.50E-02
1.00E-02
5.00E-03
0.00E+00
MMP1_1
MMP1_2
MMP9_1
MMP9_2
SB12_1_chip
SB12_1_bulk
SB12_2_chip
SB12_2_bulk

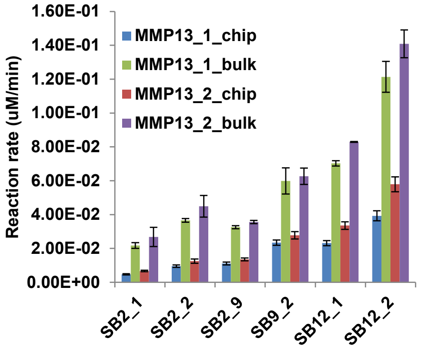
Reaction rate (uM/min)
1.60E-01
1.40E-01
1.20E-01
1.00E-01
8.00E-02
6.00E-02
4.00E-02
2.00E-02
0.00E+00
SB2_1
SB2_2
SB2_9
SB9_2
SB12_1
SB12_2
MMP13_1_chip
MMP13_1_bulk
MMP13_2_chip
MMP13_2_bulk

Fig 5.6 Largest reagent dilution generated on the device: Left panel: The data trace indicates four repeats of a sequence of droplets generated to test the largest reagent (Alexa Fluor 546) dilution that can be produced on our device. Each sequence ends with an undiluted reagent droplet to indicate the scale of dilution. **Right panel:** Average fluorescence intensities of the droplets in the sequence shown in the left panel. Error bars indicate standard deviation over four repeats of the sequence.

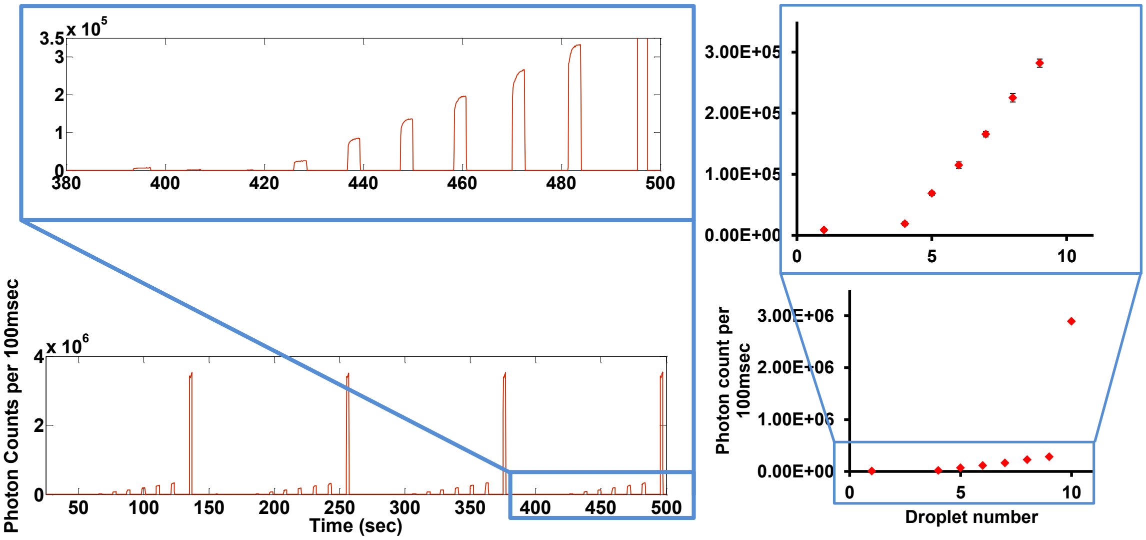

x 10^5
3.5
3
2
1
0
380
400
420
440
460
480
500
Photon Counts per 100msec
x 10^6
4
2
0
50
100
150
200
250
300
350
400
450
500
Time (sec)
3.00E+05
2.00E+05
1.00E+05
0.00E+00
0
5
10
Photon count per 100msec
3.00E+06
2.00E+06
1.00E+06
0.00E+00
0
5
10
Droplet number

Fig 5.7 Standard curves. Left panel: The data trace on top shows four repeats of a droplet sequence generated on device with different concentrations of fluorescent substrate reference standard. The average fluorescence intensity data extracted from this droplet sequence is plotted against the known reference standard concentrations in the droplets in the bottom plot to generate a standard curve for on-chip experiments. **Right panel:** A plot of measured fluorescence intensity (on the CFX96 Real-Time PCR detection system) against corresponding concentrations of the reference standard.

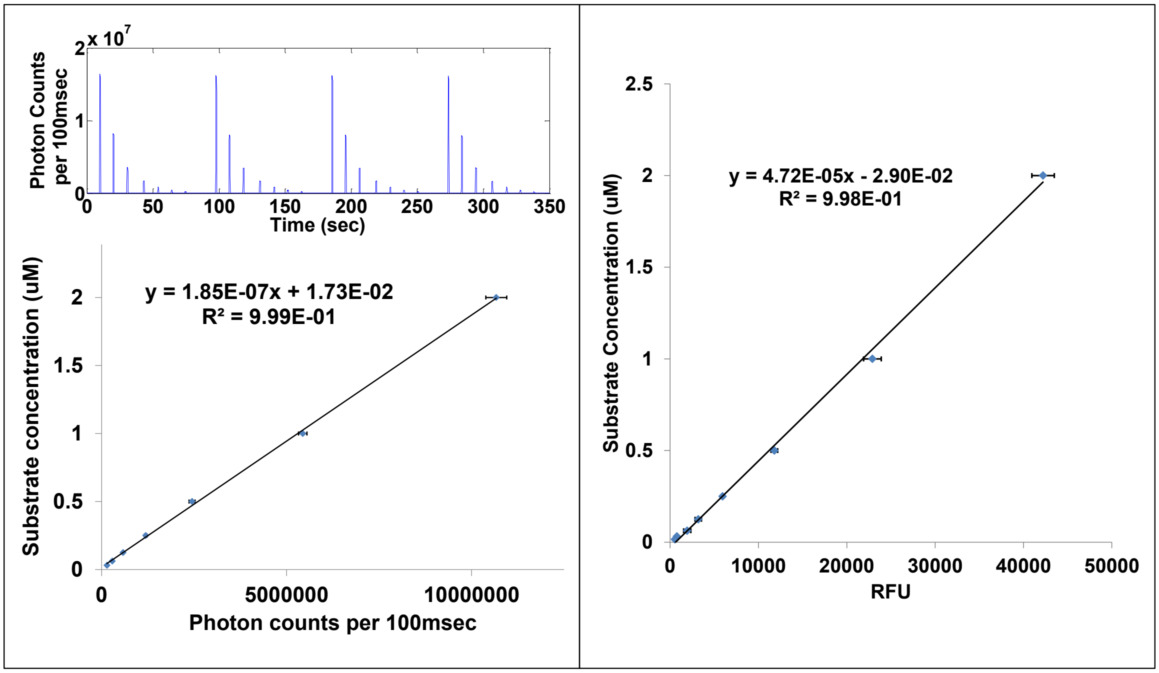
Photon Counts per 100msec
2 x 10^7
1
0
0
50
100
150
200
250
300
350
Time (sec)
Substrate concentration (uM)
y = 1.85E-07x + 1.73E-02
R² = 9.99E-01
2
1.5
1
0.5
0
0
5000000
10000000
Photon counts per 100msec
Substrate Concentration (uM)
2.5
2
1.5
1
0.5
0
y = 4.72E-05x - 2.90E-02
R² = 9.98E-01
0
10000
20000
30000
40000
50000
RFU

Fig 5.8 MMP activity comparison between on and off-chip experiments: (**MMP1_chip:** MMP1 at 1X concentration on-chip, **MMP1_bulk:** MMP1 at 1X concentration off-chip, **SB3_1:** Substrate SB3 at 1X concentration)

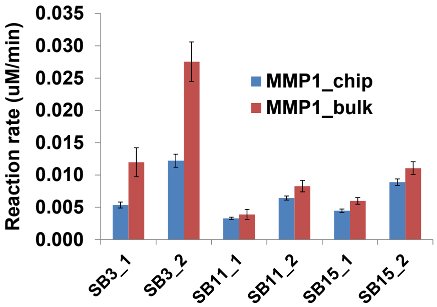
Reaction rate (uM/min)
0.035
0.030
0.025
0.020
0.015
0.010
0.005
0.000
MMP1_chip
MMP1_bulk
SB3_1
SB3_2
SB11_1
SB11_2
SB15_1
SB15_2

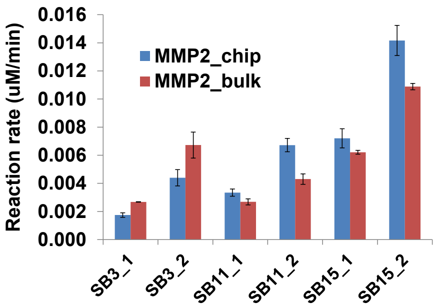
Reaction rate (uM/min)
0.016
0.014
0.012
0.010
0.008
0.006
0.004
0.002
0.000
MMP2_chip
MMP2_bulk
SB3_1
SB3_2
SB11_1
SB11_2
SB15_1
SB15_2

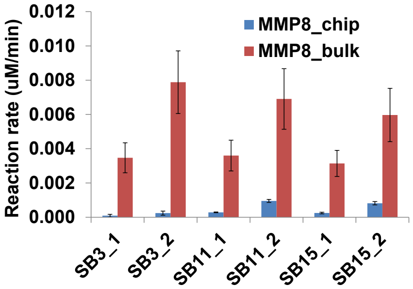
Reaction rate (uM/min)
0.012
0.010
0.008
0.006
0.004
0.002
0.000
MMP8_chip
MMP8_bulk
SB3_1
SB3_2
SB11_1
SB11_2
SB15_1
SB15_2

Fig 5.9 Average measured droplet fluorescence intensities from two repeats of 650 unique MMP-substrate combinations. The numbers on both axes indicate concentrations (1:1X concentration, 2: 2X concentration etc) while the labels indicate the corresponding reagent (e.g. SB3, MMP1 etc)

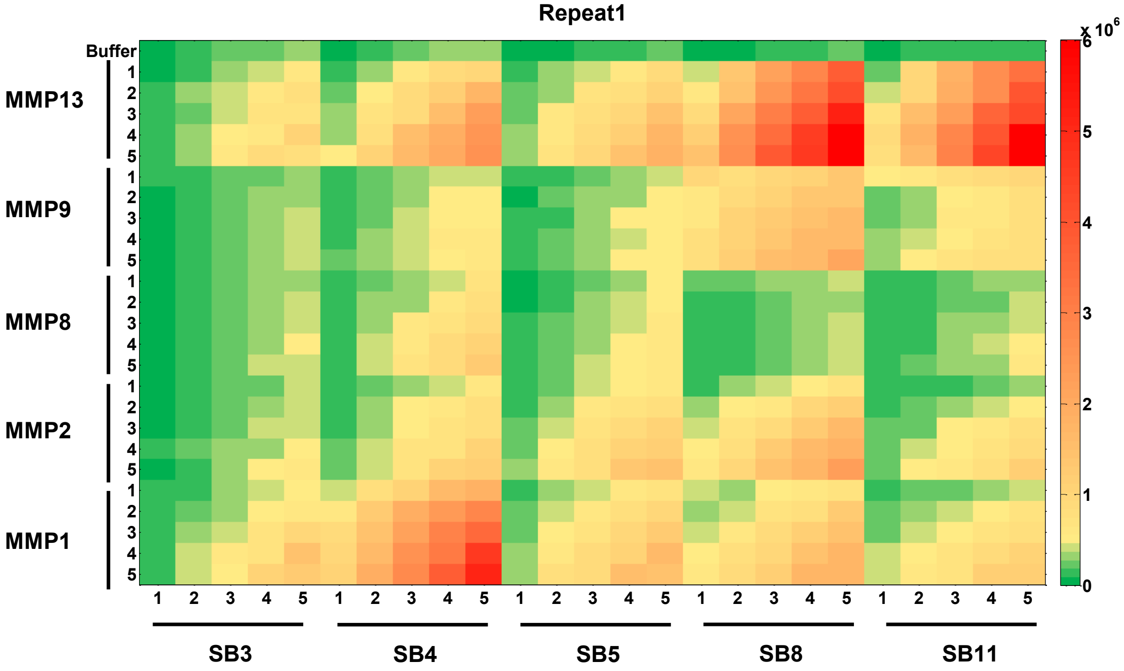
Repeat1

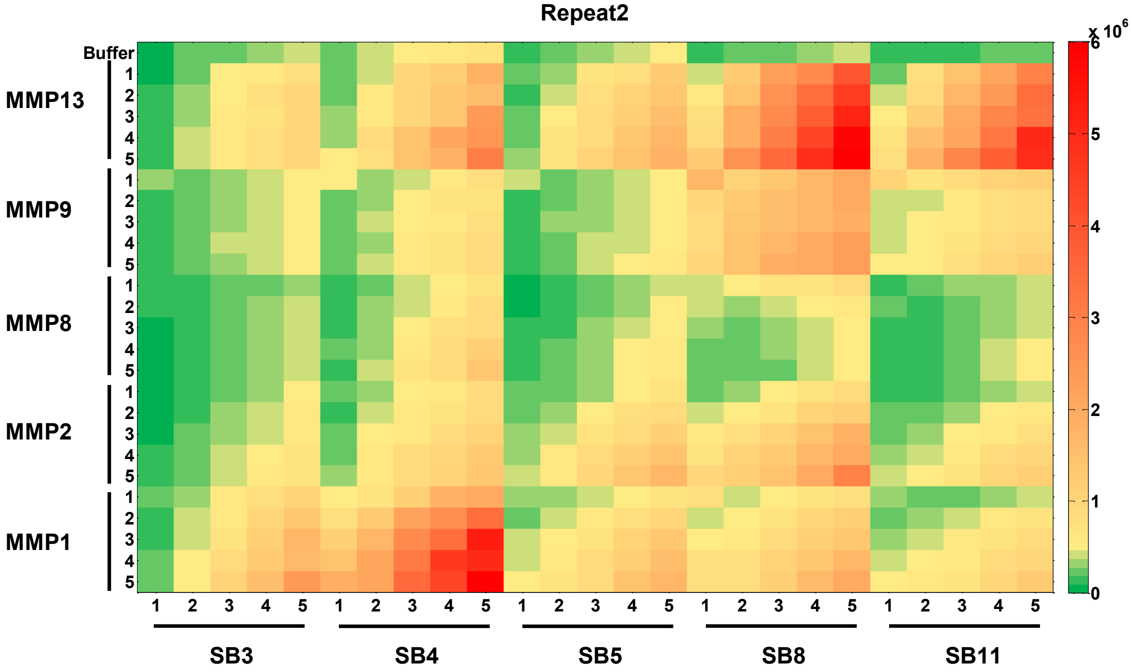
Repeat2

Fig 5.10 Average fluorescence intensities measured from different repeats for each unique MMP-substrate combination plotted against each other: good linear correlation indicating repeatable operation of the device over long periods of time can be seen.

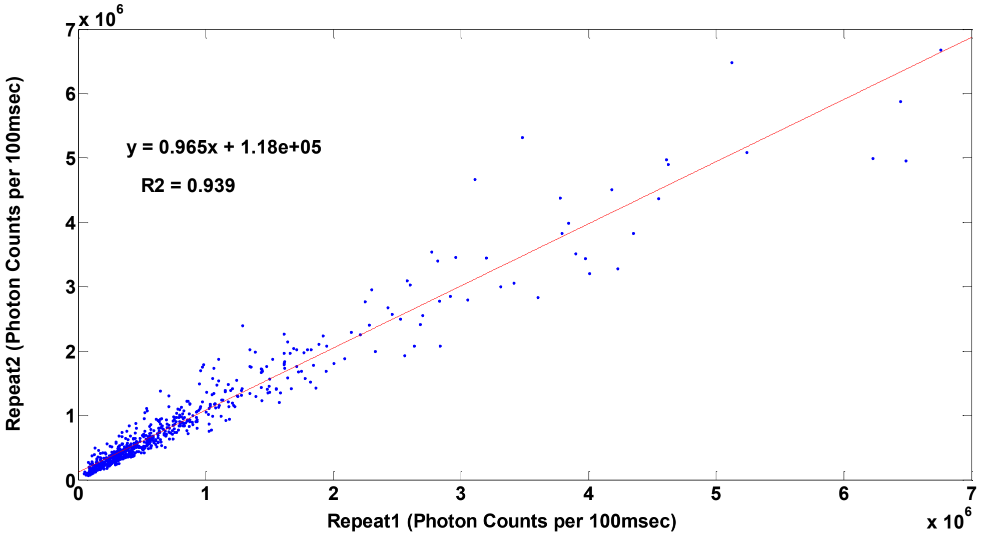
x 10^6
y = 0.965x + 1.18e+05
R2 = 0.939
Repeat2 (Photon Counts per 100msec)
Repeat1 (Photon Counts per 100msec)
x 10^6
0
1
2
3
4
5
6
7

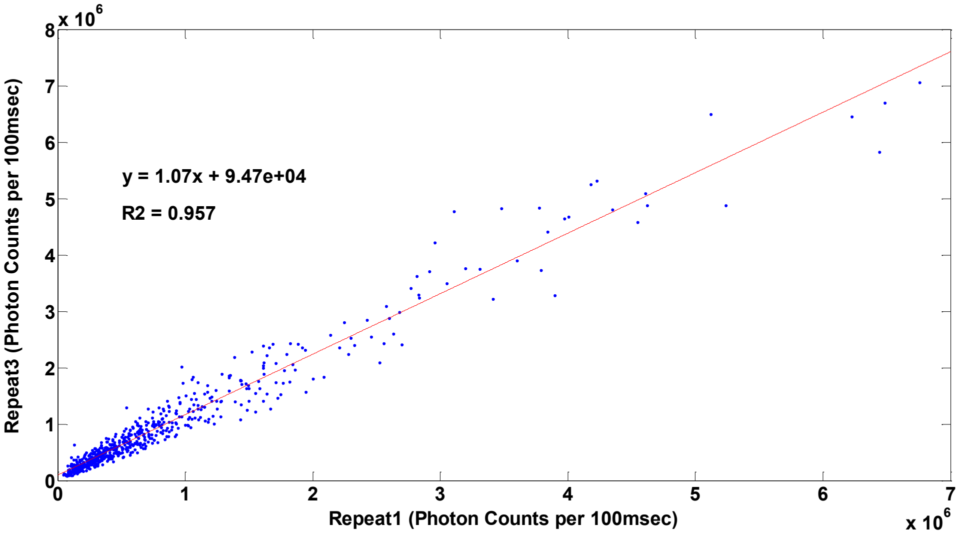
x 10^6
y = 1.07x + 9.47e+04
R2 = 0.957
Repeat3 (Photon Counts per 100msec)
Repeat1 (Photon Counts per 100msec)
x 10^6
0
1
2
3
4
5
6
7
8

Chapter 6: Microfluidic platform for on-demand generation of spatially indexed combinatorial droplets

Zec, Helena, Tushar D. Rane, and Tza-Huei Wang. "Microfluidic platform for on-demand generation of spatially indexed combinatorial droplets." Lab on a Chip12.17 (2012): 3055-3062. Reproduced by permission of The Royal Society of Chemistry

6.1 Background

Droplet microfluidic platforms are in the early stages of revolutionizing high throughput and combinatorial sample screening for bioanalytical applications(1, 2, 86, 87). Droplet-based systems have many advantages over conventional microtiter techniques for combinatorial screening applications. Microfluidic droplets function as miniaturized reaction containers consist of pico or nanolitre volumes, thereby facilitating reduced reagent consumption and background noise(87). Furthermore, carrier fluid shields each droplet, mitigating the problems of absorption onto solid surfaces and contamination. The high surface area to volume ratio of droplets also facilitates shorter heat and mass transfer times, leading faster reaction kinetics in droplets(1, 19).

Recent publications in the microfluidic domain boast high throughput capability of their respective droplet-based platforms. Compartmentalization of many small droplets allows isolation of interfering molecules into separate volumes, thereby facilitating digital analysis of biological entities. Several examples have been demonstrated including: droplet platforms for high throughput single copy DNA amplification(21, 69, 88), droplet platforms for high throughput single cell screening(20, 22, 89) as well as droplet platforms for single organism screening(90, 91). These droplet platforms are capable of high resolution screening of the biological contents at the level of the fundamental unit. However, they are limited to the analysis of a single sample under a homogeneous reagent condition.

The aforementioned droplet platforms are incapable of addressing the needs of numerous applications which require high degrees of multiplexing as well as high-throughput analysis of multiple samples. Some examples include genetic fingerprinting for forensics(92), single nucleotide polymorphism (SNP) analysis for crop improvement and domestication(93), genotyping required for identification of genes associated with common diseases(94) and generation of a blood donor genotype database for better matching between recipient and donor to prevent adverse transfusion reactions(95). All these applications require multiplexed screening of a single sample with a panel of reagents (or markers) and rapid screening of a large number of samples to generate the required databases.

In recent years, there have been attempts to expand the capacity of droplet platforms for the analysis of a biological or chemical sample with multiple reagents. One of the well-tested platforms has been the droplet platform developed by RainDance Technologies, for massively parallel PCR enrichment for DNA sequencing(96). This platform involves a multistep approach with generation of a large library of PCR reagent droplets by a microchip, followed by merging of these reagent droplets with sample droplets generated from a DNA sample on a second device. These sample-reagent hybrid droplets are then collected in standard PCR tubes for thermocycling, followed by fluorescence detection and sequencing. In this platform, the content of each individual droplet is unknown and is decoded only by offline nucleic acid sequencing. Therefore, it cannot be applied to other applications that require real-time detection(87). A solution to this problem is to associate a unique optical-code with each reagent prior to mixing with the sample(5). However, an optical-coding scheme based on fluorescence intensity is practically limited to a small number of 'codes' due to the small allowable number of fluorophores without spectral crosstalk and the limited dynamic range of the optical detection setup being used(87). Furthermore, the electrocoalescence technique used in such platforms for droplet merging is susceptible to errors of no fusion caused by an excess of droplets of a reagent or unintended fusion of more than two droplets due to highly stringent synchronization requirements(97). A recent article demonstrated a picoinjector which can overcome this problem and be used to add controlled volumes of multiple reagents to sample droplets using electromicrofluidics(98). However, similar to droplet platforms discussed earlier, the content of each individual droplet is unknown unless a barcode is included in each individual droplet.

Alternatively, a series of articles adopted a cartridge technique for increasing the throughput of the droplet platform(99). This technique involves generation of an array of reagent plugs in a capillary (cartridge), which are sequentially introduced to a simple microfluidic device for merging with a single substrate. The reagent plugs can be further digitized into smaller droplets prior to merging with the sample. As the length of the capillary can be very long, the number of reagents to screen against the sample is virtually limitless. This technique has been applied to many applications including protein crystallization(99) and study of bacterial susceptibility to antibiotics(25). Although the aforementioned droplet and cartridge platforms are capable of high throughput and multiplexed analysis, they are still limited to screening of a single sample at a time. Recently, a microfluidic platform was proposed for combinatorial chemical synthesis in picolitre droplets, where droplets of one library of reagents were fused at random with droplets containing a different set of reagents(97). This platform has the potential of generating a large set of possible combinations of different reagents. However, as afore-discussed, the unknown identity of the compounds within individual droplets precludes its use for many screening applications that require real-time detection.

Here we present a droplet platform capable of on-demand generation of nanolitre droplets of combinational mixtures of samples and reagents, needed for biochemical screening applications that require multiplexing and high-throughput capability. On-demand droplet generation and manipulation using pneumatic valves has been demonstrated by other groups in the past(100-102). However, these platforms have focused on generating multiple reagent combinations using fixed number of inputs to the device, severely limiting the number of possible sample-reagent combinations being generated on the device. The droplet platform reported in this article uses a linear array of sample plugs as an input to the device, removing the limitation imposed by the number of inputs to the device. Initially, a preformed linear array of sample plugs separated by a carrier fluid is flowed from the cartridge into the microfluidic device, wherein each plug is digitized by a pneumatic valve into smaller sample daughter droplets. The volume of the resulting daughter droplet can be precisely controlled by varying the valve opening time and the back pressure on the cartridge containing sample plugs. The daughter droplets are then directly injected with reagents in a synchronization-free manner. The microfluidic design features a robust fusion module which exploits local channel geometry for synchronization-free injection of reagents into each sample daughter droplet. After reagent injection into a sample droplet, our microfluidic device introduces additional carrier fluid containing surfactant to the channel containing the sample-reagent hybrid droplet array to prevent unwanted merging of these droplets on the device. In the proposed microfluidic device, droplets are indexed by their layout in a 1D array, enabling the identification of the contents of each droplet by spatial indexing.

Spatial indexing as a means for identification of droplet content obviates the need for a limiting optical barcoding scheme.

6.2 Materials and Methods

6.2.1 Serial Sampling Loading System

The sample library was generated using a custom-designed Serial Sample Loading System (SSL). Fig 6.2 is a schematic illustrating the functioning of the SSL system. Briefly, the SSL system was designed to be compatible with Costar 96-well plates (Corning). Initially the wells on a Costar 96-well plate are filled with the samples and the carrier fluid to be used for generating the sample plug array. An Aquapel (PPG Industries) treated silica capillary is then attached to a capillary adapter on the SSL system, which is also connected to a positive pressure input. A sample well is then interfaced with the capillary through the capillary adapter. Application of positive pressure to the sealed sample well for a controlled amount of time is then used to drive a sample plug from the well into the capillary. This sequence of steps is then repeated to load alternating sample and carrier fluid plugs into the capillary (Fig. 6.2b). More detailed information on the structure and operation of different components of the SSL system can be found in the section 6.5.4.

6.2.2 Fabrication of the Master Molds for the Microfluidic Device

The fluidic layer on the microfluidic device features five different heights of microfluidic channels (Fig. 6.3b and c). As a result, the fluidic mold consists of five different layers of photoresist. The fluidic channel heights in these five different photoresist layers were expected to be 25 µm, 50 µm, 100 µm, 200 µm and 360 µm. The photoresist used for the 25 um layer was SPR 220-7.0 (Rohm & Haas), while the rest of the layers were fabricated using SU-8 3050 (MicroChem). Fabrication was performed using standard photolithography techniques. Briefly, a SPR 220-7.0 layer was spin coated on a 4 inch silicon wafer. This layer was patterned using photolithography and hard baked to generate a rounded channel cross section, required for effective valve closure, as has been described earlier(36). For all other layers, SU-8 3050 was spin-coated on the wafer and patterned using standard photolithography, excluding the developing step. This technique was found to be very effective in preventing generation of bubbles and non-uniform coating of photoresist on the wafer due to the presence of features from earlier layers on the wafer. A single developing step for all four SU-8 3050 layers was used to remove excess photoresist on the wafer (Fig 6.7). The control layer for the microfluidic device on the other hand consisted of microfluidic channels of a single height. As a result, the mold fabrication for the control layer was relatively simpler, with a single layer of SU-8 3050 photoresist, 50 µm in height.

6.2.3 Microfluidic Device Fabrication

The microfluidic devices were fabricated using multilayer soft lithography techniques(36). The protocol differed slightly from our standard protocol(33, 34, 48) due to the need for proper functioning of push-down valves(103) while accommodating tall features (up to 360 μm) on the fluidic layer. The thickness of the polydimethylsiloxane (PDMS) membrane separating the control layer and the fluidic layer in a microfluidic device needs to be less than ~50 μm, for complete valve closure at reasonable pressure (~30 PSI). However, the presence of fluidic regions as tall as 360 μm on the fluidic layer mold precluded the possibility of covering the entire fluidic layer mold with PDMS, while maintaining the thickness of the PDMS layer to a value less than 50 μm in the regions of the device containing valves. To overcome this problem, a modified three-layer fabrication process was developed. Detailed description of the fabrication process is included in section 6.5.2.

6.2.4 Capillary–to–Chip Interface

Following the microfluidic device fabrication, a silica capillary was attached to the 'capillary inlet' on the microfluidic device (Fig. 6.3b). The 360 μm tall channel region at the capillary inlet accommodates a silica capillary with an OD of 360μm. A 10 mm section of silica capillary is inserted horizontally into this tall channel on the device until it is flush with the 200 μm tall fluidic channel on the device. To seal the capillary to the chip and prevent leakage, PDMS was dispensed around the capillary at the interface between the capillary and the device. The PDMS tended to crawl into the 360 μm channel and surround the capillary, effectively sealing the capillary-to-chip connection. The final assembly was baked for at least 2 hours at 80ºC before usage.

6.2.5 Device control

All the inputs on the device were kept under constant pressure, with independent input pressure for 1) carrier fluid input, 2) all four reagent inputs and 3) carrier fluid with surfactant input. The pressure applied to the capillary input was controlled directly by the pressure controller used for the SSL system. All the valves on the device were controlled by an array of off-chip solenoid valves, as has been demonstrated earlier(34). We developed Matlab (Mathworks, Natick MA) software for computer control of the valve array. This software allowed us to execute a predetermined sequence of valve actuation with independent time control for each actuation. The opening of a valve corresponding to an input on the device led to the release of a droplet of fluid from that inlet into a central channel on the device. The volume of this droplet could be controlled through variation of the opening time of the valve.

6.2.6 Reagents

All the devices and capillaries were treated with Aquapel to render their surface hydrophobic. The testing of our platform was performed using food dyes (Ateco, Glen Cove, NY) to mimic different samples and reagents for easy visualization. The carrier fluid used to maintain the separation between sample plugs consisted of a perfluorocarbon (FC-3283) and a non-ionic fluorous-soluble surfactant (1H,1H,2H,2H-Perfluoro-1-octanol) mixed in a ratio of 8:1 by volume. The carrier fluid with surfactant consisted of FC-40 (3M) and 2% 'EA' surfactant (Raindance Technologies) by weight.

6.2.7 Sample plug and droplet volume estimation

We estimated the volume of sample plugs and sample droplets generated using the SSL system and the microfluidic device respectively. This volume estimation was performed by processing the images of these sample plugs or droplets using the software ImageJ(104). Specifically, for sample plug volume estimation, a series of sample (blue food dye) plugs were generated in a silica capillary using the SSL system. A colour image of these plugs was taken against the while background of a 'letter' sized sheet of paper using a standard Digital Single-Lens Reflex (DSLR) camera. This image was imported in ImageJ and the length scale was set to true length using the known length of the letter sized paper in the image. The lengths of the sample plugs were then manually measured for each plug using the 'Measure' function in ImageJ. The plug lengths could be converted to plug volumes with the known cross sectional area of the capillary.

For sample droplet volume estimation, we generated droplets made of blue food dye using one of the four reagent inlets on the microfluidic device, until the whole incubation region on the device was full of droplets. The whole device was then imaged using a DSLR camera. The image was imported in ImageJ and cropped to obtain an image of the incubation region on the device. This image was then converted to a binary image using colour thresholding to identify droplets over the background image. An estimate of the droplet area for each droplet in the image was then obtained using the 'Analyze Particles' function. This analysis was limited to particle areas larger than a lower threshold to exclude any particles and occasional satellite droplets from the analysis. The droplet areas thus estimated were then converted to droplet volume using the known depth of the incubation channel region (200 µm).

6.3 Results and Discussion

6.3.1 Overall Work Flow

Fig 6.1 is a schematic illustrating the functioning of the platform. Initially a cartridge (capillary) is loaded with a library of sample plugs forming a serial sample plug array: plugs are separated from each other by an immiscible carrier fluid. This cartridge is interfaced with a microfluidic device featuring multichannel architecture and pneumatic microvalves. The microfluidic device digitizes sample plugs into smaller daughter droplets on. Each sample daughter droplet then moves to the downstream fusion region where a specific reagent is injected into the sample daughter droplet. The reagent droplets are injected into the sample daughter droplet through controlled actuation of valves corresponding to the reagent inlets. Supp.

Video 6 shows this sequence of events. No strict synchronization or droplet detection module is necessary for fusion of sample and reagent to occur as the sample droplet is elongated in the fusion area (Supp. Video 7), exploiting the local channel geometry. The resulting sample-reagent droplet undergoes mixing and travels downstream to the incubation region on the device. After reagent injection, additional carrier fluid containing surfactant is released into the central channel on the device to stabilize sample-reagent hybrid droplets. The sequence of droplets is maintained throughout the device, precluding the need for a complicated barcoding scheme to identify the contents of each individual droplet.

6.3.2 Capillary-to-Chip Interface

Our prototype platform necessitated the capillary-to-chip interface design to allow for sample plug introduction on chip. This objective presented a unique challenge, since proper functioning of the platform requires smooth transition of sample plugs from the large ID of the capillary to shallow channels on the device in the valve regions. There have been demonstrations of capillary-to-chip interfaces in the past for introducing sample plugs from a capillary to a microfluidic device. However, the devices used don’t face this problem as they typically feature large channels with a valve-less design(25, 99). The capillary interface we designed (Fig. 6.3b and c) between the capillary and microfluidic chip was found to be effective in minimizing plug break up as plugs moved from the high ID (200 μm) of the capillary to the shallow channels on chip (25 µm). This transition consisted of 5 different channel sections with gradually reducing channel heights of 360 µm, 200 µm, 100 µm, 50 µm and 25 µm. This gradual transition minimizes the shear stress on the sample plug as it traverses from a capillary to the shallow channels on the chip, preventing its breakup in transit.

6.3.3 Droplet uniformity using mechanical valve based droplet generation

We examined the performance of the mechanical valves on our microfluidic device for their capability to control the droplet size generated. To conduct this experiment, we primed the incubation channel on the device with the carrier fluid. We then used one of the reagent inlets on the device for generating droplets made of blue-colored food dye into the incubation channel region. The two parameters which could be used to control the droplet size generated from a reagent inlet are 1) Input pressure to the reagent inlet ($P_{reagent}$) and 2) The opening time of the valve corresponding to the reagent inlet (T_{open}). Initially, we fixed the value of $P_{reagent}$ and generated droplets on the device for different values of T_{open}. Droplet generation was continued for each condition tested, until the incubation region on the device was completely full of droplets. We then estimated the volume for all these droplets using the image processing technique discussed in the 'Materials and Methods' section. The mean and standard deviation of fifty droplets generated for each condition was plotted against T_{open} in Fig. 6.4b. This experiment was repeated for three different fixed values of $P_{reagent}$. As expected, the linear relationship between droplet volume and T_{open} indicates excellent and predictable control of the device over droplet volume. Small standard deviation observed on the droplet volume also indicates excellent droplet uniformity for identical droplet generation conditions. This result is very important to ensure the capability of the device to generate droplets of various compositions on-demand.

6.3.4 Sample Digitization

We examined the capability of our device to digitize a set of sample plugs being supplied to the device into smaller sample daughter droplets. To conduct this experiment, we generated a set of sample plugs into a silica capillary using the SSL system. These sample plugs were delivered to the microfluidic device through the capillary inlet, under pressure provided by the pressure controller on the SSL system. For this experiment, the repeating sequence of steps executed on the device was as following: 1) Generate small droplet from a sample plug in the central channel, 2) Move the droplet towards incubation region with carrier fluid 3) Release small amount of carrier fluid with surfactant in the central channel. Repeating this set of steps led to generation of an array of sample droplets generated through digitization of sample plugs on the device. Examples of unmerged sample daughter droplets are shown in Fig. 6.6a (Sample droplets A, B, C and D). The order of the sample plugs in the capillary is consistently maintained on the device, even after the digitization operation. One shortcoming of this operation is the generation of non-uniform droplets towards the beginning and the end of the sample plugs. This is because the valve actuation sequence is continuously executed without any sensing of sample plug arrival on the device. However, the sample droplet uniformity is maintained throughout the rest of the sample plug. As the droplets generated on the device are stabilized with surfactant, undesirable merging of non-uniform droplets originating from the front- or back-end of plugs is avoided on the device.

6.3.5 Generation of droplets of combinatorial mixtures

In this section we demonstrate proof-of-concept generation of combinatorial mixtures from sample plugs and reagent droplets on our device. For discernibility, we chose to use different food dye solutions to simulate different samples and reagents. Fig. 6.5 shows how reagent injection operations are performed in the fusion region on our device (also shown in Supp. Video 6). First, a sample plug travels from the capillary on to the microfluidic device. This plug is then chopped into a smaller sample daughter droplet. This droplet is then moved to the downstream fusion zone through release of carrier fluid in the central channel on the device. As every single input on the device is controlled with an individual valve, the device functions like an assembly line with complete temporal and spatial control over every single operation, as against typical droplet generating devices where the carried fluid flow is continuous. This level of control also implies that the operation of the device can be paused and resumed with a completely new valve actuation sequence, on demand without affecting the existing droplets on the device. None of the droplet devices reported in literature so far has this capability to the best of our knowledge. A reagent droplet is then injected directly into the sample daughter droplet (Fig. 6.5a). The volume of reagent solution injected into the sample droplet can be controlled through variation of the opening time for the valve corresponding to the reagent inlet. Supp. Video 7 provides a close-up view to how reagent injection is performed. The fusion zone is designed such that the sample daughter droplet is sufficiently elongated within a region, which overlaps with all the injection ports of the interrogating reagents. This elongated droplet state removes the need for strict positioning accuracy requirements on the sample droplet for reliable injection of reagent into the sample droplet. In addition to demonstrating injection of a single reagent in a sample droplet, we have demonstrated injection of up to four reagents into a single sample droplet as shown in Fig. 6.5b. The concept of droplet elongation to aid reagent injection can be easily scaled to accommodate tens of reagent inlets, if desired.

After reagent injection, the sample-reagent droplet is driven further downstream with the help of carrier fluid. Following this, a small plug of carrier fluid with surfactant is released in the central channel for stabilizing the droplets in the incubation region. Using this scheme we can simultaneously take advantage of a surfactant-free zone in one area of the chip to promote sample-reagent merging while deliberately using surfactant in another area to increase droplet stability and prevent unwanted droplet merging.

Fig. 6.6 demonstrates the reliability of the fusion mechanism on our device. Fig. 6.6a is a table of 16 different sample-reagent combinations generated on a single chip through all possible merging combinations of four different sample daughter droplets (A: blue, B: yellow, C: green, D: water) with four different reagents (Reagent 1: orange, Reagent 2: water, Reagent 3: blue, Reagent 4: yellow) with the condition of merging exactly one sample with one reagent.

The micrographs in Fig. 6.6b show a repeating sequence of the sample-reagent hybrid droplets in the incubation region of the chip. The chip is operated such that the sample daughter droplets are merged with a repeating sequence of four different reagents. As a result a repeating sequence of four possible combinations generated through mixing a single sample with four different reagents can be seen in each individual micrograph. Once a sample plug is exhausted, the sample daughter droplets generated from the next incoming sample plug start merging with the same repeating sequence of reagents generating a repeating sequence of a new set of four different sample-reagent combinations in the incubation region on the chip.

The droplet monodispersity as well as the uniform spacing between droplets is clearly visible in these micrographs. The inset in Fig. 6.6b displays zoomed-in view of these micrographs of the incubation region illustrating two repeats of each sequence in the incubation region. These images also demonstrate the capability of the device to maintain the order in which droplets are generated, throughout the incubation region on the device. We have demonstrated 16 combinations in this instance, but by employing multiple (2, 3 or 4) reagent merging with sample daughter droplets, as demonstrated in Fig. 6.5b, many more combinations can be generated using our prototype device.

6.4 Conclusion

In summary, we have demonstrated a platform capable of preparing droplets from combinational mixtures of a large number of samples and reagents. This is accomplished by synchronization-free and detection-free fusion of sample daughter droplets and reagents. A key benefit of this architecture is the ability to scale this device to analyze N samples against M reagents (N x M) where N can range from hundreds to thousands without accompanying increase in device complexity. Additional reagent set multiplexing can be accomplished analogously by introducing linear arrays of reagent set plugs similar to sample introduction. Furthermore, this design allows for spatial indexing, by maintaining the sequence of droplets from generation throughout incubation, precluding the need for barcoding.

This platform presents a novel design with several important components: a unique SSL system which uses pressure to inject uniform volumes of sample into a capillary directly from an industry standard multi-well plate. This capillary is then interfaced with a microfluidic device using a novel capillary-to-chip connection. The microfluidic device is capable of combinatorial screening operations. Robust synchronization-free reagent injection is performed on the device based on a design which capitalizes on droplet elongation in the fusion zone on the device. In our prototype design up to 4 reagent droplets can be fused with a single sample droplet. However, by employing the same concept many more reagent inlets can be introduced on chip to perform merging operations. In addition, we have demonstrated a technique for reagent injection in droplets that capitalizes on controlling droplet surface chemistry by controlling surfactant concentration at different regions on the chip. That is, we have demonstrated a surfactant-free environment in the fusion zone on the device, thereby promoting reagent injection in sample droplets while the droplets are stabilized by surfactant in the incubation region.

For the microfluidic chip design, several areas can be explored to further enhance the operation of the chip. To make the transition of sample plugs from a capillary to the microfluidic device more gradual a photolithography process employing a grayscale mask could be used. This approach can generate very gradual reduction in channel cross section from a large capillary to shallow microfluidic channels on the device as against the 5 step reduction demonstrated in the current version of the device. Furthermore, reagents may be loaded in cartridge format to further enhance multiplexing capabilities. We expect the platform described here to be a promising candidate for combinatorial screening applications using droplet microfluidics.

6.5 Supplementary section

6.5.1 Mold Fabrication

The work flow used for fabricating the fluidic layer mold is illustrated in Fig 6.7. The mold consists of five different layers of photoresist with heights of 25 µm, 50 µm, 100 µm, 200 µm and 360 µm. The photoresist used for the 25 µm layer was SPR 220-7.0 (Rohm & Haas), while the rest of the layers were fabricated using SU-8 3050 (MicroChem). Initially a 25um tall SPR 220-7.0 layer was spin coated on a silicon wafer. This layer was patterned using photolithography and hard baked to generate a rounded channel cross section, required for effective valve closure. Rest of the layers were fabricated by stacking and patterning multiple layers of SU-8 3050 on the wafer. All the steps required for standard photolithography (Soft Bake, Exposure and Post Exposure Bake) are conducted for each layer of SU-8 3050, except the developing step. This step is conducted in common for all layers after the last SU-8 layer is patterned to remove excess unexposed photoresist from the wafer (Fig 6.7). This technique was found to be very effective in preventing generation of bubbles and non-uniform coating of photoresist on the wafer due to the presence of features from earlier layers on the wafer.

6.5.2 Device Fabrication and Operation

The microfluidic device for our experiments was fabricated using multilayer soft lithography technique. Standard dual layer microfluidic devices with push-down valves fabricated using polydimethylsiloxane (PDMS) require shallow fluidic channels to make sure the layer of PDMS between the fluidic and control layer is sufficiently thin (~50um) for complete closure of valves at low pressures (<30psi). The requirement of shallow fluidic channels is incompatible with our chip design. So we developed a modified fabrication process for our device. This modified soft lithography process is outlined in Fig 6.8. For this modified fabrication process, three different batches of PDMS were mixed. These varied in composition, and base to crosslinking agent ratios of 15:1, 10:1 and 6:1 were used, respectively. These batches were thoroughly mixed and degassed prior to use for device fabrication. The control layer mold was spin coated with a thick layer (~1 mm) of 6:1 PDMS and baked at 80°C for 7 mins. A thin layer of 15:1 PDMS was spin coated on the fluidic layer mold. The device was designed such that the valve regions on the device were placed in areas surrounded by shallow fluidic channels, ensuring uniform coverage of these regions with a thin layer of PDMS. The PDMS on the fluidic layer mold was then baked at 80°C for 6 minutes. The PDMS was removed from the control layer mold and the control layer was cut to the exact size of the valve regions on the device, while not covering any channels higher than 50 μm on the device (Fig 6.8). The control layer PDMS pieces were aligned with baked PDMS layer on the fluidic layer mold under a stereoscope. The fluidic layer mold with the aligned control layer was baked at 80°C for 20 mins to promote adhesion between the control layer and the fluidic layer. Following this, 49.5 g of 10:1 PDMS was poured on the fluidic layer mold, covering all features on the fluidic layer mold with a 3-4 mm thick layer of PDMS. The fluidic layer mold was then baked for at least 30 minutes at 80°C. Following this, the PDMS was removed from the fluidic layer mold and individual devices were cut. Fluidic access holes were then punched into the device and the device was bonded to a coverglass through oxygen plasma treatment.

6.5.3 Fusion Zone design

An important aspect of our microfluidic device is the robust synchronization-free fusion mechanism. This mechanism utilizes the cross-sectional area of the central channel on the microfluidic device for the merging operation. Fig 6.9 demonstrates the design criteria of the fusion region on our device. In our current design, the dimensions of the fusion zone, defined as the distance between the first and last reagent inlet (3800 μm), height (50 μm) and width (100 μm) of the central channel determine the volume of the fusion zone (19 nL). This volume of the fusion zone corresponds to the minimum volume of the sample daughter droplet, such that the droplet spans the entire length of all the reagent injection sites on the chip. As a result, the sample daughter droplet position doesn’t need to be finely controlled to inject different reagents in it. If there is a need for smaller reaction volumes, the cross-sectional area of the central channel can be modified to reduce the minimum volume of the sample daughter droplet required. For instance, reducing the fusion zone channel height from 50 μm to 10 μm will results in reduction in minimum required droplet volume from 19 nL to 3.8 nL (Fig 6.9). A similar approach can be used to accommodate more than four reagent inlets on the chip.

6.5.4 Serial Sample Loading System

6.5.4.1 Background

High throughput sample processing is a critical requirement for a large number of industries. Some examples include the agricultural, pharmaceutical and biotechnological industries(105). As a result, there is a constant drive for innovation in sample processing techniques, supporting these industries. One major breakthrough in this domain has been the application of various robotic sample handling techniques, to improve the speed of sample processing as well as to reduce the volume of reagents used per reaction. Although the robotic systems have become incredibly fast at sample processing operations, they are typically limited to operating with standard multi-well (96, 384 and 1536 well) plates. As a result, the typical sample volume consumption is on the order of microliters per reaction for such systems(105). Recent advances in the microfluidic domain show promise in overcoming this limitation of the robotic systems. Droplet-based microfluidic systems have been shown to be capable of performing biomolecular screening with sample volumes as low as picoliters(1, 5, 8, 48, 69). However, introducing a large number of samples on a miniature microfluidic device is difficult since it is impractical to have hundreds to thousands of sample inlets to a single microfluidic device. Furthermore, the tubing used for supplying the samples to such a microfluidic device would already consume orders of magnitude more sample than is required for the actual analysis on the microfluidic device. So, there is a need for an efficient way to transport a large number of samples to a microfluidic device. Ideally such a sample transport system would be flexible enough to supply variable number of samples to a microfluidic device without any modifications in the transport system or the device.

The 'plug-in cartridge' technique developed by the Whitesides group(106) provides an elegant solution to the problem of introducing a large number of reagents on a microfluidic device through a single inlet. Under this approach, a series of sample plugs are loaded into a capillary, with air bubbles present between sample plugs acting as spacers. This capillary is connected to a microfluidic device, for serial delivery of these sample plugs. However, in this approach, the sample plugs are constantly in contact with the capillary inner surface, leading to the problem of cross contamination between plugs(106). Another modification of this approach developed by the Ismagilov group(107) utilizes an immiscible carrier fluid instead of an air bubble to act as a spacer between sample plugs. The carrier fluid in this approach preferentially wets the inner surface of the capillary, thus preventing direct contact between sample plugs and the capillary surface. As a result, the problem of cross contamination between sample plugs is eliminated. The carrier fluids typically used for generating these sample plug arrays are fluorinated oils, which also reduce the problem of reagents leaking from sample plugs into the carrier fluid due to their low solubility for most reagents(107).

Although this approach is promising, the current techniques used under this approach for generating the 'sample plug cartridges' have some issues which need to be resolved. The common technique of using a syringe pump for aspirating sample plugs from a sample well(99, 108, 109) in a multi-well plate can be extremely slow. Another technique of using vacuum for aspirating a sample plug can be much faster(106). However, this technique can only provide a maximum driving pressure of 1 atm (~15 psi). As a result, the driving force may not be sufficient to load large numbers of sample plugs into a capillary due to the increasing fluidic resistance of the capillary with the introduction of sample plugs. Furthermore, both these techniques require the free end of the capillary to be attached to either a syringe or a vacuum source, thus excluding the possibility of operating this sample loading system in sync with the operations on a downstream microfluidic device. This can be a major setback to throughput as the possibility of conducting assays in continuous flow manner on microfluidic devices, as has been demonstrated earlier(110), is precluded.

To overcome these issues, we conceptualized and fabricated a sample plug loading system, which utilizes positive pressure for loading sample plugs from an industry standard multi-well plate to a capillary. Fig 6.10 shows a schematic illustrating the working principle of this system. A critical component of this system is a ‘capillary adapter’ which acts as an interface between a capillary, to be used for holding the sample plug array, and a multi-well plate used for holding samples. As shown in the schematic, the capillary adapter can be sealed with a sample well on the multi-well plate, creating a temporary pressure chamber in the sample well. In this sealed mode, the capillary attached to the capillary adapter is immersed in the sample present in the well. The pressure input on the capillary adapter can then be used to apply pressure to the sample in the well for a controlled amount of time. As a result, a small plug of sample is pushed from the well into the capillary. The size of this plug can be controlled by varying the input pressure and the pressure application time. Repeating this process with multiple sample wells can be used to generate an array of sample plugs in the capillary. As is clear from Fig 6.10, this whole sample plug loading process only requires one end of the capillary to be engaged, while the other end of the capillary is free to be interfaced with a downstream microfluidic device, where further operations can be carried out with the sample plug array.

Fig 6.11 shows a detailed model of the capillary adapter we designed in the CAD software ‘Solidworks’ (Solidworks Corp.). The wider backside of the adapter with the three large holes is used to bolt the capillary adapter to a stable support. The narrower front side is the actual functioning head of the capillary adapter. The functioning head consists of three disc shaped recesses on three sides (top, left and right), which are used to seat three NanoPorts (Idex Health and Science). The NanoPorts can be used to make a leak free connection with different types of tubing. The NanoPort on the top side is used to attach the capillary to the capillary adapter. The NanoPort on left side is used to attach the pressure supply line to the capillary adapter, while the NanoPort on the right side can be used to gauge pressure in the sample well, if required. All these NanoPorts holding locations on the capillary adapter have holes drilled in the center and routed to the bottom of the capillary adapter, as shown in the bottom view (Fig 6.11). When in use, the capillary goes through the straight hole drilled from the top of the capillary adapter to the bottom side. The bottom side of the capillary adapter has a disc shaped recess and a protruding circle. The disc shaped recess holds a silicone sealing ring, which is used to temporarily seal the capillary adapter with a sample well on a 96-well plate. The protruding circle acts as a centering feature, which is used for centering the capillary adapter into a sample well.

Our assembled Serial Sample Loading (SSL) platform is shown in Fig 6.12. All the components of the SSL platform are attached to an aluminum breadboard for support. A vertical stainless steel post bolted to the aluminum breadboard provides strong support structure for the capillary adapter. The capillary adapter is bolted to an angle bracket, which can slide on the post. This assembly allows us to manipulate the height of the capillary adapter from the aluminum base, as required. The capillary adapter is fixed at a suitable height to leave sufficient space for an assembly for XYZ motion of a 96-well plate below it. To control the cost of the pilot system, we chose to keep the motion of the 96-well plate in the XY plane manual by using simple rails. However, these rails can be easily replaced with a motorized XY stage for automated motion of the 96-well plate. Controlled motion of the 96-well plate in the Z dimension, however, is critical for providing a reproducible seal between the capillary adapter and a sample well. So the motion in the Z-dimension was motorized. Typical linear translation stages are ill-suited for this application due to the limitation on the load supported by these stages along the direction of travel. Hence, a Motorized Lab Jack was used for automated motion of the 96-well plate in the Z dimension. Fig 6.12 also shows an Electronic Pressure Controller, which can control the pressure applied to a sample well through the capillary adapter.

6.5.4.2 Materials and Methods

The capillary adapter was designed in Solidworks (Solidworks Corp.) and then fabricated at the Physical Sciences Machine Shop at Johns Hopkins University. The capillary adapter was fabricated using stainless steel as substrate, to prevent corrosion due to contact with biological samples and buffers. All other structural components for the SSL system were purchased from Thorlabs (Newton, NJ). A Motorized Lab Jack (L490MZ/M, Thorlabs) was purchased to use for computer controlled vertical motion of the 96-well plate in the SSL system. The electronic pressure controller used with the SSL system was purchased from Alicat Scientific Inc. (Tucson, AZ). The pressure controller used is a dual valve pressure controller (PCD-100PSIG-D-PCV03), which eliminates the need for bleed ports and relief valves typically required for pressure control in a closed volume. NanoPorts (N-124H, N-333 and N-125H Idex Health and Science) were bonded to the capillary adapter at the three ports according to the instructions provided by Idex. The sealing ring attached to the bottom of the capillary adapter was fabricated using a silicone septum (Corning). The ring shape was punched out of the silicone septum using hole punches (3/8” and 13/64” hole diameter, McMaster). The capillary adapter was designed to be compatible with Costar 96-well plates (Corning). The Motorized Lab Jack and the Electronic Pressure Controller were interfaced with a computer through USB ports. Custom software written in LabVIEW (National Instruments), allowed us to control the motion of the 96 well-plate in the vertical direction, as well as the pressure applied to a sample well through the capillary adapter.

The sample loading experiments were conducted using Silica Capillary Tubing (Polymicro Technologies). The capillaries were treated with Aquapel™ (PPG Industries) before an experiment, to render the inner surface of the capillary hydrophobic. The samples used for most experiments were food dyes (Ateco, Glen Cove, NY), unless specified otherwise. The carrier fluid used for separating sample plugs from each other was a mixture of FC-3283 (3M) and 1H,1H,2H,2H-Perfluoro-1-octanol (Sigma-Aldrich Co.) in the ratio of 8:1 by volume. For these experiments, the Aquapel treated capillary was completely filled with the carrier fluid first. Following this, a sample well on the 96-well plate was manually aligned with the capillary adapter. The LabVIEW software then raised the 96-well plate in vertical direction, to seal the sample well with the capillary adapter. The same software was then used to apply the desired pressure profile to the sample well for the desired amount of time. Following this, the 96-well plate was lowered by the LabVIEW software. We then manually aligned another well containing the carrier fluid with the capillary adapter. The same sample plug loading steps were then used to load a carrier fluid plug into the capillary. This alternating sequence of sample and carrier fluid plug loading was repeated until the desired number of sample plugs was loaded into the capillary.

For the experiments which required sample plug volume estimation, we used a 1 m long silica capillary with a 200 µm inner diameter (ID). The sample used for these experiments was a single food dye. A series of 12 sample plugs separated by carrier fluid was loaded into the capillary using the steps described above. This capillary was then placed on the white background of a 'letter' sized sheet of paper and imaged using a Digital Single-Lens Reflex (DSLR) camera. The camera was placed such that the whole letter sized paper was included in the camera's field of view. The image was then imported in ImageJ (104) for plug volume estimation. Length scale was set in the image using the known length of the letter sized sheet of paper. Following this, the length of each sample plug was measured by manually drawing a line marking the length of the plug in ImageJ. This measured length, along with the known cross sectional area of the capillary was then used to estimate the plug volume for each sample plug. The plug volume data from the last 10 sample plugs for each loading condition was then used for the data analysis.

6.5.4.3 Results

One of the first critical tests of our SSL platform was to determine its capability to provide significantly higher driving pressure than vacuum (~15 psi) for sample plug loading in a capillary. To conduct this test, we first attached a silicone sealing ring to the capillary adapter, as described in the 'Materials and Methods' section. The NanoPorts for the capillary and pressure gauge on the capillary adapter were plugged using plugs (Idex Health and Science). The electronic pressure controller was connected to an input pressure supply of 95 psi from a Nitrogen cylinder. A sample well on a Costar 96-well plate, was then sealed with the capillary adapter using the SSL system. The LabVIEW software was then used to raise the pressure in the sealed sample well to different peak pressure values (10, 20, 30, 40 and 50 psi). Fig 6.13 shows a plot of the pressure in the sample well, sensed by the pressure controller, for these 5 different tests. The pressure plot for each test consists of 3 distinct regions: Rising phase (the pressure in the sample well is raised from zero to peak value during this phase), Peak pressure phase (pressure in the sample well is maintained at peak value during this phase) and Decline phase (pressure in the sample well is reduced from peak to zero psi during this phase). The duration of each of these phases can be controlled using the LabVIEW software. All these phases were fixed at duration of 5 sec each for the plots shown in Fig 6.13. The pressure plots demonstrate that the pressure controller can easily maintain a peak pressure of 50 psi in the sealed sample well as commanded. Thus, proving that our SSL system can provide substantially higher driving pressures than a vacuum based system for sample plug loading in a capillary. The pressure controller we used was factory calibrated to a maximum pressure of 50 psi. Hence, we couldn’t test the SSL system for pressures higher than 50 psi. Furthermore, Fig 6.13 also demonstrates that the pressure controller can control the timing of the 'Rising' and 'Peak pressure' phases very precisely. The duration of the 'Decline' phase, however, being a passive process driven by the pressure difference between the sealed sample well and the atmosphere, depends to some extent on the peak pressure value.

We then tested the capability of the SSL system to load a series of sample plugs into a capillary. Initial testing was conducted using food dyes as samples for easy visibility. A silica capillary was loaded with alternate plugs of different food dyes and carrier fluid using the SSL system. Fig. 6.14a shows a micrograph of the silica microcapillary with a few food dye sample plugs. The micrograph shows excellent uniformity of plugs, the ability of the SSL system to keep sample plugs separate from each other, as well as the capability to load sample plugs without breakup into the capillary. We then tested the sample plug loading scheme with a biologically relevant sample in the form of a 'PicoGreen' (Life Technologies) stained Lambda DNA (Promega) sample. The Lambda DNA was present at a concentration of 2ug/ml concentration in the sample. Biological samples provide additional challenge to the sample plug loading process due to the lack of any visual feedback during sample plug loading. Food dyes are easily visible and their plug uniformity can be easily discerned during the loading process. However, most biological samples being transparent, it is difficult to differentiate them from the transparent carrier fluid. The variation in plug size is solely dependent on the repeatability of the SSL system. We thus loaded these Lambda DNA sample plugs into a silica capillary essentially blindly and then obtained a fluorescence image (Fig. 6.14b) of the silica capillary using a Typhoon 9410 Variable Mode Imager (GE Healthcare). The fluorescent Lambda DNA plugs can be clearly seen over the dark background of the interspersed carrier fluid plugs. Excellent uniformity of plug loading, despite lack of visual feedback is also clearly evident from this image. The ultimate purpose of the SSL system is delivery of a large array of sample plugs to a microfluidic device for further processing. So, as a proof of principle, we also demonstrated interfacing of a capillary with a simple microfluidic device (Fig. 6.14c). A series of sample plugs made from food dye using the SSL system, were then delivered from the capillary to the microfluidic device. Excellent transition of sample plugs from the capillary to the microfluidic device without break-up can be clearly seen from the image in Fig. 6.14c.

We then conducted more rigorous testing of the SSL platform to determine its capability to maintain sample plug uniformity, as well as control the sample plug size as desired. To conduct these experiments, we loaded a series of twelve sample plugs made of the same food dye into a 1m long silica capillary for each set of sample plug loading conditions, as described in the 'Materials and Methods' section. The sample plug volume estimated from the last ten sample plugs was used to estimate the mean and standard deviation of the plug volume for each loading condition. These values were then used for the plots shown in Fig. 6.15 and 6.16.

The sample plug volume depends on a few factors: 1) Peak pressure (P_{peak}) applied, 2) duration of the 'Rising' and 'Decline' phases of pressure application and 3) the duration (T_{peak}) of the Peak pressure phase. All these parameters can be precisely controlled in the SSL system with our LabVIEW software. We decided to vary the intuitive factors like P_{peak} and T_{peak} to control the sample plug volume. Initially, we held P_{peak} constant and varied T_{peak} to estimate the sample plug volume generated for different T_{peak} values. This experiment had two objectives: First to estimate the variation in plug volume for a fixed set of loading conditions and second to estimate the relationship between plug volume and T_{peak} for a fixed value of P_{peak}. Fig. 6.15 shows a plot of sample plug volume vs T_{peak} for three different values of P_{peak} (0.5, 1 and 1.5 psi). The linear relation between plug volume and T_{peak} for each individual P_{peak} value demonstrates the capability of the SSL system to precisely control the plug volume in a predictable manner, through the variation of the duration of the 'Peak pressure' phase. Furthermore, the plug size variation indicated by the error bars is fairly low with a maximum coefficient of variation of approx. 7% for all but two smallest plug volumes generated, where we were approaching the lower limit of the operation of the electronic pressure controller. We expect the system performance, in terms of plug volume variability, to improve as the motion of the 96 well plate is automated in the horizontal plane too, as the overlap of the sample well wall with the sealing ring of the capillary adapter can be reproduced across the area of the 96 well plate, providing a reproducible seal for every single sample plug loading step.

Varying T_{peak} to control plug volume can be beneficial for smaller plug volumes. However, as the plug volume increases, T_{peak} can quickly increase, reducing the speed at which sample plugs can be loaded in a capillary. For larger plug volumes, it would be beneficial to raise the peak pressure, to achieve larger plug volume in the same amount of time. Fig 6.16 shows a plot of the sample plug volume vs P_{peak} for a fixed value of T_{peak} (1 sec). This plot shows another linear relationship between sample plug volume and P_{peak}, providing an alternative predictable way to vary the sample plug volume through variation of the peak pressure applied to the sample well. The value of P_{peak} here is only limited by the pressure at which the seal between the sample well and the capillary adapter breaks down. This result, thus illustrates a limitation of applying vacuum to load sample plugs in a capillary, which can be overcome with the use of the SSL system. Although, the vacuum level can be controlled with a regulator, the driving pressure cannot be greater than 1 atm(~15psi), limiting the speed at which large sample plugs can be loaded in a capillary.

One limitation of the SSL system is its dependence on the fluidic resistance of the capillary for maintaining the uniformity of sample plug volume for the same sample plug loading conditions. However, as more and more sample plugs are loaded into the capillary, the fluidic resistance of the capillary increases, gradually reducing the sample plug volume over the course of loading of sample plugs. This effect is illustrated in Fig 6.17a. In this figure, the sample plug volume data is normalized by the plug volume of the first sample plug generated for each loading condition. The normalized sample plug volume is then plotted against the sample plug number in the loading sequence. As seen from the plot, for three independent loading conditions (P_{peak}: 1 psi, T_{peak}: 1.5, 2 and 2.5 sec), we observe a consistent gradual reduction in the sample plug volume as the number of sample plugs in the capillary increases.

This problem can be avoided through pressure compensation for the changing fluidic resistance of the capillary. We observed the sample plug volume reduce by approx. 15% for the 10th sample plug loaded into a capillary for all the three conditions shown in Fig 6.17a. So we did simple linear peak pressure (P_{peak}) increase for each sample plug in the loading sequence to compensate for the 17% (1/0.85) increase in the fluidic resistance over the course of loading 10 sample plugs in the capillary. The normalized sample plug volumes for this modified loading scheme with the same starting point as the three conditions shown in Fig 6.17a, are plotted in Fig 6.17b. These plots demonstrate that a simple compensation scheme can avoid gradual reduction in sample plug volume with increasing number of sample plugs, further improving the sample plug uniformity of the SSL system.

In the future versions of the SSL system, the compensation scheme can be further improved by devising a mathematical model of the changing fluidic resistance in the capillary and incorporating it in the LabVIEW software, to automatically compensate for the changing fluidic resistance by varying the peak pressure (P_{peak}) applied to the sample well for each consecutive sample plug being loaded into the capillary. Alternatively, an imaging based technique can be used to detect the appearance of the edge between a sample plug and the carrier fluid at a particular distance from the end of capillary immersed in the sample solution, to provide feedback for computer control of the pressure controller. This approach can enable very accurate metering of sample plug volume for each sample plug despite changing fluidic resistance in the capillary.

6.5.4.4 Discussion

In conclusion, we have devised a new technique for serial delivery of a large number of samples to a microfluidic device, directly from a standard multi-well plate. Our SSL system differs from similar techniques developed by other research groups in the past, in the application of positive pressure as a driving force for the loading of a series of sample plugs into a capillary for direct delivery to a microfluidic device. The SSL system can be used for rapid sample plug loading into a capillary with the only rate limiting step being movement of the multi-well plate, to load samples from different sample wells. We demonstrated the functioning of the SSL system as well as its capability to precisely control the sample plug volume. Since the SSL system engages only one end of the capillary in sample plug loading, it can be directly interfaced with a downstream microfluidic device for its operation in synchronization with the microfluidic device. In its current form, the SSL system was designed for loading sample plugs into a single capillary. However, the design can be easily extrapolated for simultaneous loading of sample plugs in multiple capillaries from a row of sample wells. We expect the SSL system to be instrumental in further improvement in the throughput of droplet-based microfluidic devices in future.

Fig 6.1 Schematic of the sample screening platform Step 1: A cartridge is loaded with a library of sample plugs separated by an immiscible carrier fluid. This cartridge is interfaced with a microfluidic device. Step 2: On-demand digitization of incoming sample plugs into smaller daughter droplets. The volume of individual daughter droplets can be controlled by valve opening time and back pressure on the cartridge. Step 3: By exploiting the cross sectional area of the central channel, the sample daughter droplet is stretched in the "Fusion Region". This approach allows for robust, synchronization-free injection of up to four reagents simultaneously directly into the daughter droplet. The volume of reagent injected is controlled through modulation of back pressure and valve opening time corresponding to the reagent inlet. Step 4: Once sample and reagent have been combined into one droplet, the droplets are stabilized with carrier fluid containing surfactant to prevent unwanted droplet coalescence downstream. Step 5: Sample-reagent droplets travel to an incubation channel. Step 6: The sample-reagent droplets are incubated while maintaining their sequence in downstream incubation channels. This approach allows for droplet identification through spatial indexing in a 1-Dimensional array.

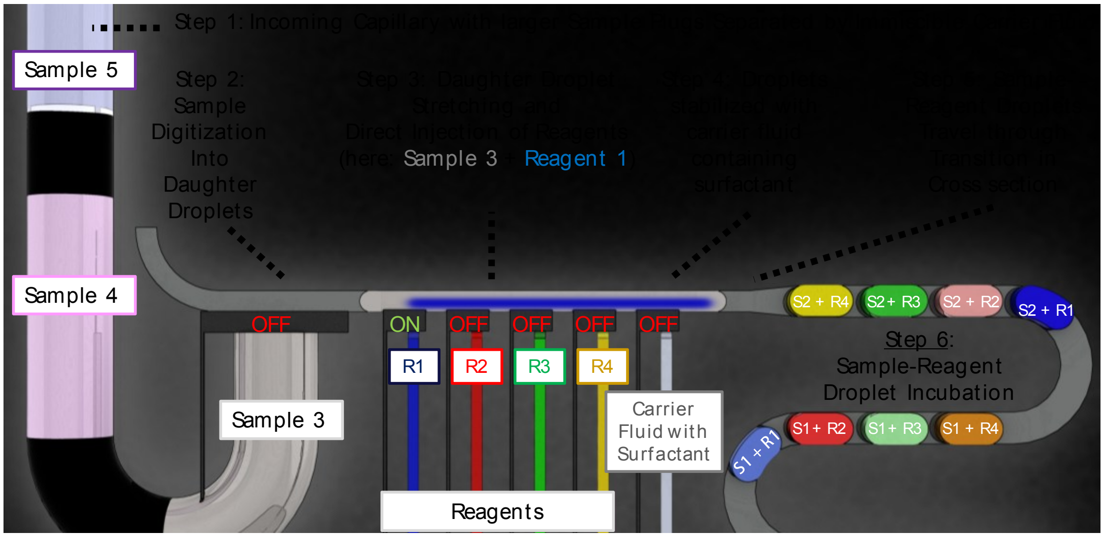
Step 1: Incoming Capillary with larger Sample Plugs Separated by Immiscible
Sample 5
Sample 4
Sample 3
Step 2: Sample Digitization Into Daughter Droplets
Step 3: Daughter Droplet Stretching and Direct Injection of Reagents (here: Sample 3 + Reagent 1)
Step 4: Droplets stabilized with carrier fluid containing surfactant
Step 5: Sample-Reagent Droplets Travel through Transition in Cross section
OFF
ON
OFF
OFF
OFF
OFF
R1
R2
R3
R4
Carrier Fluid with Surfactant
Reagents
S2 + R4
S2 + R3
S2 + R2
S2 + R1
Step 6: Sample-Reagent Droplet Incubation
S1 + R1
S1 + R2
S1 + R3
S1 + R4

Step 2: Sample Digitization (Yellow) into Daughter Droplets

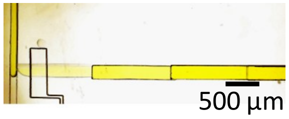

Step 3: Sample Daughter Droplet (Yellow) Stretching And Injection of Reagent (Blue)

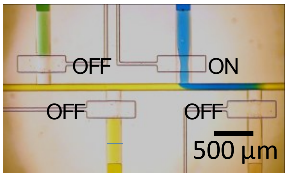
OFF
ON
OFF
OFF
500 µm

Step 5: Sample-Reagent Droplet (Green) Travels through Transition

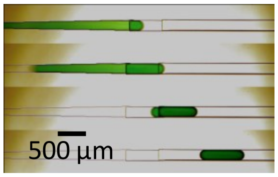

Fig 6.2 'Serial Sample Loading' (SSL) system a) Schematic: A custom SSL system was designed which employs positive pressure to inject a sample plug into a microcapillary from a standard multi-well plate. A custom capillary adapter in the SSL system provides an interface between a microcapillary and a multi-well plate. This adapter can seal a well on the multi-well plate, thus generating a temporary pressure chamber inside the sample well. A pressure input on the adapter can then be used to apply controlled pressure to the fluid inside the sample well. This positive pressure drives a small plug of sample from the well into the microcapillary. Following this, the seal is broken and the multi-well plate is moved to seal another sample well with the capillary adapter. This sequence of steps is repeated to generate a sample library into the microcapillary. **b)** An image of a food dye sample plug array generated using the SSL system. Each sample plug is separated from each other by an immiscible carrier fluid.

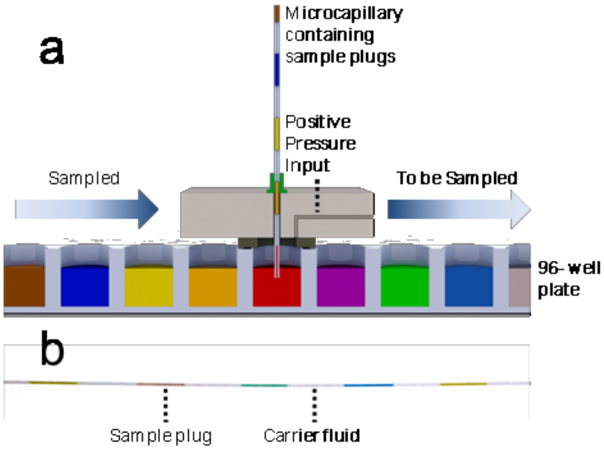
a
Microcapillary containing sample plugs
Positive Pressure Input
Sampled
To be Sampled
96-well plate
b
Sample plug
Carrier fluid

Fig 6.3: Microfluidic Device Design a) Photograph of a prototype device. The microfluidic device has a multichannel architecture: 1) The central channel with fusion region and incubation region (purple), 2) Capillary inlet, 3) Reagent inlets: reagent 1 (pink), reagent 2 (orange), reagent 3 (green), reagent 4 (turqoise) and surfactant oil inlet (yellow). The valves on the device (V1-V7) are indicated by a turquoise dye. **b)** A scan of the capillary inlet region, indicating the height difference between different sections of the capillary inlet to facilitate smooth sample plug transition from the large ID of the capillary to the shallow channels on the microfluidic device.

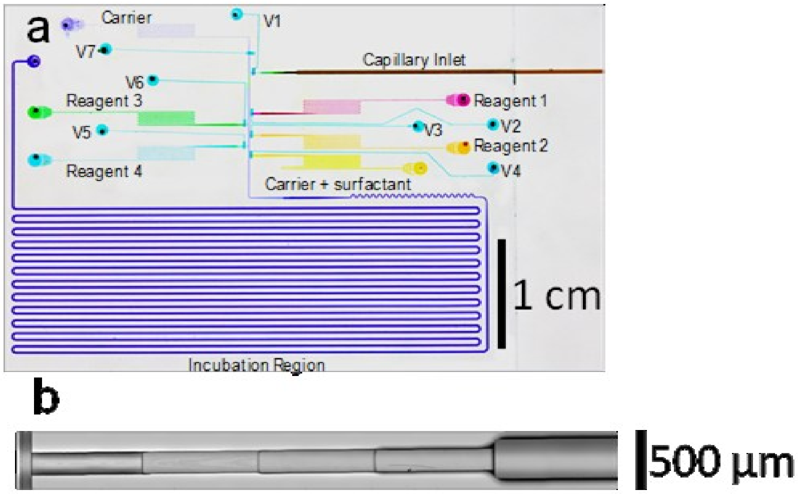
a
Carrier
V1
V7
Capillary Inlet
V6
Reagent 3
Reagent 1
V5
V3
V2
Reagent 2
Reagent 4
V4
Carrier + surfactant
1 cm
Incubation Region
b
500 µm

Fig 6.4 Control of droplet volume and droplet uniformity using mechanical valve based droplet generation a) Micrograph of the incubation region on the microfluidic device filled with reagent droplets generated using sequentially increasing valve opening times (T_{on} = 0.3, 0.4, 0.5, 0.6, 0.7, 0.8 seconds) for a fixed back pressure on the reagent inlet ($P_{reagent}$= 5 psi). This resulted in a linear array of repeats of a sequence of six droplets, with each droplet increasing in volume. **b)** A plot of droplet volume versus the valve opening time (T_{on}) for a valve corresponding to a reagent inlet for three different values of back pressures applied to the reagent inlet ($P_{reagent}$= 2.5, 5 and 7.5 psi). The droplet volumes plotted are an average of volumes estimated from 50 droplets for each condition. The error bars in the volume data are too small to be seen on the plot.

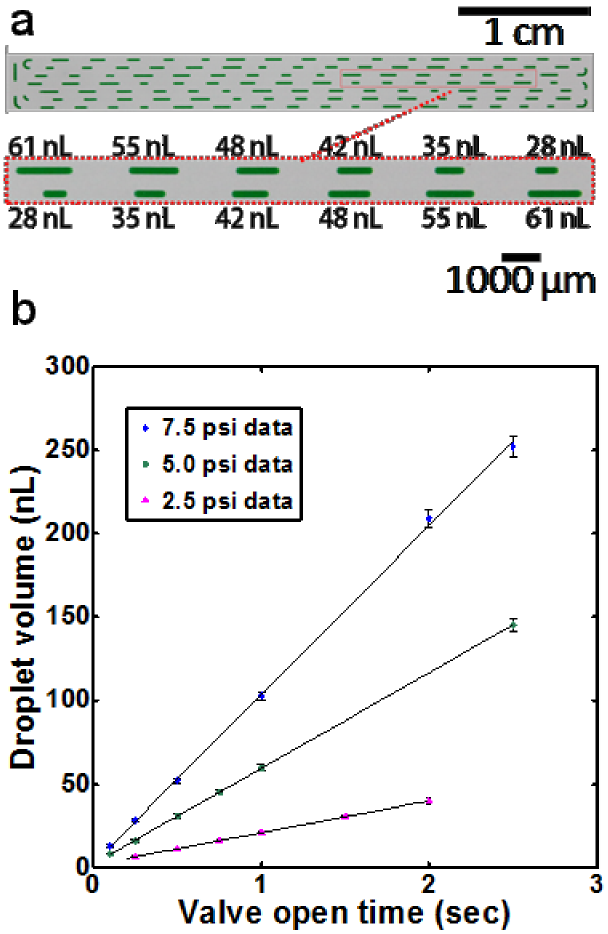
a
1 cm
61 nL
55 nL
48 nL
42 nL
35 nL
28 nL
28 nL
35 nL
42 nL
48 nL
55 nL
61 nL
1000 µm
b
Droplet volume (nL)
Valve open time (sec)
7.5 psi data
5.0 psi data
2.5 psi data
0
50
100
150
200
250
300
0
1
2
3

Fig 6.5 Demonstration of reagent injection in sample daughter droplets merging with reagents a) Time series of images indicating reagent injection into sample daughter droplets at the 'Fusion zone' on the device. A sample daughter droplet (yellow) is released from the capillary inlet and is halted in the 'Fusion zone' by actuating a valve upstream which controls carrier fluid injection into the central channel on the device. A reagent (blue) is released and injected directly into the sample droplet. The elongated configuration of the sample daughter droplet in the 'Fusion zone' ensures robust reagent injection operation on the device without the need for precise sample droplet positioning. **b)** A series of photographs demonstrating injection of different numbers of reagents into a sample daughter droplet simultaneously.

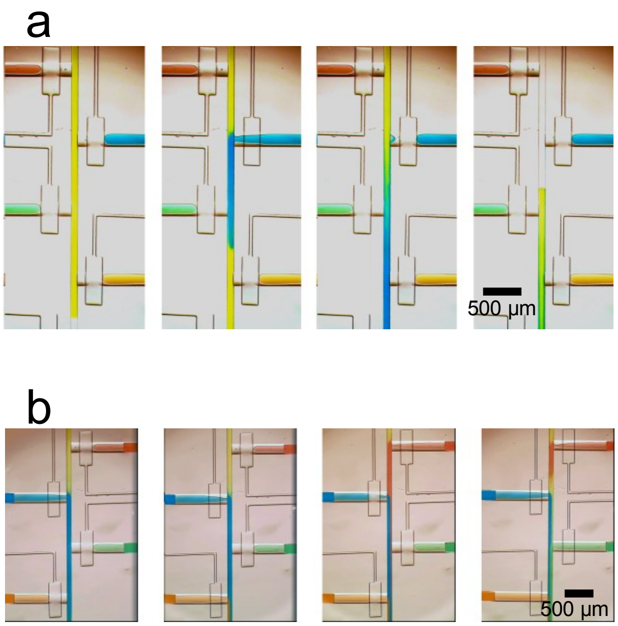

Sample (yellow) + 1 Reagent (blue)

Sample (yellow) + 2 Reagents (blue, orange)

Sample (yellow) + 3 Reagents (red, blue, orange)

Sample (yellow) + 4 Reagents (red, blue, green, orange)

Fig 6.6 Photographs of the incubation region indicating multiplexing capability of the device a) Table with micrographs indicating combinatorial mixture droplets generated on the device using four different samples [Sample A (blue), Sample B (yellow), Sample C (green), Sample D (water)] and four different reagents [Reagent 1 (orange), Reagent 2 (water), Reagent 3 (light blue), Reagent 4 (yellow)]. Droplets 1A-4A, 1B-4B, 1C-4C, and 1D-4D are each generated from a combination of the sample and reagent in the corresponding column and row respectively. For example, Droplet 1A is the combination of sample A with reagent 1. **b)** Left panel shows four different micrographs showing repeating sequences of sample daughter droplets generated from a single sample plug merged with four different reagents on a single device. The right panel shows zoomed in version of a small section of the micrographs from the left panel for easy visualization of the droplet sequence. The droplet identification codes in this panel are the same as those used in subfigure a. Note: The sequence of droplets seems to be going in opposite direction in alternate channels due to the changing direction of flow in serpentine channels.

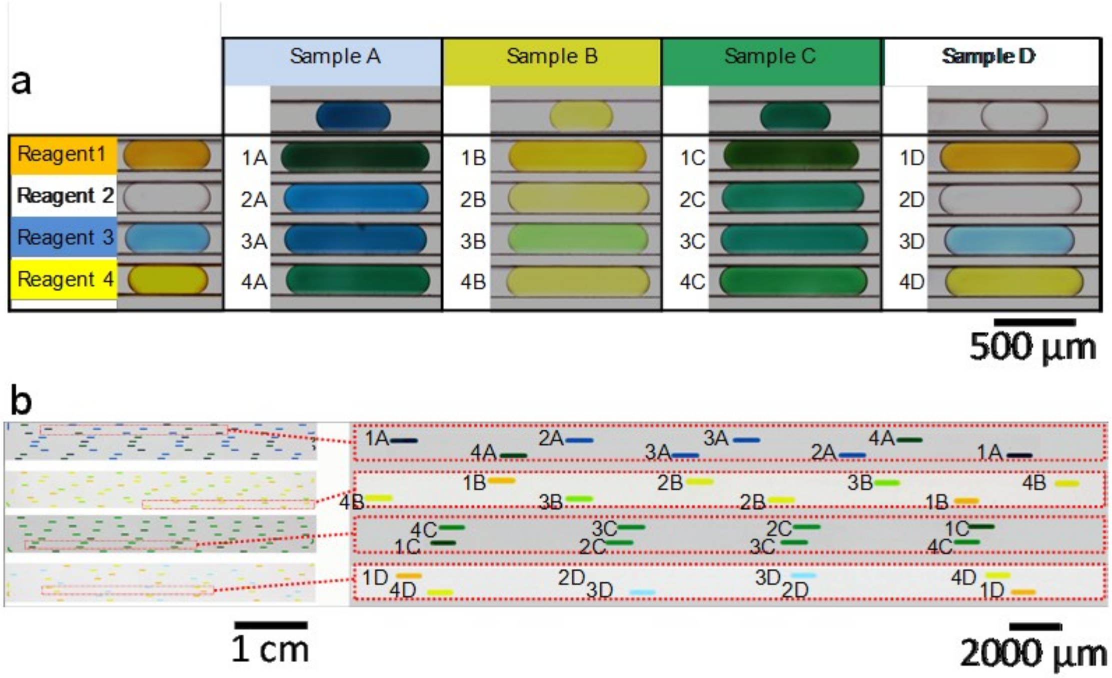
a
Sample A
Sample B
Sample C
Sample D
Reagent1
Reagent 2
Reagent 3
Reagent 4
1A
2A
3A
4A
1B
2B
3B
4B
1C
2C
3C
4C
1D
2D
3D
4D
500 µm
b
1A 4A 2A 3A 3A 2A 4A 1A
4B 1B 3B 2B 2B 3B 1B 4B
4C 1C 3C 2C 2C 3C 1C 4C
1D 4D 2D 3D 3D 2D 4D 1D
1 cm
2000 µm

Fig 6.7 Microfabrication Process with Single Developing Step: Four consecutive layers of SU8 photoresist are spin coated and patterned on a single silicon wafer using photolithography. Each layer undergoes all standard photolithography steps like soft bake (SB), exposure and post-exposure bake (PEB). However, the developing step is conducted in common for all layers after patterning the last photoresist layer.

Spincoat 1st SU8 layer, 50 µm
SB → Exposure → PEB

Spincoat 2nd SU8 layer, 100 µm
SB → Exposure → PEB

Spincoat 3rd SU8 layer, 200 µm
SB → Exposure → PEB

Spincoat 4th first SU8 layer, 360 µm
SB → Exposure → PEB

Single Development Step
Hardbake

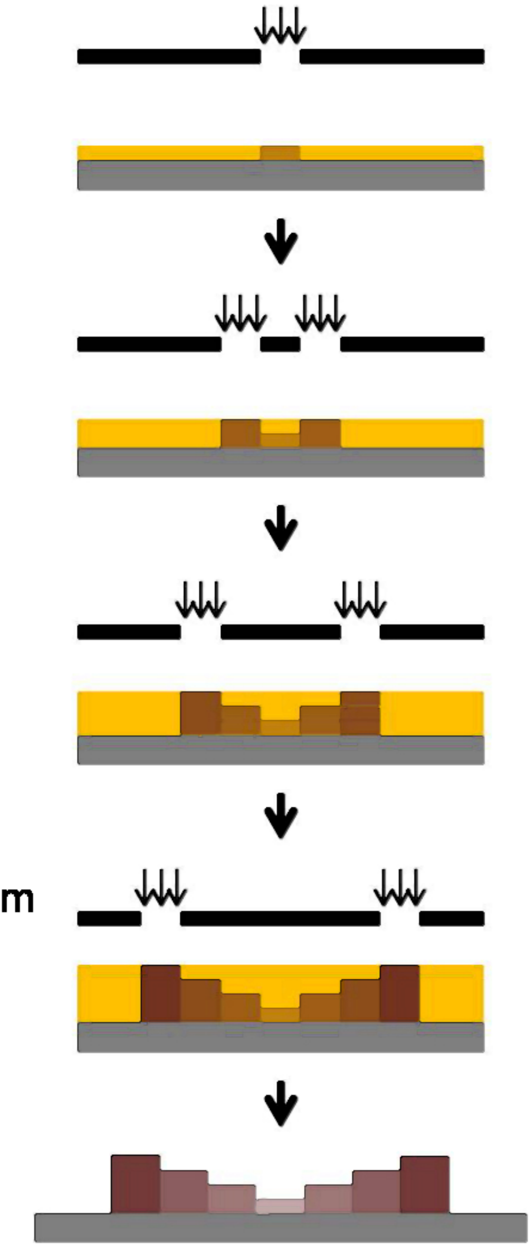

Fig 6.8 Modified microfluidic device fabrication: The process flow used for fabrication of our microfluidic devices to accommodate tall channels in the fluidic layer while maintaining the functionality of push-down valves. (6:1, 10:1 and 15:1 refer to the ratio of the base to curing agent used to mix a batch of PDMS)

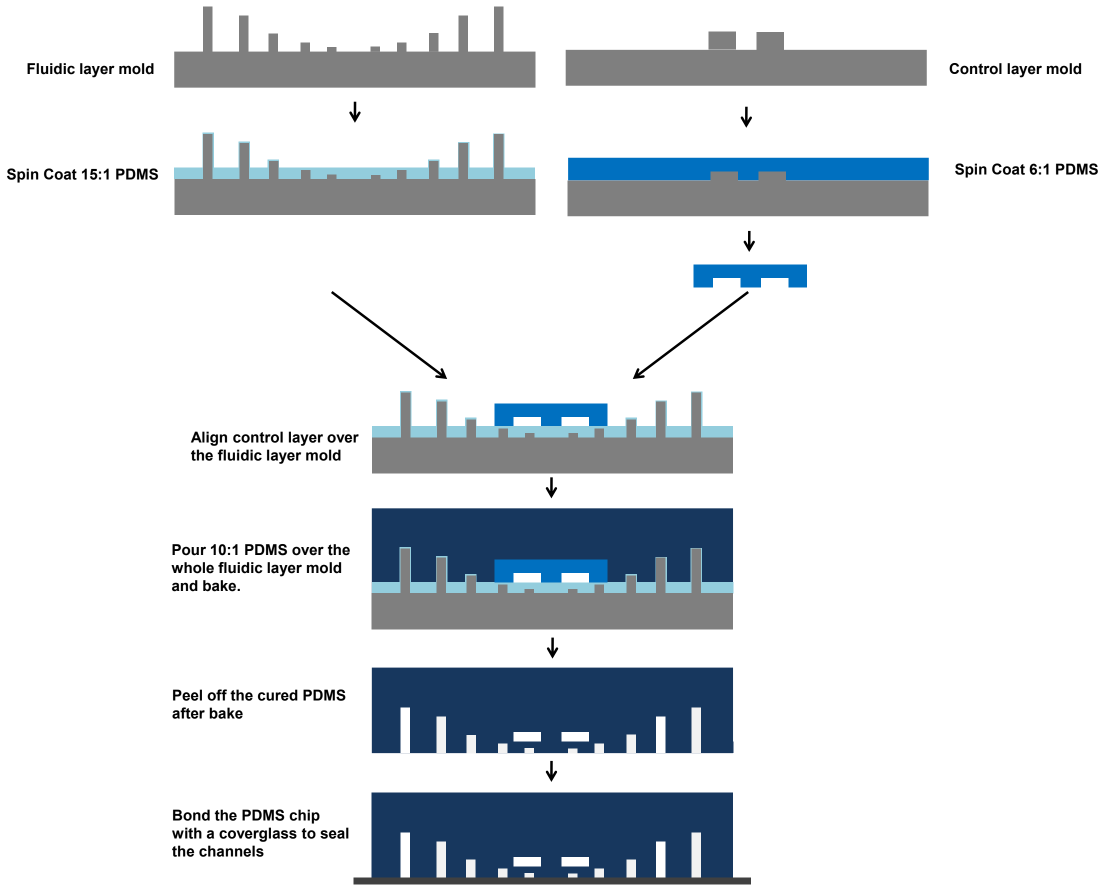
Fluidic layer mold
Control layer mold
Spin Coat 15:1 PDMS
Spin Coat 6:1 PDMS
Align control layer over the fluidic layer mold
Pour 10:1 PDMS over the whole fluidic layer mold and bake.
Peel off the cured PDMS after bake
Bond the PDMS chip with a coverglass to seal the channels

Fig 6.9 Fusion zone design for robust reagent injection in sample droplets with different volumes

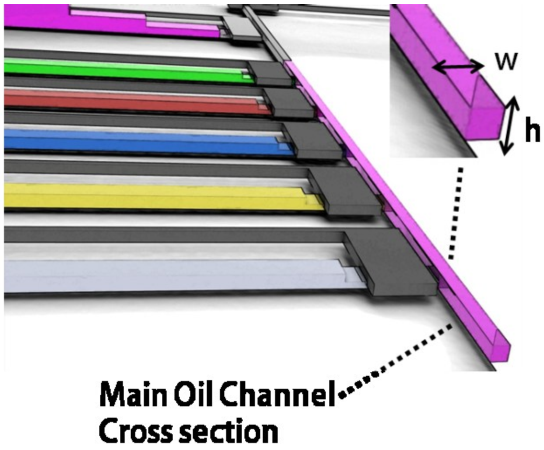
w
h
Main Oil Channel
Cross section

Current Design:
Width fusion zone: 100 μm
Height fusion zone: 50 μm
Length fusion zone: 3800 μm
Minimum Droplet Volume: 19 nL

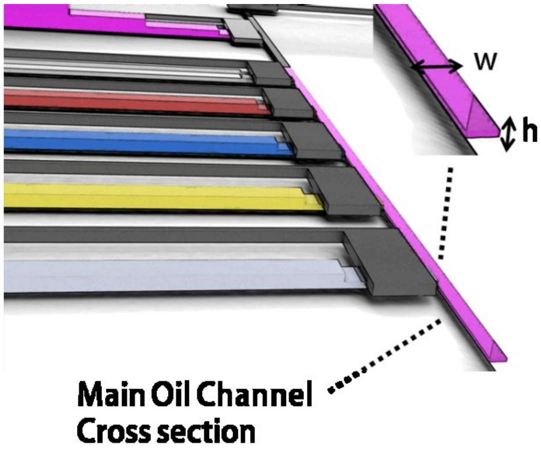
w
h
Main Oil Channel
Cross section

Alternative Design:
Width fusion zone: 100 μm
Height fusion zone: 10 μm
Length fusion zone: 3800 μm
Minimum Droplet Volume: 3.8 nL

Fig 6.10 A schematic illustrating the working principle of the sample plug loading system. This positive pressure based sample loading system involves interfacing a capillary with a sample well through a capillary adapter. The capillary adapter can be used to seal a sample well from a multi-well plate, creating a temporary pressure chamber in the sample well. Application of pressure to this sealed sample well through the capillary adapter leads to introduction of a sample plug from the sample well into the capillary.

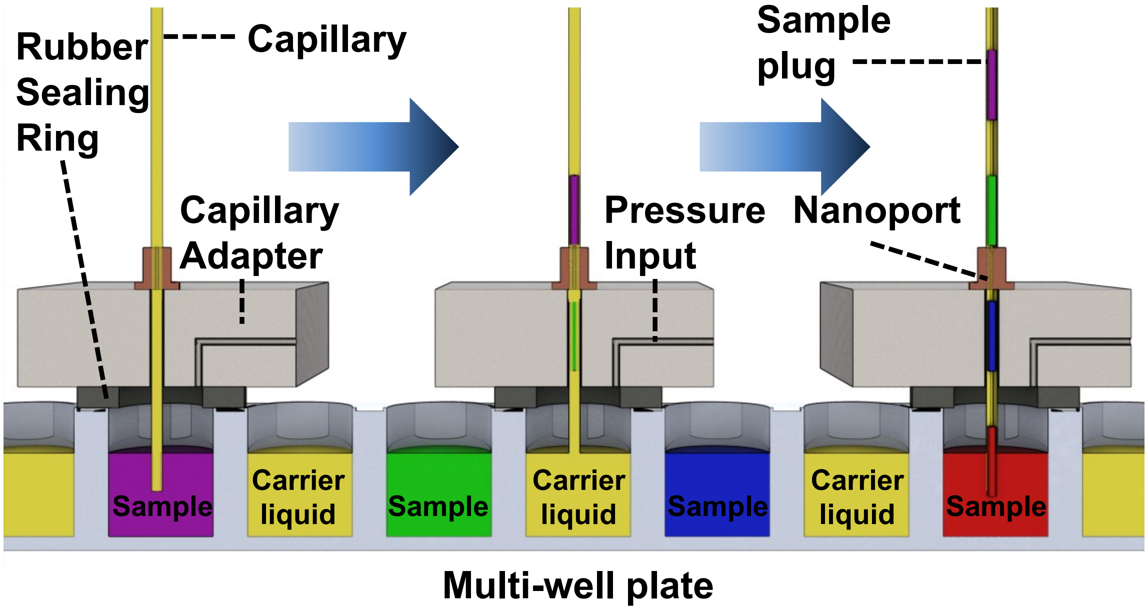
Rubber Sealing Ring
Capillary
Capillary Adapter
Pressure Input
Sample plug
Nanoport
Sample
Carrier liquid
Sample
Carrier liquid
Sample
Carrier liquid
Sample
Multi-well plate

Fig 6.11 Different views of a CAD model of the capillary adapter actually used for fabrication of the capillary adapter: The wider backside of the adapter with the three large holes is used to bolt the capillary adapter to a stable support. The narrower front side is the actual functioning head of the capillary adapter.

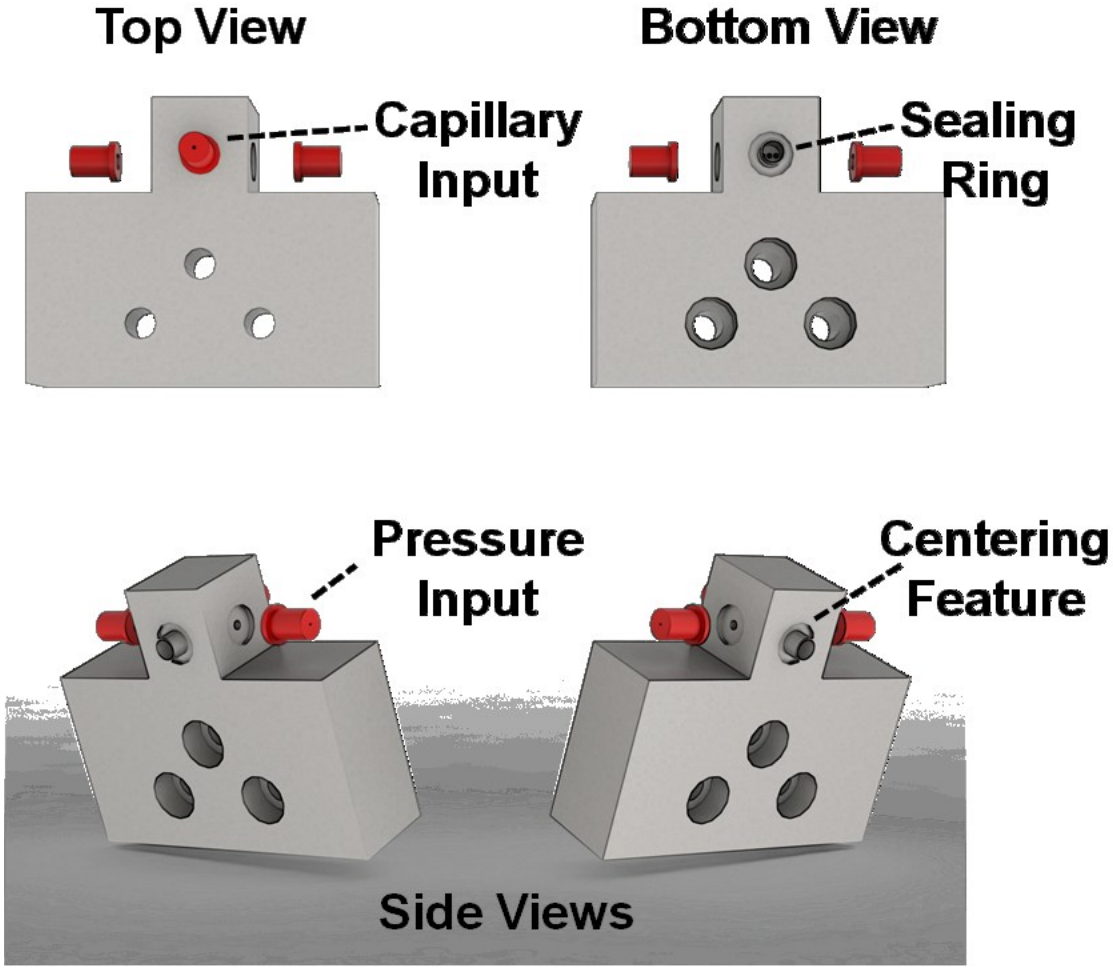
Top View
Bottom View
Capillary Input
Sealing Ring
Pressure Input
Centering Feature
Side Views

Fig 6.12 A photograph of the actual assembled Serial Sample Loading (SSL) system: The SSL system features a custom made capillary adapter to interface a capillary with the multi-well plate, a Motorized Lab Jack for vertical motion of the multi-well plate and an Electronic Pressure Controller to control to pressure applied to a sample well for sample plug loading into the capillary.

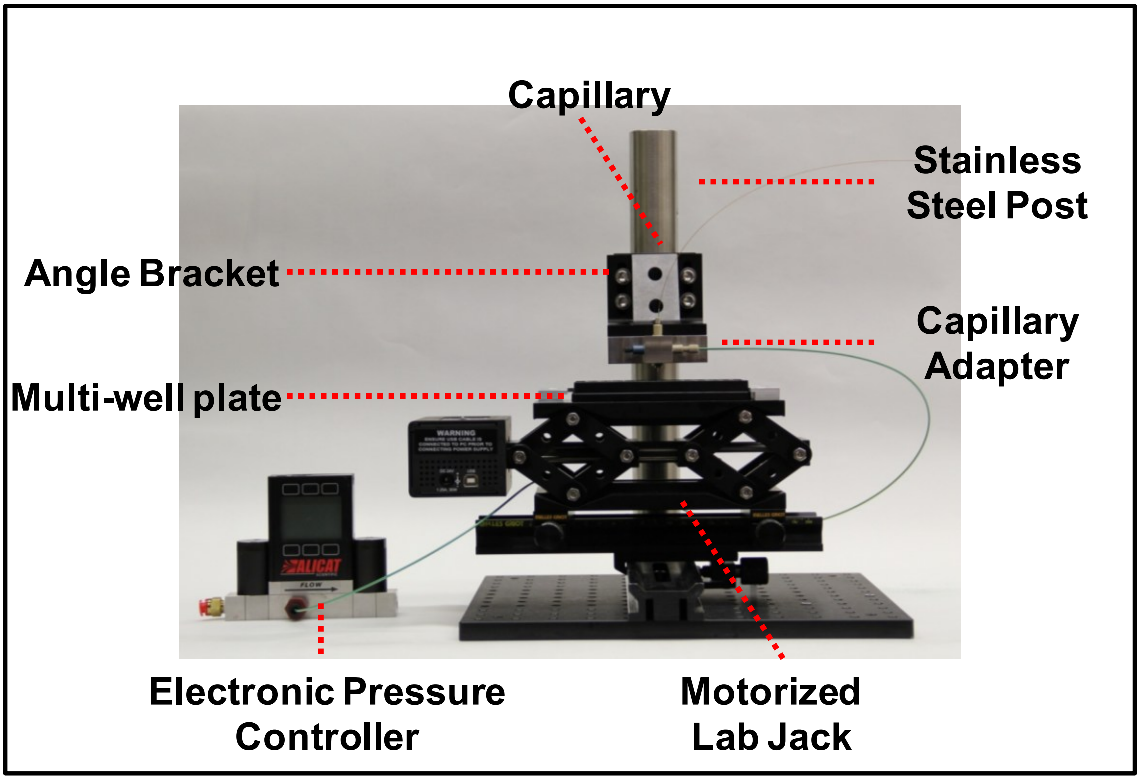
Capillary
Stainless Steel Post
Angle Bracket
Capillary Adapter
Multi-well plate
Electronic Pressure Controller
Motorized Lab Jack

Fig 6.13 A plot of pressure variation in the sample well over time, for different peak pressures (10, 20, 30, 40 and 50 psi) applied to the sample well. The pressure variation is sensed by the Electronic Pressure Controller in the SSL system. Each individual plot shows three distinct phases of pressure application to the sample well: 1) Rising phase (The pressure is raised from zero to peak pressure during this phase), 2) Peak pressure phase (Pressure is maintained at its peak value during this phase) and 3) Decline phase (The pressure is reduced from peak pressure to zero during this phase). The duration of all these phases was maintained constant at 5 sec each for all the plots in the figure. The plots demonstrate precise timing and pressure control of the SSL system in the sample well. Furthermore, the plots also demonstrate that peak pressure of up to 50 psi could be easily maintained in the sample well.

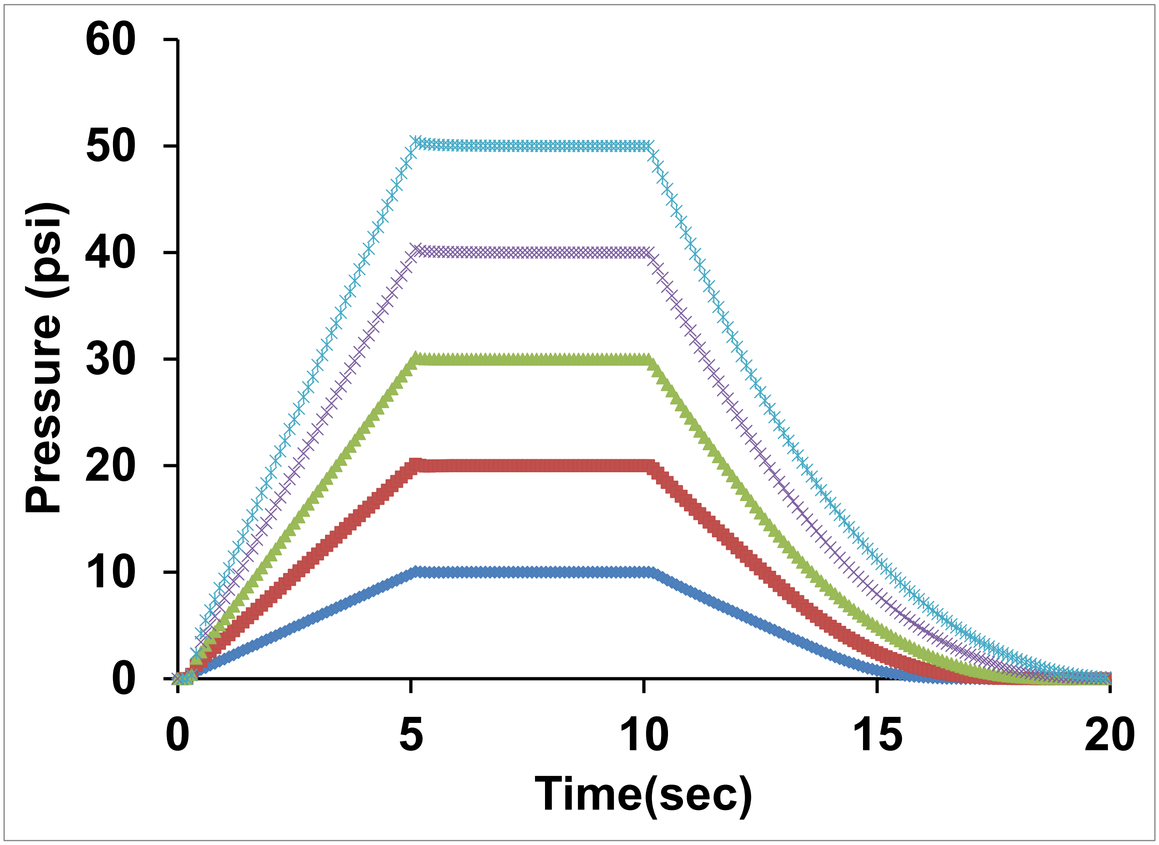
60
50
40
30
20
10
0
Pressure (psi)
0
5
10
15
20
Time(sec)

Fig 6.14 Micrographs demonstrating capability of the SSL system to load uniform sample plugs into a capillary: a) The micrograph shows a series of sample plugs in the form of different food dyes loaded into a capillary by the SSL system. **b)** This micrograph shows a fluorescence image of a series of sample plugs made from PicoGreen stained Lambda DNA, loaded into a capillary by the SSL system. The capillary loaded with these sample plugs was imaged using a Typhoon 9410 Variable Mode Imager and the false color was added to the fluorescence intensity image using ImageJ. **c)** A photograph of a simple microfluidic chip interfaced with a capillary. The image shows transition of a series of sample plugs generated using the SSL system from the capillary to the microfluidic device without break-up.

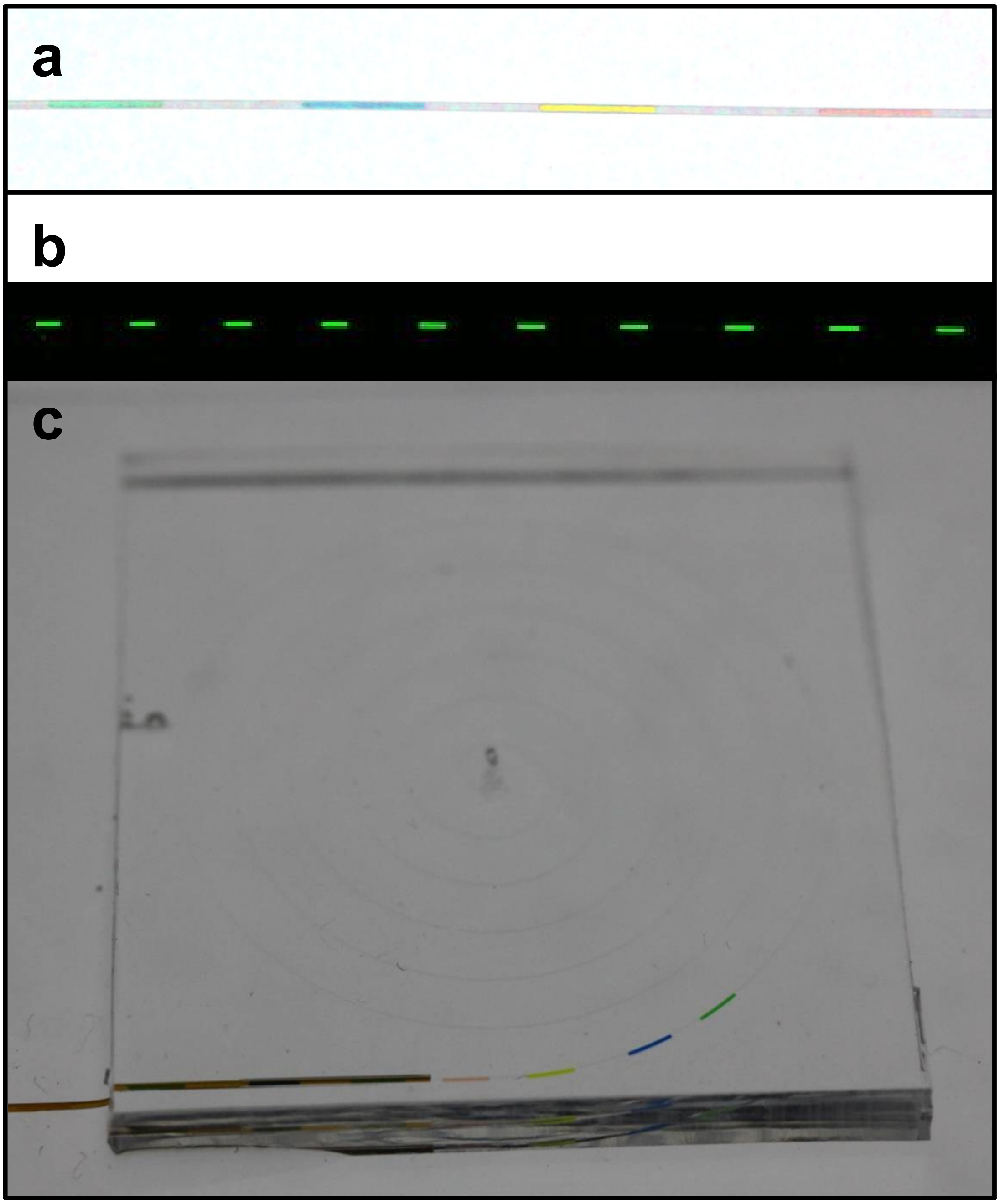
a
b
c

Fig 6.15 Plots showing the linear relationship between sample plug volume and the duration of the peak pressure phase (Tpeak) for three different fixed values of peak pressure (Ppeak: 0.5, 1 and 1.5 psi) applied. Each data point shows the mean and standard deviation of the volume of ten sample plugs generated for each sample plug loading condition.

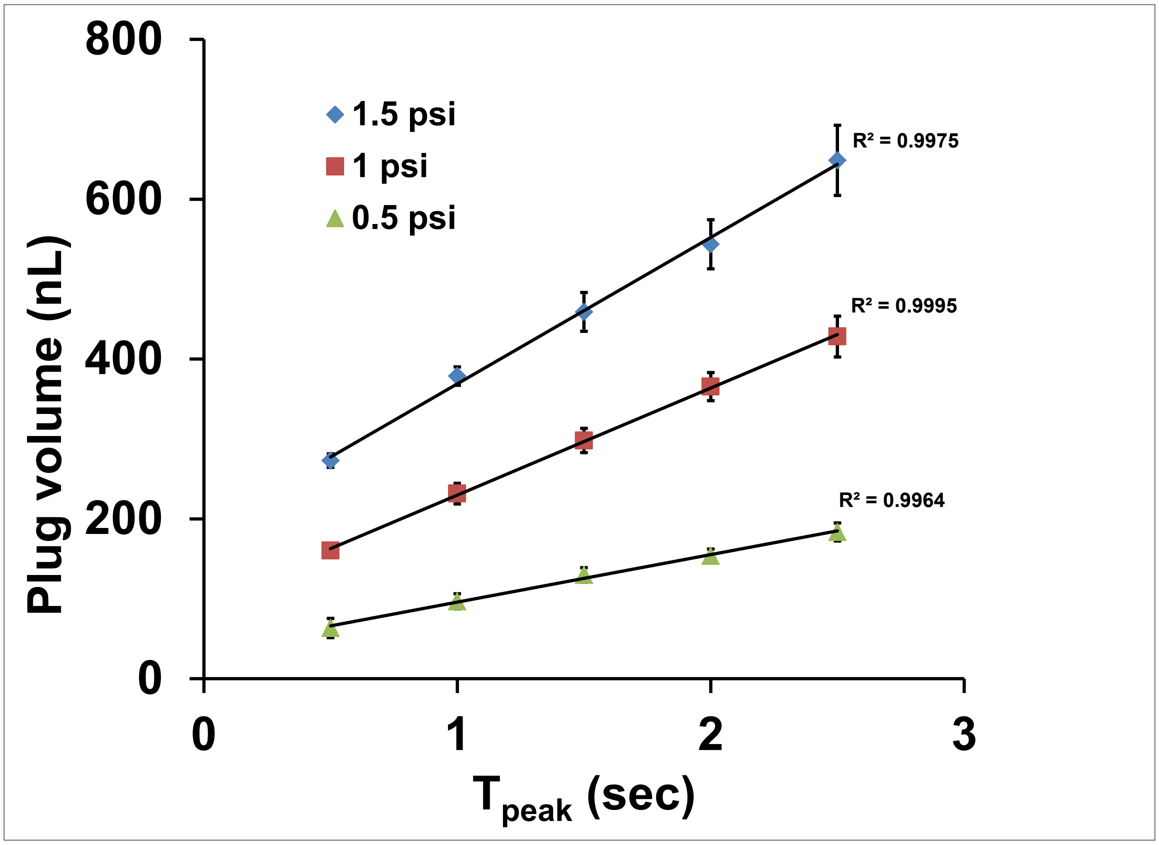
800
600
400
200
0
Plug volume (nL)
0
1
2
3
T_{peak} (sec)
1.5 psi
1 psi
0.5 psi
R² = 0.9975
R² = 0.9995
R² = 0.9964

Fig 6.16 Plot showing the linear relationship between the sample plug volume and the peak pressure (Ppeak) applied for a fixed duration of the peak pressure phase (Tpeak: 1 sec). Each data point shows the mean and standard deviation of the volume of ten sample plugs generated for each sample plug loading condition.

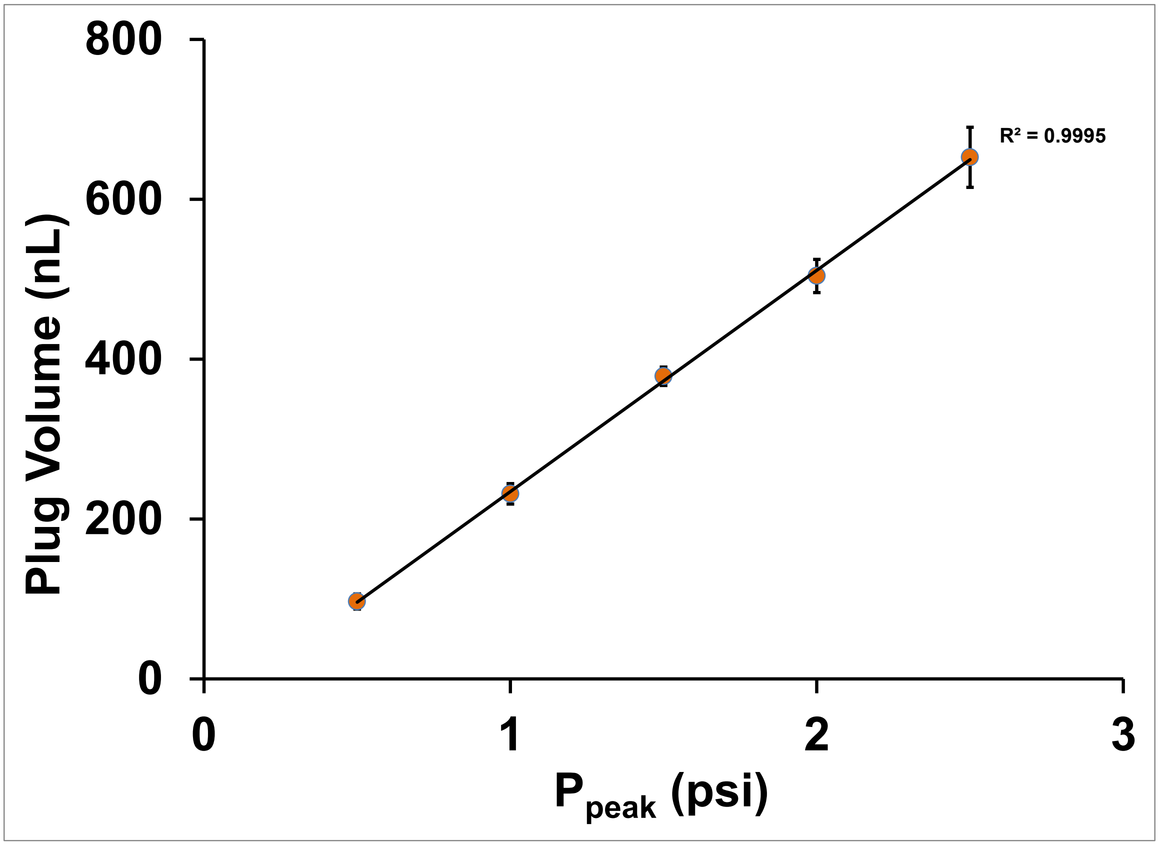

800
600
400
200
0
Plug Volume (nL)
0
1
2
3
P_{peak} (psi)
R² = 0.9995

Fig 6.17 Sample plug volume variation with plug number Left) Plot showing the gradual reduction of sample plug volume as the number of sample plugs loaded into a capillary increases for three loading conditions (P_{peak}: 1 psi, T_{peak}: 1.5, 2, 2.5 sec). The sample plug volume is normalized by the volume of the first sample plug loaded into the capillary for each sample plug loading condition. **Right)** A plot of Sample plug volume versus the plug number in the sequence in which sample plugs are loaded in a capillary, with peak pressure (P_{peak}) compensation to overcome the increase in fluidic resistance of the capillary with each additional plug being loaded into the capillary. The gradual plug volume reduction observed in the left figure is reduced with pressure compensation.

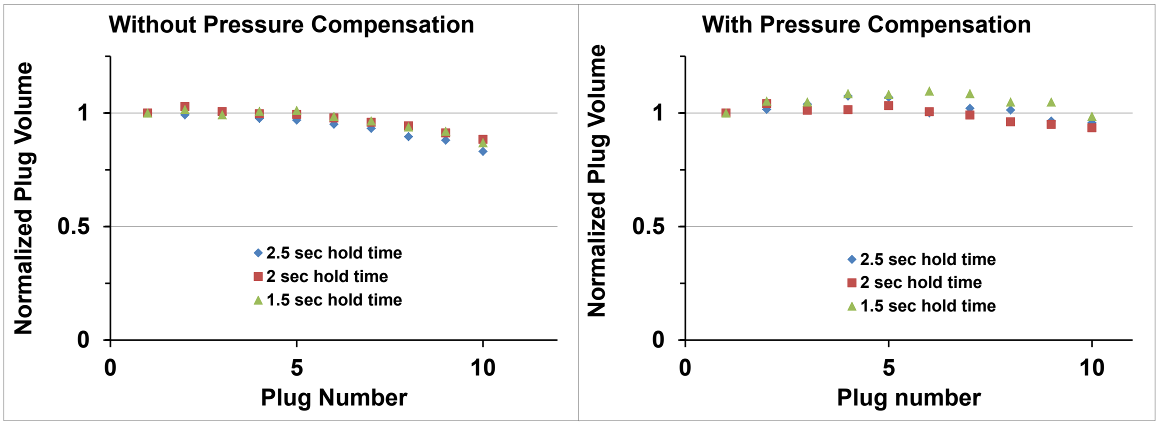
Without Pressure Compensation
Normalized Plug Volume
0
0.5
1
0
5
10
Plug Number
◆ 2.5 sec hold time
■ 2 sec hold time
▲ 1.5 sec hold time
With Pressure Compensation
Normalized Plug Volume
0
0.5
1
0
5
10
Plug number
◆ 2.5 sec hold time
■ 2 sec hold time
▲ 1.5 sec hold time

Chapter 7: Conclusion and Future directions

In conclusion, this thesis contributed a set of tools using droplet microfluidic technology with applications including single cell analysis, single molecule analysis, pathogen detection and high throughout combinatorial screening. The technology developed in the second chapter demonstrated single molecule sensing and quantification within individual droplets. This sensitive technique when coupled with single cell encapsulation in droplets can be used for ultra-sensitive and high throughput molecular expression analysis from single cells. The continuous flow sample-to-answer devices developed in chapters three and four provide an alternative to the current fragmented droplet digital PCR workflow which requires three separate instruments for target nucleic acid sensing at single molecule level. Further development of these continuous flow devices for delivery of multiple samples in a serial manner will make this analysis workflow a viable alternative to current commercially available droplet digital PCR instruments with the added flexibility of screening virtually any range of sample volumes desired. Finally the technology developed in chapters five and six provides a solution for performing high-throughput screening operations using droplet microfluidics. Further development of this technology for increased throughput and continuous flow PCR capabilities can make this an attractive technology for next generation of drug discovery and plant genomic screening workflow.

References

1. Teh SY, Lin R, Hung LH, Lee AP. Droplet microfluidics. Lab Chip. 2008 Feb; 8(2): 198-220.

2. Huebner A, Sharma S, Srisa-Art M, Hollfelder F, Edel JB, Demello AJ. Microdroplets: A sea of applications? Lab Chip. 2008 Aug; 8(8): 1244-1254.

3. Kobayashi I, Uemura K, Nakajima M. Formulation of monodisperse emulsions using submicron-channel arrays. Colloids Surf Physicochem Eng Aspects. 2007 3/15; 296(1-3): 285-289.

4. Ottesen EA, Hong JW, Quake SR, Leadbetter JR. Microfluidic digital PCR enables multigene analysis of individual environmental bacteria. Science. 2006 Dec 1; 314(5804): 1464-1467.

5. Brouzes E, Medkova M, Savenelli N, Marran D, Twardowski M, Hutchison JB, Rothberg JM, Link DR, Perrimon N, Samuels ML. Droplet microfluidic technology for single-cell high-throughput screening. Proc Natl Acad Sci U S A. 2009 Aug 25; 106(34): 14195-14200. PMCID: PMC2732882.

6. Zeng Y, Novak R, Shuga J, Smith MT, Mathies RA. High-performance single cell genetic analysis using microfluidic emulsion generator arrays. Anal Chem. 2010 Apr 15; 82(8): 3183-3190. PMCID: PMC2859697.

7. Hindson BJ, Ness KD, Masquelier DA, Belgrader P, Heredia NJ, Makarewicz AJ, Bright IJ, Lucero MY, Hiddessen AL, Legler TC, Kitano TK, Hodel MR, Petersen JF, Wyatt PW, Steenblock ER, Shah PH, Bousse LJ, Troup CB, Mellen JC, Wittmann DK, Erndt NG, Cauley TH, Koehler RT, So AP, Dube S, Rose KA, Montesclaros L, Wang S, Stumbo DP, Hodges SP, Romine S, Milanovich FP, White HE, Regan JF, Karlin-Neumann GA, Hindson CM, Saxonov S, Colston BW. High-throughput droplet digital PCR system for absolute quantitation of DNA copy number. Anal Chem. 2011 Nov 15; 83(22): 8604-8610. PMCID: PMC3216358.

8. Zhong Q, Bhattacharya S, Kotsopoulos S, Olson J, Taly V, Griffiths AD, Link DR, Larson JW. Multiplex digital PCR: Breaking the one target per color barrier of quantitative PCR. Lab Chip. 2011 Jul 7; 11(13): 2167-2174.

9. Baker M. Digital PCR hits its stride. Nat Meth. 2012 print; 9(6): 541-544.

10. Fallah-Araghi A, Baret JC, Ryckelynck M, Griffiths AD. A completely in vitro ultrahigh-throughput droplet-based microfluidic screening system for protein engineering and directed evolution. Lab Chip. 2012 Mar 7; 12(5): 882-891.

11. Zheng B, Roach LS, Ismagilov RF. Screening of protein crystallization conditions on a microfluidic chip using nanoliter-size droplets. J Am Chem Soc. 2003 Sep 17; 125(37): 11170-11171.

12. Shestopalov I, Tice JD, Ismagilov RF. Multi-step synthesis of nanoparticles performed on millisecond time scale in a microfluidic droplet-based system. Lab Chip. 2004 Aug; 4(4): 316-321.

13. Nie Z, Li W, Seo M, Xu S, Kumacheva E. Janus and ternary particles generated by microfluidic synthesis: Design, synthesis, and self-assembly. J Am Chem Soc. 2006 Jul 26; 128(29): 9408-9412.

14. Hwang DK, Dendukuri D, Doyle PS. Microfluidic-based synthesis of non-spherical magnetic hydrogel microparticles. Lab Chip. 2008 Oct; 8(10): 1640-1647.

15. Choi CH, Jung JH, Rhee YW, Kim DP, Shim SE, Lee CS. Generation of monodisperse alginate microbeads and in situ encapsulation of cell in microfluidic device. Biomed Microdevices. 2007 Dec; 9(6): 855-862.

16. Song H, Ismagilov RF. Millisecond kinetics on a microfluidic chip using nanoliters of reagents. J Am Chem Soc. 2003 Nov 26; 125(47): 14613-14619. PMCID: PMC1769313.

17. Chiu DT, Lorenz RM. Chemistry and biology in femtoliter and picoliter volume droplets. Acc Chem Res. 2009 May 19; 42(5): 649-658. PMCID: PMC2684575.

18. Nie Z, Xu S, Seo M, Lewis PC, Kumacheva E. Polymer particles with various shapes and morphologies produced in continuous microfluidic reactors. J Am Chem Soc. 2005 Jun 8; 127(22): 8058-8063.

19. Song H, Chen DL, Ismagilov RF. Reactions in droplets in microfluidic channels. Angew Chem Int Ed Engl. 2006 Nov 13; 45(44): 7336-7356. PMCID: PMC1766322.

20. Huebner A, Srisa-Art M, Holt D, Abell C, Hollfelder F, deMello AJ, Edel JB. Quantitative detection of protein expression in single cells using droplet microfluidics. Chem Commun (Camb). 2007 Mar 28; (12)(12): 1218-1220.

21. Kumaresan P, Yang CJ, Cronier SA, Blazej RG, Mathies RA. High-throughput single copy DNA amplification and cell analysis in engineered nanoliter droplets. Anal Chem. 2008 May 15; 80(10): 3522-3529.

22. Clausell-Tormos J, Lieber D, Baret JC, El-Harrak A, Miller OJ, Frenz L, Blouwolff J, Humphry KJ, Koster S, Duan H, Holtze C, Weitz DA, Griffiths AD, Merten CA. Droplet-based microfluidic platforms for the encapsulation and screening of mammalian cells and multicellular organisms. Chem Biol. 2008 May; 15(5): 427-437.

23. Schaerli Y, Wootton RC, Robinson T, Stein V, Dunsby C, Neil MA, French PM, Demello AJ, Abell C, Hollfelder F. Continuous-flow polymerase chain reaction of single-copy DNA in microfluidic microdroplets. Anal Chem. 2009 Jan 1; 81(1): 302-306.

24. Beer NR, Wheeler EK, Lee-Houghton L, Watkins N, Nasarabadi S, Hebert N, Leung P, Arnold DW, Bailey CG, Colston BW. On-chip single-copy real-time reverse-transcription PCR in isolated picoliter droplets. Anal Chem. 2008 Mar 15; 80(6): 1854-1858.

25. Boedicker JQ, Li L, Kline TR, Ismagilov RF. Detecting bacteria and determining their susceptibility to antibiotics by stochastic confinement in nanoliter droplets using plug-based microfluidics. Lab Chip. 2008 Aug; 8(8): 1265-1272. PMCID: PMC2612531.

26. Schmitz CH, Rowat AC, Koster S, Weitz DA. Dropspots: A picoliter array in a microfluidic device. Lab Chip. 2009 Jan 7; 9(1): 44-49.

27. Castro A, Williams JG. Single-molecule detection of specific nucleic acid sequences in unamplified genomic DNA. Anal Chem. 1997 Oct 1; 69(19): 3915-3920.

28. de Mello AJ. Seeing single molecules. Lab Chip. 2003 May; 3(2): 29N-34N.

29. Li H, Zhou D, Browne H, Balasubramanian S, Klenerman D. Molecule by molecule direct and quantitative counting of antibody-protein complexes in solution. Anal Chem. 2004 Aug 1; 76(15): 4446-4451.

30. Neely LA, Patel S, Garver J, Gallo M, Hackett M, McLaughlin S, Nadel M, Harris J, Gullans S, Rooke J. A single-molecule method for the quantitation of microRNA gene expression. Nat Methods. 2006 Jan; 3(1): 41-46.

31. Yeh HC, Chao SY, Ho YP, Wang TH. Single-molecule detection and probe strategies for rapid and ultrasensitive genomic detection. Curr Pharm Biotechnol. 2005 Dec; 6(6): 453-461.

32. Yeh HC, Ho YP, Shih I, Wang TH. Homogeneous point mutation detection by quantum dot-mediated two-color fluorescence coincidence analysis. Nucleic Acids Res. 2006 Mar 3; 34(5): e35. PMCID: PMC1390686.

33. Puleo CM, Yeh HC, Liu KJ, Wang TH. Coupling confocal fluorescence detection and recirculating microfluidic control for single particle analysis in discrete nanoliter volumes. Lab Chip. 2008 May; 8(5): 822-825.

34. Puleo CM, Wang TH. Microfluidic means of achieving attomolar detection limits with molecular beacon probes. Lab Chip. 2009 Apr 21; 9(8): 1065-1072.

35. Liu KJ, Wang TH. Cylindrical illumination confocal spectroscopy: Rectifying the limitations of confocal single molecule spectroscopy through one-dimensional beam shaping. Biophys J. 2008 Sep 15; 95(6): 2964-2975. PMCID: PMC2527274.

36. Unger MA, Chou HP, Thorsen T, Scherer A, Quake SR. Monolithic microfabricated valves and pumps by multilayer soft lithography. Science. 2000 Apr 7; 288(5463): 113-116.

37. Yeh HC, Ho YP, Shih I, Wang TH. Homogeneous point mutation detection by quantum dot-mediated two-color fluorescence coincidence analysis. Nucleic Acids Res. 2006 Mar 3; 34(5): e35. PMCID: PMC1390686.

38. Diehl F, Li M, He Y, Kinzler KW, Vogelstein B, Dressman D. BEAMing: Single-molecule PCR on microparticles in water-in-oil emulsions. Nat Methods. 2006 Jul; 3(7): 551-559.

39. Liu KJ, Wang TH. Cylindrical illumination confocal spectroscopy: Rectifying the limitations of confocal single molecule spectroscopy through one-dimensional beam shaping. Biophys J. 2008 Sep 15; 95(6): 2964-2975. PMCID: PMC2527274.

40. Huang B, Wu H, Bhaya D, Grossman A, Granier S, Kobilka BK, Zare RN. Counting low-copy number proteins in a single cell. Science. 2007 Jan 5; 315(5808): 81-84.

41. Vogelstein B, Kinzler KW. Digital PCR. Proc Natl Acad Sci U S A. 1999 Aug 3; 96(16): 9236-9241. PMCID: PMC17763.

42. Lun FM, Chiu RW, Allen Chan KC, Yeung Leung T, Kin Lau T, Dennis Lo YM. Microfluidics digital PCR reveals a higher than expected fraction of fetal DNA in maternal plasma. Clin Chem. 2008 Oct; 54(10): 1664-1672.

43. Joensson HN, Samuels ML, Brouzes ER, Medkova M, Uhlen M, Link DR, Andersson-Svahn H. Detection and analysis of low-abundance cell-surface biomarkers using enzymatic amplification in microfluidic droplets. Angew Chem Int Ed Engl. 2009; 48(14): 2518-2521.

44. Baret JC, Miller OJ, Taly V, Ryckelynck M, El-Harrak A, Frenz L, Rick C, Samuels ML, Hutchison JB, Agresti JJ, Link DR, Weitz DA, Griffiths AD. Fluorescence-activated droplet sorting (FADS): Efficient microfluidic cell sorting based on enzymatic activity. Lab Chip. 2009 Jul 7; 9(13): 1850-1858.

45. Clausell-Tormos J, Lieber D, Baret JC, El-Harrak A, Miller OJ, Frenz L, Blouwolff J, Humphry KJ, Koster S, Duan H, Holtze C, Weitz DA, Griffiths AD, Merten CA. Droplet-based microfluidic platforms for the encapsulation and screening of mammalian cells and multicellular organisms. Chem Biol. 2008 May; 15(5): 427-437.

46. Koster S, Angile FE, Duan H, Agresti JJ, Wintner A, Schmitz C, Rowat AC, Merten CA, Pisignano D, Griffiths AD, Weitz DA. Drop-based microfluidic devices for encapsulation of single cells. Lab Chip. 2008 Jul; 8(7): 1110-1115.

47. Shim JU, Olguin LF, Whyte G, Scott D, Babtie A, Abell C, Huck WT, Hollfelder F. Simultaneous determination of gene expression and enzymatic activity in individual bacterial cells in microdroplet compartments. J Am Chem Soc. 2009 Oct 28; 131(42): 15251-15256.

48. Rane TD, Puleo CM, Liu KJ, Zhang Y, Lee AP, Wang TH. Counting single molecules in sub-nanolitre droplets. Lab Chip. 2010 Jan 21; 10(2): 161-164.

49. Lane DJ, Pace B, Olsen GJ, Stahl DA, Sogin ML, Pace NR. Rapid determination of 16S ribosomal RNA sequences for phylogenetic analyses. Proc Natl Acad Sci U S A. 1985 Oct; 82(20): 6955-6959. PMCID: PMC391288.

50. Fuhrman JA, Davis AA. Widespread archaea and novel bacteria from the deep sea as shown by 16S rRNA gene sequences. Mar Ecol Prog Ser. 1997; 150: 275-285.

51. Ludwig W, Schleifer KH. Bacterial phylogeny based on 16S and 23S rRNA sequence analysis. FEMS Microbiol Rev. 1994 Oct; 15(2-3): 155-173.

52. Zwirglmaier K, Ludwig W, Schleifer KH. Recognition of individual genes in a single bacterial cell by fluorescence in situ hybridization--RING-FISH. Mol Microbiol. 2004 Jan; 51(1): 89-96.

53. Wang TH, Peng Y, Zhang C, Wong PK, Ho CM. Single-molecule tracing on a fluidic microchip for quantitative detection of low-abundance nucleic acids. J Am Chem Soc. 2005 Apr 20; 127(15): 5354-5359.

54. Tyagi S, Kramer FR. Molecular beacons: Probes that fluoresce upon hybridization. Nat Biotechnol. 1996 Mar; 14(3): 303-308.

55. Tyagi S, Kramer FR. Molecular beacons: Probes that fluoresce upon hybridization. Nat Biotechnol. 1996 Mar; 14(3): 303-308.

56. Zhang CY, Chao SY, Wang TH. Comparative quantification of nucleic acids using single-molecule detection and molecular beacons. Analyst. 2005 Apr; 130(4): 483-488.

57. Xi C, Balberg M, Boppart SA, Raskin L. Use of DNA and peptide nucleic acid molecular beacons for detection and quantification of rRNA in solution and in whole cells. Appl Environ Microbiol. 2003 Sep; 69(9): 5673-5678. PMCID: PMC194960.

58. Yang J, Liu Y, Rauch CB, Stevens RL, Liu RH, Lenigk R, Grodzinski P. High sensitivity PCR assay in plastic micro reactors. Lab Chip. 2002 Nov; 2(4): 179-187.

59. Waters LC, Jacobson SC, Kroutchinina N, Khandurina J, Foote RS, Ramsey JM. Microchip device for cell lysis, multiplex PCR amplification, and electrophoretic sizing. Anal Chem. 1998 Jan 1; 70(1): 158-162.

60. Wilding P, Kricka LJ, Cheng J, Hvichia G, Shoffner MA, Fortina P. Integrated cell isolation and polymerase chain reaction analysis using silicon microfilter chambers. Anal Biochem. 1998 Mar 15; 257(2): 95-100.

61. Lee WC, Lien KY, Lee GB, Lei HY. An integrated microfluidic system using magnetic beads for virus detection. Diagn Microbiol Infect Dis. 2008 Jan; 60(1): 51-58.

62. Brosius J, Palmer ML, Kennedy PJ, Noller HF. Complete nucleotide sequence of a 16S ribosomal RNA gene from escherichia coli. Proc Natl Acad Sci U S A. 1978 Oct; 75(10): 4801-4805. PMCID: PMC336208.

63. Hoshino T, Yilmaz LS, Noguera DR, Daims H, Wagner M. Quantification of target molecules needed to detect microorganisms by fluorescence in situ hybridization (FISH) and catalyzed reporter deposition-FISH. Appl Environ Microbiol. 2008 Aug; 74(16): 5068-5077. PMCID: PMC2519275.

64. Strain MC, Lada SM, Luong T, Rought SE, Gianella S, Terry VH, Spina CA, Woelk CH, Richman DD. Highly precise measurement of HIV DNA by droplet digital PCR. PLoS One. 2013; 8(4): e55943. PMCID: PMC3616050.

65. Heredia NJ, Belgrader P, Wang S, Koehler R, Regan J, Cosman AM, Saxonov S, Hindson B, Tanner SC, Brown AS, Karlin-Neumann G. Droplet digital PCR quantitation of HER2 expression in FFPE breast cancer samples. Methods. 2013 Jan; 59(1): S20-3.

66. Heyries KA, Tropini C, Vaninsberghe M, Doolin C, Petriv OI, Singhal A, Leung K, Hughesman CB, Hansen CL. Megapixel digital PCR. Nat Methods. 2011 Jul 3; 8(8): 649-651.

67. Shen F, Du W, Kreutz JE, Fok A, Ismagilov RF. Digital PCR on a SlipChip. Lab Chip. 2010 Oct 21; 10(20): 2666-2672. PMCID: PMC2948063.

68. Zec H, Rane TD, Wang T. Microfluidic platform for on-demand generation of spatially indexed combinatorial droplets. Lab on a Chip. 2012; 12(17): 3055-3062.

69. Kiss MM, Ortoleva-Donnelly L, Beer NR, Warner J, Bailey CG, Colston BW, Rothberg JM, Link DR, Leamon JH. High-throughput quantitative polymerase chain reaction in picoliter droplets. Anal Chem. 2008 Dec 1; 80(23): 8975-8981. PMCID: PMC2771884.

70. Notomi T, Okayama H, Masubuchi H, Yonekawa T, Watanabe K, Amino N, Hase T. Loop-mediated isothermal amplification of DNA. Nucleic Acids Res. 2000 Jun 15; 28(12): E63. PMCID: PMC102748.

71. Tomita N, Mori Y, Kanda H, Notomi T. Loop-mediated isothermal amplification (LAMP) of gene sequences and simple visual detection of products. Nat Protoc. 2008; 3(5): 877-882.

72. Sternlicht MD, Werb Z. How matrix metalloproteinases regulate cell behavior. Annu Rev Cell Dev Biol. 2001; 17: 463-516. PMCID: PMC2792593.

73. Amalinei C, Caruntu ID, Giusca SE, Balan RA. Matrix metalloproteinases involvement in pathologic conditions. Rom J Morphol Embryol. 2010; 51(2): 215-228.

74. Miller MA, Barkal L, Jeng K, Herrlich A, Moss M, Griffith LG, Lauffenburger DA. Proteolytic activity matrix analysis (PrAMA) for *simultaneous determination of multiple protease activities. Integr Biol (Camb). 2011 Apr; 3(4): 422-438. PMCID: PMC3173501.*

75. Brouzes E, Medkova M, Savenelli N, Marran D, Twardowski M, Hutchison JB, Rothberg JM, Link DR, Perrimon N, Samuels ML. Droplet microfluidic technology for single-cell high-throughput screening. Proc Natl Acad Sci U S A. 2009 Aug 25; 106(34): 14195-14200. PMCID: PMC2732882.

76. Hindson BJ, Ness KD, Masquelier DA, Belgrader P, Heredia NJ, Makarewicz AJ, Bright IJ, Lucero MY, Hiddessen AL, Legler TC, Kitano TK, Hodel MR, Petersen JF, Wyatt PW, Steenblock ER, Shah PH, Bousse LJ, Troup CB, Mellen JC, Wittmann DK, Erndt NG, Cauley TH, Koehler RT, So AP, Dube S, Rose KA, Montesclaros L, Wang S, Stumbo DP, Hodges SP, Romine S, Milanovich FP, White HE, Regan JF, Karlin-Neumann GA, Hindson CM, Saxonov S, Colston BW. High-throughput droplet digital PCR system for absolute quantitation of DNA copy number. Anal Chem. 2011 Nov 15; 83(22): 8604-8610. PMCID: PMC3216358.

77. Song H, Chen DL, Ismagilov RF. Reactions in droplets in microfluidic channels. Angew Chem Int Ed Engl. 2006 Nov 13; 45(44): 7336-7356. PMCID: PMC1766322.

78. Song H, Ismagilov RF. Millisecond kinetics on a microfluidic chip using nanoliters of reagents. J Am Chem Soc. 2003 Nov 26; 125(47): 14613-14619. PMCID: PMC1769313.

79. Zhong Q, Bhattacharya S, Kotsopoulos S, Olson J, Taly V, Griffiths AD, Link DR, Larson JW. Multiplex digital PCR: Breaking the one target per color barrier of quantitative PCR. Lab Chip. 2011 Jul 7; 11(13): 2167-2174.

80. Abate AR, Hung T, Mary P, Agresti JJ, Weitz DA. High-throughput injection with microfluidics using picoinjectors. Proc Natl Acad Sci U S A. 2010 Nov 9; 107(45): 19163-19166. PMCID: PMC2984161.

81. Chen CH, Miller MA, Sarkar A, Beste MT, Isaacson KB, Lauffenburger DA, Griffith LG, Han J. Multiplexed protease activity assay for low-volume clinical samples using droplet-based microfluidics and its application to endometriosis. J Am Chem Soc. 2013 Feb 6; 135(5): 1645-1648. PMCID: PMC3566300.

82. Zec H, Rane TD, Wang TH. Microfluidic platform for on-demand generation of spatially indexed combinatorial droplets. Lab Chip. 2012 Sep 7; 12(17): 3055-3062.

83. Jambovane S, Kim DJ, Duin EC, Kim SK, Hong JW. Creation of stepwise concentration gradient in picoliter droplets for parallel reactions of matrix metalloproteinase II and IX. Anal Chem. 2011 May 1; 83(9): 3358-3364.

84. Holtze C, Rowat AC, Agresti JJ, Hutchison JB, Angile FE, Schmitz CH, Koster S, Duan H, Humphry KJ, Scanga RA, Johnson JS, Pisignano D, Weitz

DA. Biocompatible surfactants for water-in-fluorocarbon emulsions. Lab Chip. 2008 Oct; 8(10): 1632-1639.

85. Roach LS, Song H, Ismagilov RF. Controlling nonspecific protein adsorption in a plug-based microfluidic system by controlling interfacial chemistry using fluorous-phase surfactants. Anal Chem. 2005 Feb 1; 77(3): 785-796. PMCID: PMC1941690.

86. Pompano RR, Liu W, Du W, Ismagilov RF. Microfluidics using spatially defined arrays of droplets in one, two, and three dimensions. Annu Rev Anal Chem (Palo Alto Calif). 2011; 4: 59-81.

87. Guo MT, Rotem A, Heyman JA, Weitz DA. Droplet microfluidics for high-throughput biological assays. Lab Chip. 2012 Feb 9.

88. Beer NR, Hindson BJ, Wheeler EK, Hall SB, Rose KA, Kennedy IM, Colston BW. On-chip, real-time, single-copy polymerase chain reaction in picoliter droplets. Anal Chem. 2007 Nov 15; 79(22): 8471-8475.

89. Baret JC, Miller OJ, Taly V, Ryckelynck M, El-Harrak A, Frenz L, Rick C, Samuels ML, Hutchison JB, Agresti JJ, Link DR, Weitz DA, Griffiths AD. Fluorescence-activated droplet sorting (FADS): Efficient microfluidic cell sorting based on enzymatic activity. Lab Chip. 2009 Jul 7; 9(13): 1850-1858.

90. Shi W, Qin J, Ye N, Lin B. Droplet-based microfluidic system for individual caenorhabditis elegans assay. Lab Chip. 2008 Sep; 8(9): 1432-1435.

91. Shi W, Wen H, Lu Y, Shi Y, Lin B, Qin J. Droplet microfluidics for characterizing the neurotoxin-induced responses in individual caenorhabditis elegans. Lab Chip. 2010 Nov 7; 10(21): 2855-2863.

92. Sobrino B, Brion M, Carracedo A. SNPs in forensic genetics: A review on SNP typing methodologies. Forensic Sci Int. 2005 Nov 25; 154(2-3): 181-194.

93. Gupta PK, Rustgi S, Mir RR. Array-based high-throughput DNA markers for crop improvement. Heredity (Edinb). 2008 Jul; 101(1): 5-18.

94. Ragoussis J. Genotyping technologies for genetic research. Annu Rev Genomics Hum Genet. 2009; 10: 117-133.

95. Veldhuisen B, van der Schoot CE, de Haas M. Blood group genotyping: From patient to high-throughput donor screening. Vox Sang. 2009 Oct; 97(3): 198-206.

96. Tewhey R, Warner JB, Nakano M, Libby B, Medkova M, David PH, Kotsopoulos SK, Samuels ML, Hutchison JB, Larson JW, Topol EJ, Weiner MP, Harismendy O, Olson J, Link DR, Frazer KA. Microdroplet-based PCR enrichment for large-scale targeted sequencing. Nat Biotechnol. 2009 Nov; 27(11): 1025-1031. PMCID: PMC2779736.

97. Theberge AB, Mayot E, El Harrak A, Kleinschmidt F, Huck WT, Griffiths AD. Microfluidic platform for combinatorial synthesis in picolitre droplets. Lab Chip. 2012 Mar 7; 12(7): 1320-1326.

98. Abate AR, Hung T, Mary P, Agresti JJ, Weitz DA. High-throughput injection with microfluidics using picoinjectors. Proc Natl Acad Sci U S A. 2010 Nov 9; 107(45): 19163-19166. PMCID: PMC2984161.

99. Li L, Mustafi D, Fu Q, Tereshko V, Chen DL, Tice JD, Ismagilov RF. Nanoliter microfluidic hybrid method for simultaneous screening and optimization validated with crystallization of membrane proteins. Proc Natl Acad Sci U S A. 2006 Dec 19; 103(51): 19243-19248. PMCID: PMC1748211.

100. Zeng S, Li B, Su X, Qin J, Lin B. Microvalve-actuated precise control of individual droplets in microfluidic devices. Lab Chip. 2009 May 21; 9(10): 1340-1343.

101. Guo F, Liu K, Ji X, Ding H, Zhang M, Zeng Q, Liu W, Guo S, Zhao X. Valve-based microfluidic device for droplet on-demand operation and static assay. Appl Phys Lett. 2010 12/06; 97(23): 233701-3.

102. Wang H, Liu K, Chen KJ, Lu Y, Wang S, Lin WY, Guo F, Kamei K, Chen YC, Ohashi M, Wang M, Garcia MA, Zhao XZ, Shen CK, Tseng HR. A rapid pathway toward a superb gene delivery system: Programming structural and functional diversity into a supramolecular nanoparticle library. ACS Nano. 2010 Oct 26; 4(10): 6235-6243. PMCID: PMC2992838.

103. Melin J, Quake SR. Microfluidic large-scale integration: The evolution of design rules for biological automation. Annu Rev Biophys Biomol Struct. 2007; 36: 213-231.

104. Abramoff MD, Magalhaes PJ, Ram SJ. Image processing with ImageJ. Biophotonics International. 2004; 11: 36-42.

105. Mayr LM, Bojanic D. Novel trends in high-throughput screening. Curr Opin Pharmacol. 2009 Oct; 9(5): 580-588.

106. Linder V, Sia SK, Whitesides GM. Reagent-loaded cartridges for valveless and automated fluid delivery in microfluidic devices. Anal Chem. 2005 Jan 1; 77(1): 64-71.

107. Chen DL, Ismagilov RF. Microfluidic cartridges preloaded with nanoliter plugs of reagents: An alternative to 96-well plates for screening. Curr Opin Chem Biol. 2006 Jun; 10(3): 226-231. PMCID: PMC1764868.

108. Zheng B, Ismagilov RF. A microfluidic approach for screening submicroliter volumes against multiple reagents by using preformed arrays of nanoliter plugs in a three-phase liquid/liquid/gas flow. Angew Chem Int Ed Engl. 2005 Apr 22; 44(17): 2520-2523. PMCID: PMC1766320.

109. Adamson DN, Mustafi D, Zhang JX, Zheng B, Ismagilov RF. Production of arrays of chemically distinct nanolitre plugs via repeated splitting in microfluidic devices. Lab Chip. 2006 Sep; 6(9): 1178-1186. PMCID: PMC1851925.

110. Zhang Y, Ozdemir P. Microfluidic DNA amplification--a review. Anal Chim Acta. 2009 Apr 13; 638(2): 115-125.

Curriculum Vitae

Tushar D. Rane	05/25/14
Name	**Date of this version**

Education History:

Ph. D. expected	2014	Program in Biomedical Engineering Mentor: Dr. Jeff TH Wang	Johns Hopkins School of Medicine
M.S.E	2007	Biomedical Engineering	Johns Hopkins University
B. Tech	2004	Mechanical Engineering	Indian Institute of Technology, Bombay

Professional experience:

Research Internship	Summer, 2003	Tata Research Development and Design Centre, Pune, India

Scholarships:

- Siebel Scholar Class of 2014 (Awarded to 85 students at the top of their class based on academic performance and leadership from 17 top graduate programs every year)
- Indian Institute of Technology, Bombay, Heritage Fund Scholarship (2001-2004, awarded to approximately 100 students with limited family income every year, based on academic performance)

Peer-Reviewed Journal Publications

1) **Rane, T. D.**, Zec, H. C., Puleo, C., Lee, A., & Wang, J. T. H. (2012). Droplet microfluidics for amplification-free genetic detection of single cells. *Lab on a Chip, 12(18), 3341-3347*
2) Zec, H. C.*, **Rane, T. D.***, & Wang, J. T. H. (2012). Microfluidic platform for on-demand generation of spatially indexed combinatorial droplets. *Lab on a Chip, 12(17), 3055-3062*

3) **Rane, T. D.***, Zec, H. C.*, & Wang, T. H. (2012). A Serial Sample Loading System Interfacing Multiwell Plates with Microfluidic Devices. *Journal of Laboratory Automation*, *17*(5), 370-377
4) Liu, K. J., **Rane, T. D.**, Zhang, Y., & Wang, T. H. (2011). Single-Molecule Analysis Enables Free Solution Hydrodynamic Separation Using Yoctomole Levels of DNA. *Journal of the American Chemical Society*, *133*(18), 6898-6901
5) **Rane, T. D.***, Puleo, C. M.*, Liu, K. J., Zhang, Y., Lee, A. P., & Wang, T. H. (2010). Counting single molecules in sub-nanolitre droplets. *Lab on a Chip*,*10*(2), 161-164
6) Izawa, J., **Rane, T.**, Donchin, O., &Shadmehr, R. (2008). Motor adaptation as a process of reoptimization. *The Journal of Neuroscience*, *28*(11), 2883-2891
7) **Rane, T. D.**, Dewri, R., Ghosh, S., Chakraborti, N., &Mitra, K. (2005). Modeling the recrystallization process using inverse cellular automata and genetic algorithms: Studies using differential evolution. *Journal of phase equilibria and diffusion*, *26*(4), 311-321
8) Diedrichsen, J., Hashambhoy, Y., **Rane, T.**, &Shadmehr, R. (2005). Neural correlates of reach errors. *The Journal of neuroscience*, *25*(43), 9919-9931

(*: These authors contributed equally to this article)

Peer-Reviewed Conference Articles

1) H.C. Zec, **T.D. Rane,** P. Ma, T.H. Wang (2013). Parallelization of fission and fusion operations for high throughput generation of combinatorial droplets. *IEEE 27th International Conference on Micro Electro Mechanical Systems*
2) **Tushar D Rane**, Helena C. Zec, Tza-Huei Wang (2013) A multiplexed microfluidic droplet platform for matrix metalloproteinase screening. *The 17th International Conference on Miniaturized Systems for Chemistry and Life Sciences(MicroTAS)*
3) H.C. Zec, **T.D. Rane**, W.C. Chu, V.W. Wang, T.H. Wang (2013). A microfluidic droplet platform for multiplexed single nucleotide polymorphism analysis of an array plant genomic DNA samples. *IEEE 26th International Conference on Micro Electro Mechanical Systems*
4) K.J. Liu, **T.D. Rane**, Y. Zhang, C. Beh, D.J. Shin, T.H. Wang (2012). An Integrated Platform for Single Molecule Free Solution Hydrodynamic Separation Using Yoctomoles of DNA and Picoliter Samples. *ASME 10th International Conference on Nanochannels, Microchannels and Minichannels (ICNMM)*
5) Helena Zec, **Tushar D. Rane**, Wen-Chy Chu & Jeff Wang. (2012) Multiplexed Screening Of A Large Library Of Biological Samples Through On-Demand Droplet Generation And Fusion. *Proceedings of the ASME 10th International Conference on Nanochannels, Microchannels, and Minichannels (ICNMM)*
6) **Rane T. D.**, Zec H., Puleo C., Lee A. P., & Wang T. H. (2011) High-throughput single-cell pathogen detection on a droplet microfluidic platform. *IEEE 24th International Conference on Micro Electro Mechanical Systems*
7) **Tushar Rane**, Chris Puleo, Helena Zec, Kelvin Liu, Yi Zhang, Abraham Lee & Tza-Huei Wang (2009) Analyte Detection in Droplets: One Molecule at a Time. *13th International Conference on Miniaturized Systems for Chemistry and Life Sciences(MicroTAS)*
8) C.M. Puleo, H.C. Yeh, K.J. Liu, **T. Rane**, T.H. Wang (2008). Coupling evaporation-based, microfluidic concentration and confocal fluorescence spectroscopy. *IEEE 21st International Conference on Micro Electro Mechanical Systems*
9) Izawa J., **Rane T.**, Donchin O., & Shadmehr R. (2006) Changing the noise in dynamics of reaching predictably changes control of reaching. *Advances in Computational Motor Control*

Patent Applications

- U.S. Patent App. 13/147,742: 'MICROFLUIDIC SOLUTION FOR HIGH-THROUGHPUT, DROPLET-BASED SINGLE MOLECULE ANALYSIS WITH LOW REAGENT CONSUMPTION' Inventors: Jeff T.H. Wang, K.J. Liu, C.M. Puleo, **T.D. Rane**
- U.S. Patent App. 13/708,510: 'SYSTEM AND METHOD FOR SCREENING A LIBRARY OF SAMPLES'
  Inventors: Jeff T.H. Wang, H.C. Zec, **T.D. Rane**, W.C. Chu

Service and Leadership

Spring 2005	Teaching assistant for ‘Computational Modeling Lab’
Spring 2006	Teaching assistant for ‘Computational Modeling Lab’
Spring 2007	Teaching assistant for ‘Learning Theory’ class
Fall 2009	Teaching assistant for ‘Microfabrication Lab’
Spring 2010	Teaching assistant for ‘Systems Bioengineering II’
Spring 2013	Teaching assistant for ‘Biosensing and BioMEMS’ class
Fall 2011-Spring 2013	Volunteer consultant for the ‘Study Consulting’ program at Johns Hopkins University